A NOVEL FLUORESCENT HPLC-BASED METABOLIC LABELING TECHNIQUE REVEALS EFFECTS OF NUTRITIONAL CONTEXT ON DIETARY FATTY ACID PARTITIONING IN THE INTESTINAL ENTEROCYTES

by
Vanessa H. Quinlivan

A dissertation submitted to Johns Hopkins University in conformity with the requirements for the degree of Doctor of Philosophy

Baltimore, MD
October 2017

ABSTRACT

When dietary fatty acids are absorbed by intestinal enterocytes, they are re-assembled into complex lipids such as phospholipids, cholesterol esters, and triglycerides. Although the cellular machinery required for these processes is well known, the mechanisms regulating the partitioning of individual fatty acids among the thousands of possible complex lipid products are not as well understood. Metabolic labeling of dietary lipids, historically performed using radioactive reagents or expensive stable isotopes, is a key technique for examining the biochemical behavior of individual fatty acids in the context of a physiologically relevant mixed-lipid diet. Likewise, fluorescent lipids have been established as important tools for live imaging of the trafficking and spatial deposition of dietary lipids, yet their metabolism has not been fully characterized. I have developed a novel HPLC-based quantitative metabolic labeling method in a larval zebrafish model, wherein the same fluorescent lipid reagents and delivery methods may be used for biochemical and live imaging experiments. The characterization of fluorescent fatty acid metabolism described here opens the way for more widespread use of fluorescent lipids in metabolic studies. In this thesis I review the current literature on the zebrafish as a model for lipid uptake and metabolism. This review includes my own analysis and interpretation of a recently published developmental lipidomics data set. I then describe the application of metabolic labeling with fluorescent lipids toward a greater understanding of dietary lipid partitioning in the intestinal enterocytes, specifically addressing the interactions among dietary fatty acids, cholesterol, and ethanol. Preliminary results suggest that phospholipid synthesis from dietary fatty acids is increased in larval zebrafish exposed to ethanol before feeding. Future work will address potential physiological effects of this interaction between ethanol and dietary fatty acid partitioning. Additionally, I report results of a collaborative study in which HPLC lipid profiling methods initially developed in zebrafish were expanded into a mouse model. This enabled

measurement of changes in individual plasma lipid species resulting from perturbation of a putative lipid transport mechanism in the intestinal enterocytes. These diverse applications of the metabolic labeling methods I have developed demonstrate significant contributions to the lipid biology field: I have expanded both the amount and type of data that can be obtained using HPLC lipidomics, creating a relatively low-cost and high-throughput alternative to metabolic labeling with mass spectrometry analysis. Furthermore, ongoing work may contribute to greater understanding of both potentially beneficial interactions between ethanol and dietary lipids (e.g. the Mediterannean diet hypothesis) and possible diet-driven variability in the progression of alcoholic liver disease.

Readers: Steven Farber, G. William Wong, Marnie Halpern, David Cohen

TABLE OF CONTENTS

TABLES

Chapter 1

Chapter 2

Tables S1-4 are included as supplemental material in the electronic version of this thesis.

FIGURES

Chapter 1

Chapter 2

INTRODUCTION

In this thesis I describe novel lipidomics and metabolic labeling techniques that I developed in the larval zebrafish model. This work has addressed a need in the lipidomics field for a midpoint between expensive and resource-intensive liquid chromatography-mass spectrometry (LC-MS) lipidomics (which may yield so much information as to make interpretation unnecessarily difficult due to signal to noise issues) and thin-layer chromatography or less precise mass spectrometry techniques that either only give information on lipid classes and/or fatty acids.

In Chapter 1 I have reviewed the current literature on the embryonic and larval zebrafish as models for lipid absorption, metabolism, and transport. Additionally, drawing on a published LC-MS lipidomic data set, I have analyzed and interpreted trends in individual phospholipids over the course of yolk absorption by the developing zebrafish.

Chapter 2 was originally published as a methods article in the *Journal of Lipid Research*, and presents a novel combined biochemical and live imaging method for the study of dietary lipid metabolism. Metabolic labeling, which is the delivery of tagged analogs of nutrients to an animal or cell culture model so that the labeled molecules and their products can be assayed in context, is especially important for the study of lipid metabolism. All naturally-occuring foods and internal sources of lipid (e.g., the embryonic zebrafish yolk) are mixtures of various types of complex lipids carrying a wide variety of different fatty acids. Historically, isotopically labeled fatty acids have been used as metabolic labels to study the biochemical processing of individual fatty acids in the context of a mixed-nutrient diet, and the predominant application of fluorescently labeled lipids has been live imaging to study the spatial distribution of the products of dietary lipids. Expanding upon existing techniques, I have developed novel methods for metabolic labeling with fluorescent lipids: This is the first published application of these reagents capable of yielding both

a detailed biochemical profile of the products of individual dietary fluorescent fatty acids and live imaging data showing the spatial deposition of fluorescent lipids from the same experiment. I then used these methods to investigate the influence of nutritional context and the type of fluorescent tag on the partitioning of dietary fluorescent fatty acids into complex lipids. Additionally, I describe a novel approach to studying cholesterol metabolism by measuring cholesterol esterification with fluorescent fatty acids.

Chapter 3, reprinted from a research article in *Disease Models and Mechanisms*, includes description of a high-throughput method I developed for quantitating individual free fatty acids and cholesterol esters in mouse plasma and tissue lipid extracts. We used this method to investigate effects of diet and disrupted putative lipid transport systems on plasma, liver, and adipose tissue lipid composition in mice.

Chapter 4 describes ongoing work, which is the first investigation of how ethanol may alter metabolic channeling of individual dietary fatty acids that occurs as they are taken up by intestinal enterocytes. Ethanol is known to interfere with lipid metabolism by causing hepatic steatosis, but how lipid metabolism may be affected in other tissues is less clear. Preliminary results show a shift toward phospholipid synthesis from dietary fluorescent fatty acids in larval zebrafish exposed to ethanol. To close, I discuss experimental plans to investigate both the physiological implications and potential mechanisms for this interaction between ethanol and fatty acid metabolism.

CHAPTER 1 – LIPID UPTAKE, METABOLISM, AND TRANSPORT IN THE LARVAL ZEBRAFISH

This chapter was submitted to the *Journal of Endocrinology* for publication as a review under the topic "Energy Homeostasis in Lower Vertebrates," and is currently in review.

Abstract

The developing zebrafish is a well-established model system for studies of energy metabolism, and is amenable to genetic, physiological, and biochemical approaches. For the first five days of life, nutrients are absorbed from its endogenous maternally deposited yolk. At five days post-fertilization, the yolk is exhausted and the larva has a functional digestive system including intestine, liver, gallbladder, pancreas, and intestinal microbiota. The transparency of the larval zebrafish, and the genetic and physiological similarity of its digestive system to that of mammals make it a promising system in which to address questions of energy homeostasis relevant to human health. For example, apolipoprotein expression and function is similar in zebrafish and mammals, and transgenic animals may be used to examine both the transport of lipid from yolk to body in the embryo, and the trafficking of dietary lipids in the larva. Additionally, despite the identification of many fatty acid and lipid transport proteins expressed by vertebrates, the cell biological processes that mediate the transport of dietary lipids from the intestinal lumen to the interior of enterocytes remain to be elucidated. Genetic tractability and amenability to live imaging and a range of biochemical methods make the larval zebrafish an ideal model in which to address open questions in the field of lipid transport, energy homeostasis and nutrient metabolism.

Introduction

The developing digestive system of the embryonic and larval zebrafish is a well-established model system for the study of vertebrate gastrointestinal physiology and metabolism. Metabolic and regulatory pathways for gastrointestinal system development, intestinal and liver cell differentiation, digestion, and nutrient uptake and transport are highly conserved between zebrafish and humans (1-7). Additionally, the transparency of the developing larva makes it ideal for live imaging experiments: The larval zebrafish has a functional and visible liver, pancreas, gallbladder, intestine, and intestinal microbiota by 5 days post-fertilization (dpf) when it begins to feed. The zebrafish is also amenable to the generation of transgenic and mutant lines through a variety of techniques including CRISPR and TALENs (8-10), and is suitable for large scale forward genetic screens due to its small size and high fertility (11). Finally, as the importance of the gut microbiome to studies of nutritional physiology is becoming increasingly clear; the larval zebrafish microbiota are well-characterized, and germ-free and gnotobiotic models are available (12).

The zebrafish zygote contains a large yolk cell which is absorbed over the first five days of life and supplies the developing embryo with nutrients. The yolk consists of a lipid and protein rich core with a cellular syncytium at its periphery, called the yolk syncytial layer (YSL). The YSL exports amino acids, hydrolyzes complex lipids to release fatty acids, and synthesizes lipoproteins, which export lipid to the developing embryo until it is able to feed independently (13). The intestine of the larval zebrafish is open at both ends and ready to absorb exogenous food at 5 dpf, though the non-enterocyte secretory cell populations do not differentiate until later larval stages (14). Once the intestinal tract is open, the gut microbiota are acquired from the media. At this time colonization occurs essentially immediately and is maintained throughout life with the main source of variation in bacterial community composition being changes in diet(15).

Both the embryonic and larval zebrafish are valuable models of lipid uptake and trafficking, respectively from the yolk cell and the diet. This review encompasses the roles of lipid remodeling, lipoproteins, intestinal lipid transport proteins, and the gut microbiota in lipid processing during zebrafish development.

Yolk Lipid Uptake in the Embyronic and Larval Zebrafish

Lipoproteins transport yolk lipids to the body in the developing zebrafish embryo

The majority of the mass of a zebrafish zygote consists of the yolk, a lipid-rich structure that is gradually depleted by transport of its contents to the embryo as it develops into a free-feeding larva. Yolk lipids are packaged into lipoproteins in the YSL before being exported to the body of the developing zebrafish. Lipoproteins are lipid-transporting structures consisting of a neutral lipid interior bounded by a phospholipid and cholesterol monolayer, carrying one or more apolipoproteins. Apolipoproteins mediate interactions among lipoproteins, cellular receptors, and lipid-processing enzymes. The zebrafish genome contains analogs of every major human apolipoprotein, but there are some differences in patterns of expression and function. Due to the teleost genome duplication, zebrafish have multiple paralogs of each apolipoprotein gene. There are 11 apolipoprotein genes in the *apoB*, *apoA-IV*, *apoE*, and *apoA-I* families, and all are expressed in the YSL (16)(Figure 1). Whole-mount in-situ hybridization reveals that expression of some apolipoprotein genes is localized to subregions of the YSL, suggesting a previously uncharacterized compartmentalization of this structure. For example, mRNA encoding *apoA-IV* appears to be specific to the yolk extension at earlier stages (though different paralogs in this family are concentrated here at different points in development) while members of the other apolipoprotein families are expressed more evenly throughout the YSL (16). The significance of these potential YSL subdomains has yet to be described, but it is possible that there is a

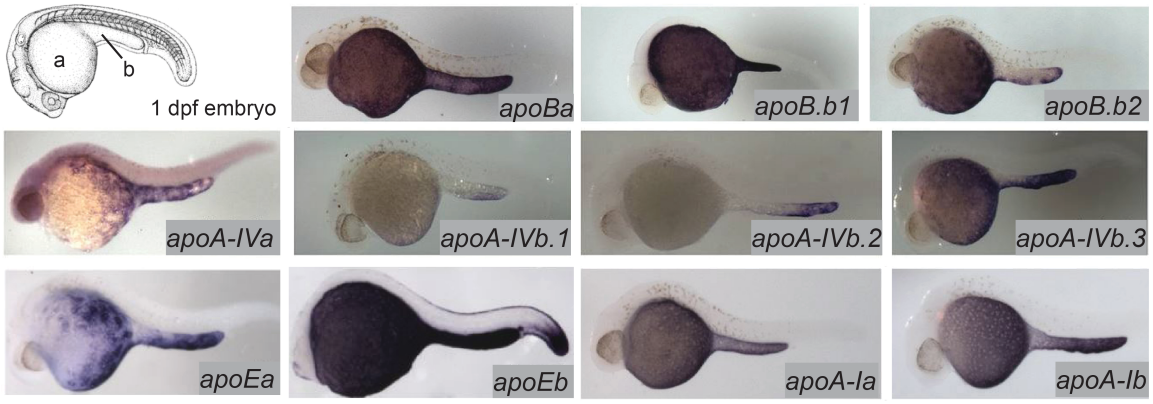

Figure 1. Zebrafish apolipoprotein genes are expressed in the yolk syncytial layer. The developing zebrafish embryo gradually absorbs lipids from its yolk (a), which is surrounded by the YSL. At 1-5 dpf, the yolk ball is lengthened along the tail of the embryo forming the yolk extension (b). In situ hybridization reveals expression of all 11 zebrafish apolipoprotein genes in the *apoB*, *apoA-IV*, *apoE*, and *apoA-I* families in the YSL at 1 day post-fertilization. Line drawing reprinted from Miyares et al, 2014. In situ hybridization images adapted and reprinted from Otis et al, 2015, Figures 2-5.

relationship to the regionalization of the developing intestine.

Although the expression of apolipoprotein genes in the developing embryo and larva has been thoroughly characterized, the lipoprotein profile at these stages is less well defined. Most work on fish lipoproteins has focused on adults, likely due to the difficulty of obtaining adequate blood samples from larvae(17). Secretion of VLDL (very low-density lipoprotein) particles from the yolk has been demonstrated by electron microscopy (18, 19). The YSL also expresses *apoA-I* and *apoA-II*, which are found in HDL (high-density lipoprotein) particles and chylomicrons but not LDL (low-density lipoprotein) or VLDL (16, 20). ApoB, which is a component of chylomicrons, LDL, and VLDL, has a vital role in the export of yolk lipids. Microsomal triglyceride transfer protein (MTP) packages triglycerides into ApoB-containing lipoproteins. ApoB is degraded if it is not associated with lipid so, in the absence of MTP function, ApoB is not functional (21). In *mtp-/-* mutant zebrafish larvae, lipids are trapped in the yolk (characterized by retention of yolk volume, an increase in yolk opacity, and a reduction in neutral lipid in the body) and larvae do not survive beyond 5 days (22). (Additionally, unlike their wild-type siblings, *mtp-/-* embryos retain fluorescent fatty acid injected into the yolk and do not export it or its fluorescent products to the circulation (23).) The ability of *mtp-/-* larvae to grow and survive to 5 dpf suggests that some lipid must be transported out of the yolk in order for membranes to be synthesized, possibly through the synthesis of HDL-like particles that contain ApoA-I and do not require MTP for their assembly.

Lipid composition of the embryo changes over the course of yolk absorption

According to a recently published developmental study of lipid composition performed by liquid chromatography-mass spectrometry (LC-MS), at the time of fertilization, embryo lipids are approximately 40% cholesterol, 35% phospholipid (PL), and 9% triglyceride (TG), with less abundant species including mono- and di-glycerides, cholesterol esters (CE), ceramides and lysophospholipids making up the remainder (24). Over the first five days of life, a linear decrease

in the molar amount of most lipid species is observed in the yolk with a corresponding increase in the embryonic/larval body. Some exceptions have been observed: TG in the body remains consistently low as it is depleted from the yolk, suggesting that yolk TGs are primarily broken down and either oxidized for energy or resynthesized into other lipid products. Interestingly, CE, the other "energy storage" lipid class, is exchanged evenly from the yolk to the body during this period of development (24). Cholesterol synthesis in animal cells is tightly controlled in response to the cholesterol content of membranes via regulation of HMG-CoA Reductase expression, and esterification is a major mechanism by which excess cholesterol is neutralized (25). One possible reason that CE is not depleted during the lecithotrophic (yolk-feeding) period of development is that breaking down CE for fatty acid oxidation would result in an overabundance of cholesterol. Favoring glycerolipids as an early energy source therefore would be important for cholesterol homeostasis, while CE from the yolk could be repackaged into intracellular lipid droplets for later oxidation, or storage in adipocytes. Free cholesterol in the yolk and the body decrease and increase respectively at the same apparent rate between 24 hours and 5 days of development, but the cholesterol content of the body at 5 dpf is less than the initial amount in the yolk (24). It is likely that this portion of the cholesterol is directed to synthesis of steroid hormones and bile, though these compounds were not measured in this study.

Phospholipid dynamics in the developing embryo also appear to be more complex than simple yolk to body trafficking: while other phospholipid classes seem to move gradually from the yolk to the body, phosphatidylcholine (PC) levels in the yolk increase over the first 24 hours, then decrease over the next four days while remaining relatively constant in the body (24). Though the specific lipid composition of zebrafish embryonic lipoproteins has not been investigated, one possible explanation is that the initial increase in PC goes to building the outer monolayer on lipoproteins exported from the yolk. It is possible that when this lipoprotein-associated PC reaches the body, it is in excess and is either oxidized or remodeled.

Although Fraher and colleagues' published analysis of their LC-MS data set was limited to discussion of developmental changes in lipid classes, quantitation of all individual lipid species was published as a supplement to the manuscript. These data provide an opportunity to examine the changes in individual lipid species that occur during the first 5 days of zebrafish development. For example, the major phospholipid classes are defined by head group (e.g. phosphatidylcholines, phosphatidylethanolamines (PE), phosphatidylserines (PS), etc.), but each of these classes comprises thousands of different molecules with different types of fatty acid "tails." Modern mass spectrometry technologies optimized for lipidomics can differentiate between individual lipid species at this level of resolution because they can precisely determine the mass to charge ratio (m/z) of each analyte in a mixture, and because they employ a second step in which the molecules are fragmented and the subsequent m/z values of these fragments is also determined. Complex lipids such as phospholipids are identified using m/z values calculated from molecular formulas and expected fragmentation patterns, and are annotated in Fraher's supplemental data and other lipidomics data sets as "Head Group (FA 1/FA 2)." The most abundant phospholipid in animal cell membranes, for example, is phosphatidylcholine with the saturated 16-carbon fatty acid palmitate and the monounsaturated 18-carbon fatty acid oleate, and is annotated as PC(16:0/18:1). When the specific fatty acid composition of a complex lipid cannot be determined, only the total fatty acid carbon chain length and number of unsaturated carbon-carbon bonds is given (e.g., PC(34:1)).

When trends in the amounts of individual lipids in Fraher's data set are examined, results suggest that changes in the phospholipid profile are consistent with an increase in membrane phospholipid in the larval body that is expected to occur with increasing growth. However, the trends in total amounts of phospholipid present in the yolk and body are skewed by changes in individual phospholipid species. Specifically, PC(18:2/20:4) is a major phospholipid in the body at the start of development and shows a large decrease by 5 dpf. However, the expected major PC components of cell membranes including PC(34:1) and other PCs with total chain lengths in the

low 30s increase over the course of larval development as expected. It is possible that longer-chain phospholipids predominate in lipoproteins but are a minor species in cell membranes, a model supported by a large increase in the amount of PC 18:2/20:4 in the yolk over the course of development (this species is the only phospholipid in the yolk whose total molar amount increases over 1-5 days, though other phospholipid species increase in the yolk in terms of percentage of total lipid). Phospholipids containing the fatty acid arachidonic acid (20:4) are the precursor of eicosanoids, a class of signaling molecules with roles in regulating inflammation, vascular physiology, and stem cell activity (26, 27).

This finding suggests eicosanoids as an important area of interest in the ongoing characterization of yolk utilization in the zebrafish. Although the physiological implications of changes in individual lipids were not within the scope of this published work, the rich MS data set that was produced highlights the importance of examining behavior of individual lipids in studies of metabolism and transport.

Complex lipid synthesis and remodeling occurs in the embryonic and larval zebrafish yolk

The embryonic and larval zebrafish yolk is metabolically active not just in lipid transport, but also in the synthesis and remodeling of complex lipids, as was demonstrated through the injection of radioactive and fluorescently labeled lipids into the larval yolk followed by thin layer chromatography (TLC) analysis of the products of these metabolic tracers (23). Fatty acids labeled with BODIPY-FL (4,4-Difluoro-5,7-Dimethyl-4-Bora-3a,4a-Diaza-*s*-Indacene; a green fluorescent small molecule tag) or radioactive fatty acids injected into the yolk of 3 dpf larval zebrafish were both metabolized into complex lipids including PL, CE, and TG and transported throughout the developing body. Furthermore, injection of radioactive oleate showed that the yolk synthesizes complex lipids at the earliest stages of development, as radioactive TG and PL products were found in embryos injected as early as 0.75 hours post-fertilization (hpf). While the

rate of incorporation of radioactive oleate into each phospholipid class was consistent in embryos and larvae aged 0.75 hpf to 3 dpf, larvae injected at 3 dpf were the only group to synthesize labeled CE, and there was a large increase in the amount of radioactive TG at later stages as well (23). When BODIPY-C12 was injected into the yolk of 24 hpf zebrafish embryos and yolk and body lipids were analyzed separately by TLC 1-6 hours post injection (hpi), fluorescent complex lipids including TG, CE, and several unidentified species were produced in the yolk at early time points. Some fluorescent complex lipids were detected in the body at 6 hpi (24). (It is not known whether fluorescent phospholipid was synthesized in this experiment as the assay only detected nonpolar lipids.) Injection of fluorescent PL into the yolk at 24 hpf resulted in fluorescent diglyceride and unidentified complex lipid species in the yolk, but no identified products in the body up to 6 hpi (24). (It is not known whether fluorescent phospholipid was synthesized in this experiment as the assay would not have detected it.) Injection of fluorescent PL into the yolk at 24 hpf resulted in fluorescent diglyceride and unidentified complex lipid species in the yolk, but no identified products in the body up to 6 hpi (24). Taken together, this and other evidence shows that the yolk is metabolically active throughout development and can both break down and synthesize complex lipids (23, 24, 28) (Table 1).

Table 1. The larval zebrafish is a versatile model system for metabolic labeling of lipids.

Labeled Lipid Substrate	**Developmental Stage/ Delivery Method**	**Assay**	**Reported In:**
Radioactive FA	1 dpf/yolk injection	TLC	Miyares et al, 2014
	3 dpf/yolk injection	TLC	Miyares et al, 2014
	6 dpf/feeding	HPLC	Quinlivan et al, 2017
Fluorescent FA	1 dpf/yolk injection	TLC	Fraher et al, 2016
	3 dpf/yolk injection	TLC	Miyares et al, 2014
	6 dpf/feeding	TLC	Carten et al, 2011
		HPLC	Quinlivan et al, 2017
Fluorescent PL	1 dpf/yolk injection	TLC	Fraher et al, 2016
Fluorescent CE	6 dpf/feeding	HPLC	Quinlivan et al, 2017

Dietary Lipid Uptake in the Larval Zebrafish

Digestion and absorption of dietary complex lipids

The larval zebrafish undergoes a switch from a lecithotrophic state to a free-feeding animal during its fifth day of development, so by the time its yolk supply is depleted it must be able to digest and absorb nutrients from exogenous food sources. The ability to precisely control timing of the first meal is an advantage of this model as processing of dietary lipids by enterocytes can be observed without interference from lipids absorbed from previous meals. Additionally, because the larva retains its transparency for several weeks after it becomes free-feeding, it is possible to perform live imaging experiments with either single meals or ongoing defined diets in the same system.

Most dietary lipid consumed by animals enters the intestine not in the form of free fatty acids, but in complex lipids. Dietary triglycerides, phospholipids, and cholesterol esters must be broken down by intestinal lipases in the lumen before the components of these molecules can cross the enterocyte membrane. As the fatty acids in these molecules are all linked by ester bonds, the intestinal lipases secreted by the exocrine pancreas are versatile and process a wide range of dietary lipids so that they can be absorbed (29). Following lipolysis, dietary lipid products form micelles in the intestinal lumen, which are emulsified in this aqueous environment by bile. The composition of bile varies between species and there are significant differences between teleost fish and humans, but its function is conserved (30, 31).

Enteroendocrine cells in the intestine regulate digestion and are influenced by the microbiota

As they do in mammals, enteroendocrine cells in zebrafish secrete a wide range of hormones including serotonin, which influences motility and appetite, and cholecystokinin (CCK), which stimulates gall bladder contraction and release of digestive enzymes from the

pancreas (32, 33). The zebrafish genome contains two CCK paralogs; *ccka* is expressed in the digestive system of adults (no data is available for larvae at this time) and both *ccka* and *cckb* are expressed in the brain starting at 24 hpf (34, 35). In mammals, CCK promotes lipid digestion by stimulating the gall bladder to secrete bile, but does not increase lipase activity (36, 37). Similarly, larval zebrafish treated with a CCK receptor antagonist show reduced protease activity while intestinal phospholipase activity is unaffected (29). Enteroendocrine cells expressing serotonin begin to appear in the larval zebrafish intestine at 5 dpf. They may be detected by immunohistochemistry for serotonin, and are distinguished from the enteric neurons (which also express serotonin) by their shape and location in the epithelium. By 8 dpf, 10-18 enteroendocrine cells per larva may be observed in the distal intestine (posterior to the swim bladder) (14). A notable difference is that the larval zebrafish intestine does not have crypts, where enteroendocrine cells would be located in mammals.

The intestinal microbiota is required for normal enteroendocrine cell development. In germ-free larval zebrafish, 0-6 enteroendocrine cells were observed at 8 dpf (the total number of cells in the distal intestinal epithelium did not vary between germ-free and conventional groups). Larvae raised germ-free until 5 dpf, and then colonized with the conventional microbiota, developed normal numbers of enteroendocrine cells, suggesting that the yet-unidentified signal from the microbiota that promotes enteroendocrine cell development is not required before 5 dpf. Higher gut motility was observed in zebrafish larvae raised germ-free, suggesting a possible connection to digestive problems (including irritable bowel disease) observed in humans when the gut microbiota is disrupted (14). The lower number of serotonin-positive cells could explain this physiological effect as serotonin regulates gut motility in humans (32).

The intestinal microbiota influences dietary lipid uptake

The bacterial population of the intestine also plays an important role in dietary lipid uptake and metabolism. Fermentation by the gut microbiota allows host animals to utilize dietary

plant polysaccharides that would otherwise be indigestible by converting them to metabolizable short-chain fatty acids and monosaccharides (38). Multiple studies over the last decade have shown effects of changes in composition of the gut microbiota on adiposity, serum lipids, and tissue lipids in mammals. However, determining mechanisms by which bacteria may cause global changes in vertebrate host physiology has been difficult as the composition of the gut microbiota also changes in response to changes in diet (39). The larval zebrafish model was recently used to investigate aspects of the relationship between gut bacteria and lipids involving processes other than short-chain fatty acid synthesis: when larvae raised germ-free were given a high-fat meal labeled with fluorescent fatty acids, less fluorescence accumulated in the intestinal epithelium when compared with conventionally raised larvae, showing that at least some members of the microbiota are necessary to promote uptake of dietary lipids. Monoassociated larvae (larvae raised germ-free and then inoculated with a single bacterial species) colonized with the Firmicutes strain *Exiguobacterium sp*. were used to demonstrate that this bacterial strain alone was sufficient to promote intestinal fatty acid uptake to a point where fluorescence could be observed in extra-intestinal tissues. Furthermore, experiments using conditioned media from this strain and two others also revealed significant increases in enterocyte lipid droplet number over untreated germ-free larvae, suggesting that a factor secreted by these species is involved in promoting dietary lipid uptake (40). The exact mechanism for this host-microbe relationship is currently uncharacterized, as is the evolutionary advantage of promoting host lipid uptake for these microbial species.

Lipid transport into enterocytes

Dietary lipids are imported from the intestinal lumen across the apical enterocyte membrane by several different mechanisms depending on their class. After complex lipids (including both glycerolipids and cholesterol esters) are digested to yield fatty acids,

monoglycerides, and/or lysophospholipids, these products may cross membranes by a variety of transport processes conserved among zebrafish and mammals.

Cholesterol is taken up by enterocytes by a mechanism that requires the Niemann-Pick C1-Like 1 (NPC1L1) transport protein (41, 42). This membrane-associated protein is located at the luminal border of enterocytes and is translocated to an intracellular compartment when cells are exposed to cholesterol; current models postulate a clathrin-dependent endocytic mechanism in which NPC1L1 is internalized along with a cholesterol cargo, which then moves through endosomes to the endoplasmic reticulum where it can be packaged into membranes or used to synthesize cholesterol ester (43, 44). NPC1L1 is encoded in the zebrafish genome, and several lines with point mutations in this gene have been created through the Sanger Institute Zebrafish Mutation Project (45). Ezetimibe, an inhibitor of NPC1L1-mediated cholesterol absorption that is used to treat hypercholesterolemia in humans, also blocks dietary cholesterol absorption in larval zebrafish (46-48). This creates an opportunity to use the zebrafish model to study physiological effects of modulating metabolic availability of a single component of a mixed-lipid diet. Regulation of NPC1L1 activity remains largely uncharacterized, although there is evidence from studies in humans given statins (inhibitors of cholesterol synthesis) that NPC1L1 expression levels increase in response to low intracellular cholesterol levels, suggesting that there may be an unidentified genetic mechanism that regulates NPC1L1 expression that could counteract the effects of statins by upregulating import of dietary cholesterol (49).

Fatty acid transfer proteins (FATPs) are a family of integral membrane proteins that facilitate transport of fatty acids into cells, including transport of dietary fatty acids into enterocytes. FATPs act in concert with acyl-coA synthetases (ACSs), which activate the newly imported fatty acids so that they are ready to form ester bonds and be incorporated into complex lipids (50, 51). There is evidence from mammalian and cell culture models that both the FATP and ACS families play roles in regulating preferential uptake of some dietary fatty acids over others, and the partitioning of dietary fatty acids among complex lipids (51, 52). The zebrafish

genome encodes 9 ACSL (ACSs specific to long-chain fatty acids, the type of fatty acid most abundant in animals including zebrafish) gene paralogs in six families. Expression of this class of genes is ubiquitous, with proteins corresponding to seven of nine paralogs detectable in the adult by Western blot in most tissues including the gut (53). Expression of ACSL genes in the larva is more regionalized: in the *acsl1* family, *acsl1b* mRNA is detectable in the YSL and gut in early larval stages. The *acsl1a* paralog is not expressed in the YSL and no expression data is available for early gut development (54). (Only *acsl1a* is expressed in the gut in adults (53).) *Acsl4a* mRNA is present in both the YSL and the larval gut (55). Expression of *acsl4b* and *acsl5* is detectable in the YSL but expression data is not available from larval stages after the gut has begun to develop (54) (Figure 2). Expression data is unavailable for the other *acsl* paralogs at any embryonic or larval stage, but what is known about expression of *acsl* genes in this model suggests potential division of function among paralogs similar to that suggested by regionalized apolipoprotein gene expression.

Compared with the ACSs there is far less coverage of zebrafish fatty acid transfer proteins in the current literature. As of now no studies of FATP function in this model system have been published and only one genomic sequence is annotated as a FATP in the Ensembl database; FATP3/ACSVL3/SLC27A3 (with 7 paralogs, all annotated as members of solute carrier family 27 (*slc27*)). The other six putative FATP paralogs are annotated as SLC27A1A and B (both with 65% protein sequence identity to human SLC27A1/FATP1/ACSVL5 (a mitochondrial long-chain FATP (56)), using the NCBI protein BLAST tool)), SLC27A2A (47% protein sequence identity to human SLC27A2/FATP2/ACSVL1), SLC27A2B (55% protein sequence identity to human SLC27A2/FATP2/ACSVL1), SLC27A4 (70% protein sequence identity to human SLC27A4/FATP4/ACSVL4), and SLC27A6 (57% protein sequence identity to human SLC27A6/FATP6/ACSVL2). The chromosomal locations of all of these putative *fatp* genes are conserved between the human and zebrafish genomes (syntenic analysis by ZFIN).

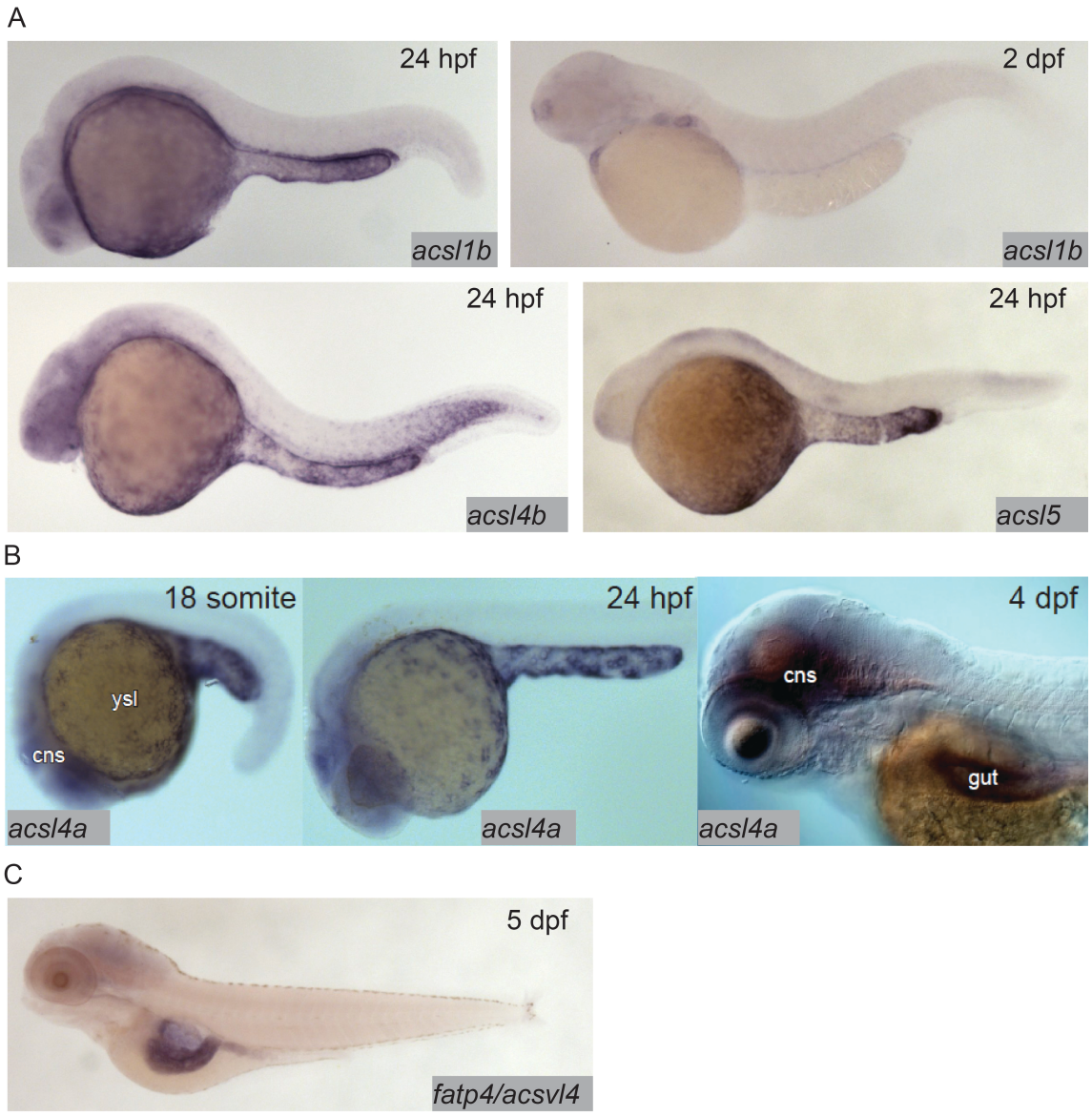

Figure 2. Acetyl-CoA synthetases are expressed in the larval zebrafish YSL and intestine. A) In situ hybridization reveals expression of *acsl1b*, *acsl4b*, and *acsl5* in the YSL at 24 hpf, and *acsl1b* in the developing gut at 2 dpf. Adapted from Thisse et al, 2004. B) acsl4a is expressed in the gut and central nervous system (cns) of the 4dpf larval zebrafish, and in the YSL at 24 hpf and earlier. Reprinted from Miyares et al, 2013, Figure S1 E. C) *fatp4*/*acsvl4* is expressed in the gut (especially the anterior bulb) of the 5 dpf larval zebrafish. Adapted from Thisse et al, 2005.

Zebrafish SLC27A2A is expressed in the adult liver (57), and SLC27A4 is expressed in the anterior gut at 5 dpf (58) (Figure 2). No expression data is available for other adult organs, earlier larval stages, or the other putative FATPs at this time. However, as FATP4 is the primary fatty acid transporter on the apical brush border of human enterocytes, the similarity in expression between zebrafish and humans supports the larval zebrafish as a model in the investigation of FATP function in dietary fatty acid absorption (59).

The relative contributions of FATP4, other membrane-associated fatty acid binding proteins, and passive diffusion to uptake of dietary fatty acids by enterocytes in larval zebrafish are not known. A recent review proposes a model in which the transmembrane receptor protein CD36, Caveolin 1 (Cav1), and FATP4 all act as fatty acid transporters at the enterocyte brush border, and in which passive diffusion of long-chain fatty acid salts across the enterocyte membrane plays a major role in adsorption (60). Larval zebrafish express CD36 and Cav1 in the intestine as well as FATP4, and therefore present an opportunity to apply live whole-animal imaging tools toward investigations of the roles of each of these proteins in dietary fatty acid processing (61, 62). (Unlike mammals, Cav1 is located on the basolateral membrane of enterocytes in zebrafish and not at the brush border (62).) In sum, despite tight conservation of FATP genes and their intestinal expression throughout the vertebrates, their physiological role in the intestine remains unclear.

Lipid processing in enterocytes for storage and export

Fatty acids taken up by enterocytes are re-packaged into complex lipids at the endoplasmic reticulum, and are subsequently stored in enterocyte lipid droplets or directed to lipoprotein synthesis for export. Lipid droplets are composed primarily of triglycerides and cholesterol esters in the interior, and bounded by a phospholipid monolayer with associated proteins such as perilipins (63). Though the mechanisms by which lipid droplets grow and shrink are well characterized, the regulation of lipid droplet size and number in various tissues is not as

well understood, and most current research efforts focus on adipose and hepatic lipid droplets (64). As the intestine is not a site of long-term lipid storage in vertebrates including larval zebrafish, enterocyte lipid droplets are highly dynamic, temporary structures that respond with high sensitivity to the nutritive state of the animal. This property combined with the relative ease of live imaging in the larval zebrafish intestine makes for an ideal system for the study of lipid droplet dynamics and regulation. When 5 dpf larvae are fed a high-fat/high-cholesterol meal of chicken egg yolk, both the average lipid droplet number per enterocyte and total area of the cell covered by lipid droplets increase significantly by 1 hour post-feeding. Lipid droplet number peaks at 1 hour and then gradually decreases, while total lipid droplet area is maintained up to three hours following the meal, suggesting that smaller lipid droplets fuse as they mature (65). The gut microbiota also influence enterocyte lipid droplet number and size. Intestinal lipid droplets are both larger and more numerous in conventionally-raised larvae after feeding than in germ-free larvae. Furthermore, conditioned media from a Firmicutes bacterial strain found to promote dietary fatty acid uptake and export to the liver was sufficient to increase enterocyte lipid droplet number but not the average lipid droplet size (40). These results have begun to reveal the diverse mechanisms by which different members of the gut microbiota influence lipid droplet dynamics and dietary lipid metabolism.

Lipoproteins are essential for the export of the products of dietary lipid from enterocytes into the circulation. Expression and function of apolipoproteins in the zebrafish is similar to that observed in mammals; at least one paralog from each of the ApoA-I, ApoB, ApoE, and ApoA-IV families is expressed in the larval zebrafish intestine (16). There is evidence that division of apolipoprotein function among organs is regulated by different mechanisms that achieve the same end in zebrafish and mammals: while different variants of ApoB are produced in the mammalian intestine and liver via RNA editing, larval zebrafish produce mRNA for the ApoB paralog b.1 in the intestine and liver and ApoBb.2 in the liver only. Similar compartmentalization of paralog expression between the liver and intestine is observed in the other apolipoprotein families as well

(16) (Figure 3). Intestinal lipid accumulation in animals treated with an MTP inhibitor shows that as in the larval zebrafish yolk, availability of functional ApoB in necessary for normal rates of lipid export from the intestine, and that enterocyte lipid droplets are the destination of excess dietary fatty acids when export is slowed (66-68). The MTP inhibitor lomitapide is effective in larval zebrafish (65). It has also been observed that in mammals as the dietary fat content increases, chylomicron number reaches a plateau but average chylomicron size continues to increase, suggesting that apolipoprotein expression is the limiting factor in the rate of lipid export from the intestine (69).

Total lipid biochemistry of the larval zebrafish reveals global effects of diet on lipid composition, and facilitates metabolic labeling studies

The larval zebrafish intestine is not only an excellent model for the study of lipid droplet and lipoprotein packaging, but also a site of differential channeling of dietary fatty acids depending on their chemical properties. The amenability of this model to biochemistry due to the ease of obtaining large numbers of embryos and larvae and performing lipid extractions from them, combined with the transparency of the larva, provides an opportunity unique among vertebrates to perform live imaging and metabolic labeling experiments in parallel using the same fluorescent lipid reagents. Additionally, the whole-body lipid composition of the larval zebrafish is highly sensitive to changes in diet: the triglyceride content of the 6 dpf larva increases 10-fold 24 hours after a single high-fat meal (compared with a standard low-fat diet, and allowing time for the intestinal lumen to clear). Working at developmental stages before adipose tissue appears (~14 dpf) avoids signal to noise problems that may occur when the neutral lipid stored in adipose is included in the whole-body lipid profile. Also, at these early developmental stages examination of dietary lipid processing in the intestine can be isolated from potential regulatory influences from adipose tissue.

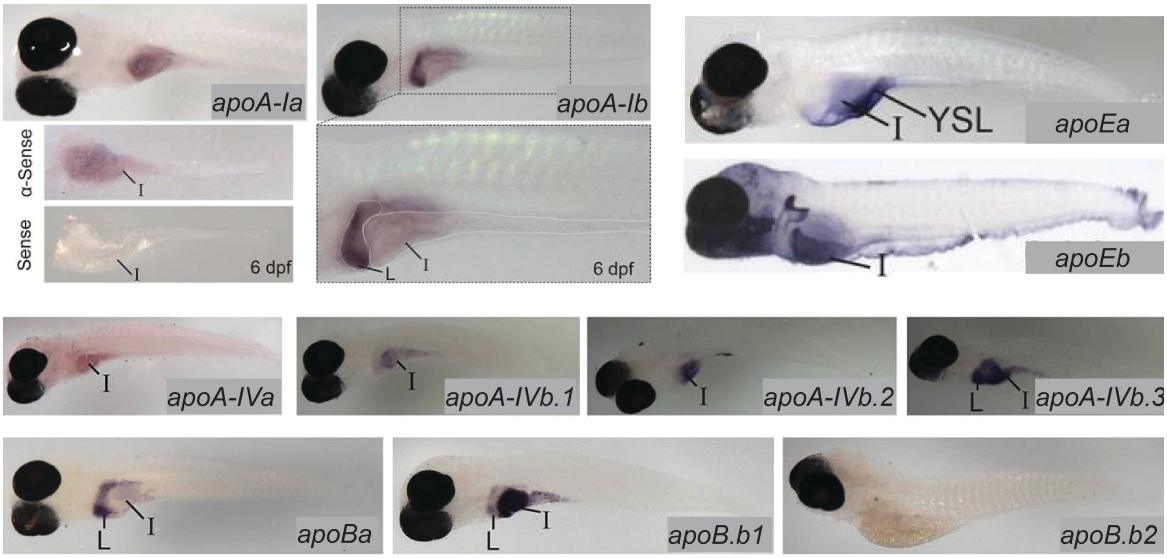

Figure 3. Zebrafish apolipoprotein genes are expressed in the larval digestive system. In situ hybridization reveals expression of 10 of the 11 zebrafish apolipoprotein genes in the *apoB*, *apoA-IV*, *apoE*, and *apoA-I* families in the liver and/or intestine of the 6 dpf larva. Dissected intestines probed for *apoA-Ia* are shown, and the gut of a larva probed for *apoA-1b* is magnified below the image of the whole larva. L = liver, I = intestine. Adapted and reprinted from Otis et al, 2015, Figures 2-5, under a CC-BY license.

Though it was beyond the scope of our recent metabolic labeling study (70), the biochemical techniques described therein could be applied to later-stage larvae in order to examine potential crosstalk between adipose tissue and the enterocytes that could influence dietary lipid partitioning. We have also developed methods for using fluorescent fatty acids as metabolic labels in the context of standard and lipid-enriched diets in larval zebrafish (Table 1). In addition to exploring the metabolic labeling potential of fluorescent lipids whose product profiles were not previously described, we have also applied HPLC with charged aerosol (total lipid detection) and fluorescence detection to obtain a greater depth of information than previous studies using fluorescent TLC (28). Initial findings (described in Chapter 2) indicate that the partitioning of saturated fluorescent fatty acids among complex lipid classes varies with carbon chain length, the total fat and cholesterol content of the diet, and the type of fluorescent tag (70). Metabolic labeling with fluorescent fatty acids in the context of lipid metabolism by the larval zebrafish is summarized in Figure 4.

Potential mechanisms regulating the rate of lipid export from the intestine beyond lipoprotein levels, the regulation and physiological effects of the size of enterocyte lipid droplets, and the channeling of newly absorbed dietary fatty acids into the different classes of complex lipids are currently largely uncharacterized. The optically clear and genetically tractable larval zebrafish model presents an ideal system in which to investigate these questions relating to energy homeostasis with a combined live imaging and biochemical approach.

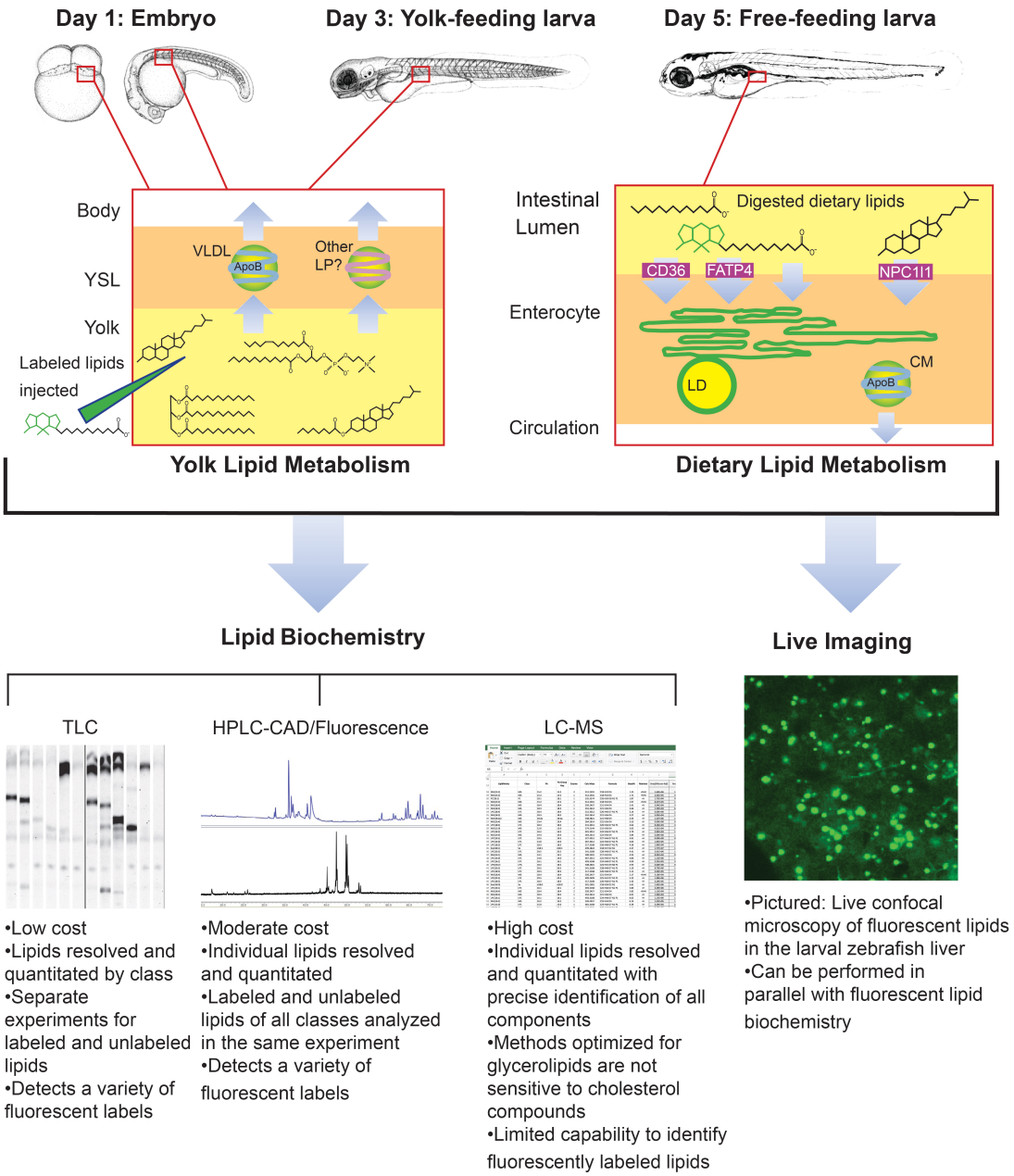

Figure 4. Metabolic labeling with fluorescent fatty acids is performed in the context of zebrafish development, yolk absorption, and dietary lipid metabolism. Fluorescent fatty acids (BODIPY FL-C12 depicted) are trafficked and metabolized along with native yolk or dietary lipids when delivered to the developing zebrafish by yolk injection or feeding. LD = cytoplasmic lipid droplet, LP = lipoprotein, VLDL = very low-density lipoprotein. Embryo and larva illustrations adapted from Miyares et al, 2014.

CHAPTER 2 – AN HPLC-CAD/FLUORESCENCE LIPIDOMICS PLATFORM USING FLUORESCENT FATTY ACIDS AS METABOLIC TRACERS

Published as a Methods article in the *Journal of Lipid Research*, May 2017.
Vanessa H. Quinlivan[1,2], Meredith H. Wilson[1], Josef Ruzicka[3] and Steven A. Farber[1,2]

[1]Department of Embryology, Carnegie Institution for Science, Baltimore, MD 21218
[2]Department of Biology, The Johns Hopkins University, Baltimore, MD 21218
[3]Thermo Fisher Scientific, Somerset, NJ 08873

Abstract

Fluorescent lipids are important tools for live imaging in cell culture and animal models, yet their metabolism has not been well-characterized. Here we describe a novel combined HPLC and LC-MS/MS method developed to characterize both total lipid profiles and the products of fluorescently labeled lipids. Using this approach we found that lipids labeled with the fluorescent tags BODIPY FL, BODIPY(558/568), and TopFluor are all metabolized into varying arrays of polar and nonpolar fluorescent lipid products when they are fed to larval zebrafish. Quantitative metabolic labeling experiments performed in this system revealed significant effects of total dietary lipid composition on fluorescent lipid partitioning. We provide evidence that cholesterol metabolism in the intestine is important in determining the metabolic fates of dietary fatty acids. Using this method we found that inhibitors of dietary cholesterol absorption and esterification both decreased incorporation of dietary fluorescent fatty acids into cholesterol esters, suggesting that cholesterol ester synthesis in enterocytes is primarily responsive to the availability of dietary cholesterol. These results are the first to comprehensively characterize fluorescent fatty acid metabolism and to demonstrate their utility as metabolic labeling reagents, effectively coupling quantitative biochemistry with live imaging studies.

Introduction

When dietary fatty acids are absorbed by intestinal enterocytes, those that are not oxidized are incorporated into complex lipids (lipid molecules containing more than one acyl chain and/or sterol group) including phospholipids, triglycerides, and cholesterol esters. This process involves a network of transporters, enzymes, and cellular components, the roles and regulation of which are still being characterized (71-73). The processes by which dietary fatty acids are distributed among various complex lipid classes and how assembly of complex lipids from dietary fatty acids may be influenced by other nutrients including dietary cholesterol are not fully understood.

To investigate dietary fatty acid metabolism in a quantitative manner, it was necessary to develop an animal model wherein individual fatty acids could be studied in the context of the digestion and absorption of a physiologically relevant mixed-lipid diet. While cell culture is a well-established model system for the study of lipid metabolism, it cannot replicate the digestive and metabolic physiology of a whole vertebrate animal with a functional liver, intestine, pancreas, and microbiota such as the larval zebrafish (15, 40, 74-79). An additional strength of this model is that live imaging and biochemical experiments may be performed in parallel using the same fluorescent lipid reagents and experimental system (2, 23, 24, 28, 29, 48, 80-83). Many publications using fluorescent lipid reagents did not examine the metabolism of these labels (with some asserting that some or all fluorescent fatty acids are not metabolizable (84-86)), but prior work has shown that BODIPY® FL (4,4-Difluoro-5,7-Dimethyl-4-Bora-3a,4a-Diaza-*s*-Indacene)-labeled fatty acids may be esterified and incorporated into products including phospholipids, triglycerides, and cholesterol esters (28, 87-91). However, with the exception of two HPLC-Fluorescence profiles of the phospholipid products of BODIPY FL-C12 (BODIPY FL-dodecanoic acid) (87, 88), all published characterization of the metabolic products of fluorescent lipids has been performed with thin layer chromatography (TLC), which unlike HPLC

does not resolve individual lipid species within each class. For this study we developed a novel total-lipid HPLC method that allowed the complex lipid product profiles of BODIPY FL-labeled fatty acids and other fluorescent lipids commonly used in imaging experiments to be described in detail, and facilitated investigation of the role of nutritional context in how fluorescent lipids are metabolized.

Emulsification of fluorescent fatty acids into chicken egg yolk (a high-fat/high-cholesterol meal relative to standard larval fish diets) has been shown to promote their metabolism when they are fed to larval zebrafish, but how the nutritional context in which fluorescent lipids are delivered regulates their partitioning has not been characterized (28). There is evidence from mammalian models for interaction between the dietary cholesterol and fatty acid uptake and metabolism pathways: cholesterol esters are synthesized in enterocytes, and dietary long-chain fatty acids enhance dietary cholesterol uptake in rats, but the mechanisms for this interaction remain unknown (30, 31(92, 93). We applied our novel fluorescent lipid profiling method to examine the effect of the metabolic availability of dietary cholesterol on intestinal cholesterol ester synthesis in order to better understand the role of cholesterol regulation mechanisms in dietary fatty acid metabolism.

In this study we describe total lipid profiles of the 6-dpf (days post-fertilization) larval zebrafish after both low-fat/low-cholesterol and high-fat/high-cholesterol meals, and the fluorescent product profiles synthesized from the most commonly used commercially available fluorescent lipids when they are fed to larval zebrafish in several different diets. This thorough characterization of the metabolism of fluorescent lipids will greatly expand the depth of physiological information that may be gained from using these reagents in well-established live fluorescent imaging methods. We also demonstrate a novel application of fluorescent fatty acids as metabolic labeling reagents by showing that pharmaceutical manipulations of intestinal cholesterol metabolism result in significant changes in dietary fluorescent fatty acid partitioning, suggesting coupling between dietary cholesterol uptake and esterification.

Materials and Methods

Zebrafish

Embryos were collected from group matings of wild-type (AB) *Danio rerio* (zebrafish) and raised to the 6 days-post-fertilization (dpf) larval stage at 28^{o}C on a 14:10 on:off light cycle in embryo media. All experiments with zebrafish (protocol #139) were approved by the Carnegie Institution Department of Embryology IACUC.

Food Preparation and Feeding

The fluorescent fatty acids BODIPY® FL-C5 (4,4-Difluoro-5,7-Dimethyl-4-Bora-3a,4a-Diaza-*s*-Indacene-3-Pentanoic Acid; Thermo Fisher Scientific), BODIPY® FL-C12 (4,4-Difluoro-5,7-Dimethyl-4-Bora-3a,4a-Diaza-*s*-Indacene-3-Dodecanoic Acid; Thermo Fisher Scientific), BODIPY® FL-C16 (4,4-Difluoro-5,7-Dimethyl-4-Bora-3a,4a-Diaza-*s*-Indacene-3-Hexadecanoic Acid; Thermo Fisher Scientific), BODIPY®(558/568)-C12 (4,4-Difluoro-5-(2-Thienyl)-4-Bora-3a,4a-Diaza-*s*-Indacene-3-Dodecanoic Acid; Thermo Fisher Scientific), and TopFluor®-C11 (dipyrrometheneboron difluoride undecanoic acid; Avanti Polar Lipids) were administered to larval zebrafish in HF/HC (high-fat/high-cholesterol) meals: Solutions of 5% chicken egg yolk liposomes containing 4 μg/mL fluorescent fatty acid were prepared as previously described (28). Larval zebrafish (6 dpf) were immersed in these solutions for 2 hours, protected from light in a shaking incubator at 30^{o}C and 30 rpm. After feeding, larvae were rinsed in fresh embryo media and screened for full intestines under a stereomicroscope. Larvae that had eaten were maintained in embryo media at room temperature for a 4-24 hour chase period (measured from the start of feeding) depending on the experiment. Samples of 10-100 pooled larvae were collected for lipid extraction and stored dry at -80^{o}C.

To compare the metabolism of BODIPY FL-C12 and palmitate, larvae were fed equimolar amounts of BODIPY FL-C12 (9.56 μM) and palmitic acid (0.85 μM ^{3}H-palmitic acid

and 8.71 μM unlabeled palmitic acid) in a HF/HC meal for two hours at 25°C and 30 rpm. Larvae were maintained at 25°C in embryo media for 18 hours, and then samples of 25 larvae each were taken for lipid extraction.

For experiments in which lipids were extracted from larval zebrafish intestines, larvae were anesthetized in tricaine (3-amino benzoic acid ethyl ester) and mounted in 3% methylcellulose. Intestines were removed using tungsten wire dissecting tools prepared according to published methods (94), and stored in lipid extraction buffer (1 mM EDTA, 20 mM Tris-Cl) at -80°C. Alternately, larvae could be fixed 24-72 hours at 4°C in 4% paraformaldehyde, transferred to PBS, and then dissected. No differences in lipid profiles as analyzed by HPLC-CAD were observed between fixed and unfixed samples. All data shown is from lipid extracts of unfixed larvae.

Preparation of LF/LC (low-fat/low-cholesterol) and LF/HC (low-fat/high-cholesterol) foods with fluorescent lipids was adapted from published methods (83). For the LF/LC diet, 2.5 nmol fluorescent lipid (BODIPY FL-C12, BODIPY®(558/568)-C12, Cholesterol BODIPY® FL-C12 [Thermo Fisher Scientific], or Cholesterol BODIPY®(576/589)-C11 [cholesterol 4,4-difluoro-5-(2-pyrrolyl)-4-bora-3a,4a-diaza-s-indacene-3-undecanoate; Molecular Probes, discontinued]) was diluted in 0.5 mL diethyl ether, combined with 0.1 g Sera® Micron larval fish food, and solvents were allowed to evaporate. For LF/HC diets, 4 mg cholesterol (4% w/w) was added as well. Larval zebrafish (5 dpf) were fed LF/LC or LF/HC meals twice per day for two days at 25°C, and then LF/LC or LF/HC meals with fluorescent lipid for three days at 25°C protected from light. Food was then withdrawn and samples of 20-75 larvae were taken after an overnight chase to allow larvae to excrete any unabsorbed food remaining in the intestinal lumen. Larger numbers of larvae per sample were required for experimental groups fed red fluorescent lipids.

Sample Preparation, HPLC, and Data Analysis

Lipids were extracted from frozen larvae samples by a Bligh-Dyer procedure, dried under vacuum, and resuspended in 100 µL HPLC-grade isopropanol per sample as the HPLC injection solvent. The components of each sample were separated and detected by an HPLC system using a LPG-3400RS quaternary pump, WPS-3000TRS autosampler (maintained at 20.0^{o}C), TCC-3000RS column oven (maintained at 40.0^{o}C), Accucore C18 column (150 x 3.0 mm, 2.6 µm particle size), FLD-3100 fluorescence detector (8 µL flow cell maintained at 45.0^{o}C), and Dionex Corona Veo charged aerosol detector (CAD) (all from Thermo Fisher Scientific). Component peaks were resolved over an 80 min time range in a multistep mobile phase gradient as follows: 0-5 min = 0.8 mL/min in 98.0% mobile phase A (methanol-water-acetic acid, 750:250:4) and 2.0% mobile phase B (acetonitrile-acetic acid, 1000:4), 5-35 min = 0.8-1.0 mL/min, 98.0-30% A, 2.0-65.0% B, and 0-5.0% mobile phase C (2-propanol), 35-45 min = 1.0 mL/min, 30%-0% A, 65.0%-95.0% B, and 5.0% C, 45-73 min = 1.0 mL/min, 95.0-60.0% B and 5.0-40.0% C, and 73-80 min = 1.0 mL/min, 60.0% B, and 40.0% C. (HPLC-grade acetic acid and 2-propanol were purchased from Fisher Scientific and HPLC-grade methanol and acetonitrile were purchased from Sigma-Aldrich.) The following adjustments were made to the solvent gradients for better separation of nonpolar products of BODIPY FL-C5 and BODIPY FL-C12: In the "B-C5" instrument method, the flow rate was decreased to 0.5 mL/min at 40-80 minutes, and in the "B-C12" method the flow rate was decreased to 0.5 mL/min at 45-80 minutes. Between 5 and 99 µL were injected per sample to produce peak shapes suitable for quantitation. For HPLC-fluorescence, the following excitation and detection wavelengths were used: 576/596 nm for products of cholesterol BODIPY(576/598)-C11, 558/578 nm for products of BODIPY(558/568)-C12, and 488/512 nm for products of BODIPY FL(503/512) and TopFluor-labeled lipids. It was not possible to use excitation and detection settings that matched the maxima for each BODIPY-lipid because for the FLD-3100 fluorescent HPLC detector these settings must be at least 20 nm apart. Optimal fluorescent detector settings were determined empirically (data not shown).

Chromatographic peaks produced by cholesterol as well as several fluorescent and non-fluorescent cholesterol esters were identified by comparison with standards (Sigma-Aldrich and Thermo Fisher Scientific). Non-cholesterol-containing lipids were identified and quantitated by mass spectrometry as described below. Additionally, acetone precipitation (adapted from (95)) was performed on some samples prior to HPLC so that fluorescent analytes that could not be precisely identified by mass spectrometry could be classified as polar or nonpolar lipids. Quantitation of lipid species was performed using Chromeleon 7.2 (Thermo Fisher Scientific, Germering, Germany). Peak baselines were drawn manually and areas were determined automatically. Further data analysis (where applicable) was performed using Microsoft Excel with the StatPlus package.

To compare the metabolic products of BODIPY FL-C12 and ^{3}H-palmitic acid, lipids extracted from larval zebrafish fed these fatty acids simultaneously as described above were subjected to HPLC-Fluorescence analysis using the "B-C12" method, after which the eluent was collected in 1-minute increments (Model 2110 Fraction Collector, Bio-Rad Laboratories) and radioactivity was quantitated using a liquid scintillation counter (Tri-Carb 2810 TR Liquid Scintillation Analyzer, Perkin-Elmer; 3a70b scintillation fluid, Research Products International Corp.). Fluorescent chromatograms were quantitated in Chromeleon 7.2 by simulated fraction collection: a flat baseline was drawn from zero to 80 minutes and each 1-minute area was assigned as a "peak" by placing a delimeter perpendicular to the baseline.

LC-MS and Data Analysis

For LC-MS experiments, chromatography was performed using the procedure and equipment described above, with eluent directed to a mass spectrometer in place of the charged aerosol detector after exiting the fluorescence detector. High-resolution accurate-mass spectrometry data were recorded on a Q Exactive Plus mass spectrometer (Thermo Fisher Scientific, Bremen, Germany) equipped with a heated electrospray-ionization probe (HESI-II).

Data were acquired in positive and negative polarity with the following source parameters: spray voltage, 3.5 kV for positive polarity and 3.2 kV for negative polarity; sheath gas flow, 70 (arbitrary units); auxiliary gas flow, 25 (arbitrary units); sweep gas flow, 1 (arbitrary units); auxiliary gas heater temperature, 400°C; capillary temperature, 285°C; S-Lens RF level, 45 %. The instrument was operated with external mass calibration without use of a lock mass. Mass spectra were recorded in data-dependent MS/MS mode as a Top-12 experiment with the following acquisition settings: mass resolution, 140,000 for full-MS and 17,500 for MS^2; full-MS scan range, 200-1600 Da; quadrupole isolation window, 1.2 Da; normalized collision energy, stepped 20-30-40%; exclusion mass list, 200 entries (created individually for each polarity mode from injection solvent blank runs). Data acquisition and quantitation was performed using Xcalibur (version 3.0.63, Thermo Fisher Scientific), and identification of non-fluorescent lipid analytes was performed with LipidSearch (version 4.0, MKI, Tokyo, Japan). Fluorescent lipids were identified manually by using Xcalibur to search for analyte peaks containing boron, as this element lends a unique isotopic signature to the BODIPY FL fluorescent tag. The two most common boron isotopes, ^{10}B and ^{11}B, exist naturally and in BODIPY FL-fatty acids (verified experimentally using standards; data not shown) in a 1:10-1:4 ratio and have a $\Delta m/z$ of 0.9964 amu. Pairs of analytes that fit this signature, eluted at the same retention time, and were specific to a single fluorescent HPLC peak were identified as specific BODIPY-lipids by comparing experimental m/z to the expected m/z of each of a range of potential products of BODIPY FL-C5, -C12, and -C16. Expected m/z was calculated from molecular formulas using the Lipid MAPS® exact mass tool at http://www.lipidmaps.org/tools/structuredrawing/masscalc.php.

Confocal Imaging

Larval zebrafish were fed both BODIPY FL-C12 and BODIPY(558/568)-C12 emulsified in 5% chicken egg yolk at 4 μg/mL for two hours at 30^{o} C as described above, and then transferred to fresh embryo media and incubated at room temperature. Live confocal imaging was

performed 6 hours after removal of larvae from the HF/HC food (Figure 4). Larvae were anesthetized with tricaine and live mounted for imaging in 3% methylcellulose under a coverslip at room temperature. Fluorescent images were acquired with a Leica TCS SP5 II confocal microscope equipped with an Argon laser, Leica 63x/1.4 oil-immersion objective, and Leica Application Suite Advanced Fluorescence 2.7.3.9723 image acquisition software. Images were adjusted for brightness and contrast using Fiji image analysis software (National Institutes of Health).

Pharmaceutical Treatments

Larval zebrafish were treated with ezetimibe using a protocol adapted from published methods which demonstrated that ezetimibe blocks dietary cholesterol uptake in larval zebrafish (65, 96): at 5 dpf larvae were immersed in a 5 μM ezetimibe (SCH58053, Santa Cruz Biotech) and 0.1% ethanol (vehicle) solution and maintained at 25.0^{o}C for 20 hours. While being fed experimental diets, larvae were treated with 10 μM ezetimibe. Following meals, larvae were returned to a 5 μM ezetimibe solution until samples were taken for lipid extraction.

A similar protocol for treatment of larval zebrafish with an ACAT inhibitor (CAY10486, N-[3-(4-hydroxyphenyl)-1-oxo-2-propenyl]-L-phenylalanine methyl ester, Cayman Chemical) was developed from a published method for ACAT inhibition in embryos (23). Beginning at 5 dpf, larvae were immersed in a 100 μM ACAT inhibitor and 0.5% DMSO (vehicle) solution and maintained at 25.0^{o}C for 20 hours. This ACAT inhibitor concentration was maintained during and after feeding, until samples were taken.

Results

A comprehensive total lipid HPLC method facilitates detection and quantitation of all classes of lipids in a single sample

In order to obtain the greatest possible depth of information from metabolic labeling with dietary fluorescent fatty acids, it was crucial to understand the lipidomic context surrounding these metabolic tracers. Lipid profiling by HPLC with various detection methods is a well-established practice (97-103) that allows for relatively high-throughput and low-cost experiments (when compared with LC-MS). However, precise identification of complex lipids resolved by HPLC using standards is often impractical, as there are thousands of possible unique phospholipid species and tens of thousands of possible triglycerides. For this reason lipid researchers often turn to MS-based lipidomics, which can provide precise identification (if high resolution, accurate mass detection methods are used) and quantitation of complex lipids, but often at the cost of limiting the number of samples and replicates that may be analyzed. Here we describe a combined HPLC-CAD and LC-MS workflow in which a lipidomic data set obtained from a short series of LC-MS experiments is used to interpret results from a large number of HPLC experiments, retaining the high-throughput/low-cost advantage of HPLC while enhancing the type and quality of data that may be obtained from HPLC lipidomics. A multistep gradient HPLC procedure for analysis of the larval zebrafish lipidome was designed to resolve the components of a mixed sample consisting of lipids of a wide range of molecular weights, degrees of polarity, and degrees of saturation. A single LC-MS/MS experiment (n = 3 biological replicates) was then performed using the chromatography component of our established HPLC method in order to identify the specific lipid contents of each analyte peak detected by HPLC-CAD/Fluorescence (Figure 1). The lipidomic data set this experiment yielded (Supplemental Table S1) could then be used to interpret the results of any HPLC experiment performed with the same instrument method. Cholesterol and most cholesterol esters were not detected by the MS

method we employed, but were detected by HPLC-CAD and identified by comparison with purchased standards (Sigma-Aldrich). The composition of each lipid peak detected by HPLC-CAD is summarized in Supplemental Table S2. Total fatty acid composition of larval zebrafish was similar in groups fed a single LF/LC or HF/HC meal, despite differences in dietary fatty acid composition. Fatty acid composition analysis of only the triglycerides shows that oleic acid is enriched 2.3-fold and linoleic acid is enriched 1.9-fold in the triglycerides of larvae fed a HF/HC meal (versus LF/LC), and that DHA is enriched 6.2-fold in larvae fed a LF/LC meal (versus LF/HC) (Supplemental Table S3). This is consistent with differences in dietary fatty acid composition, where the HF/HC diet is 35% oleic acid (vs. 14% in LF/LC) and 16.5% linoleic acid (vs. 9% in LF/LC), and the LF/LC diet is 8.6% DHA (vs. 0.5% in HF/HC). Less prevalent species enriched in the triglycerides of LF/LC-fed larvae (versus larvae fed the HF/HC meal) include 20:5, 16:1, and 20:4. No other changes in fatty acid composition greater than 1.5-fold were observed between the HF/HC and LF/LC groups in fatty acid species accounting for >0.3% of the total in triglycerides.

HPLC-CAD analysis reveals that the whole-body lipid content of larval zebrafish is enriched in a variety of triglycerides following a single HF/HC meal, while other

Figure 1 (next page). A combined HPLC-CAD and LC-MS/MS workflow for total lipid profiling of larval zebrafish. Once an HPLC method was established that resolved lipids of all classes present in larval zebrafish, the instrument was temporarily reconfigured to route sample flow to a quadrupole-Orbitrap mass spectrometer instead of the charged aerosol detector. Data obtained from a series of LC-MS/MS experiments with exact mass detection was then used to identify the components of peaks observed by HPLC-CAD/fluorescence. Through this combined workflow, peak composition data from a single LC-MS/MS experiment greatly enhances the depth of information that may be obtained from all future HPLC experiments performed using the same instrument method.

Figure 1.

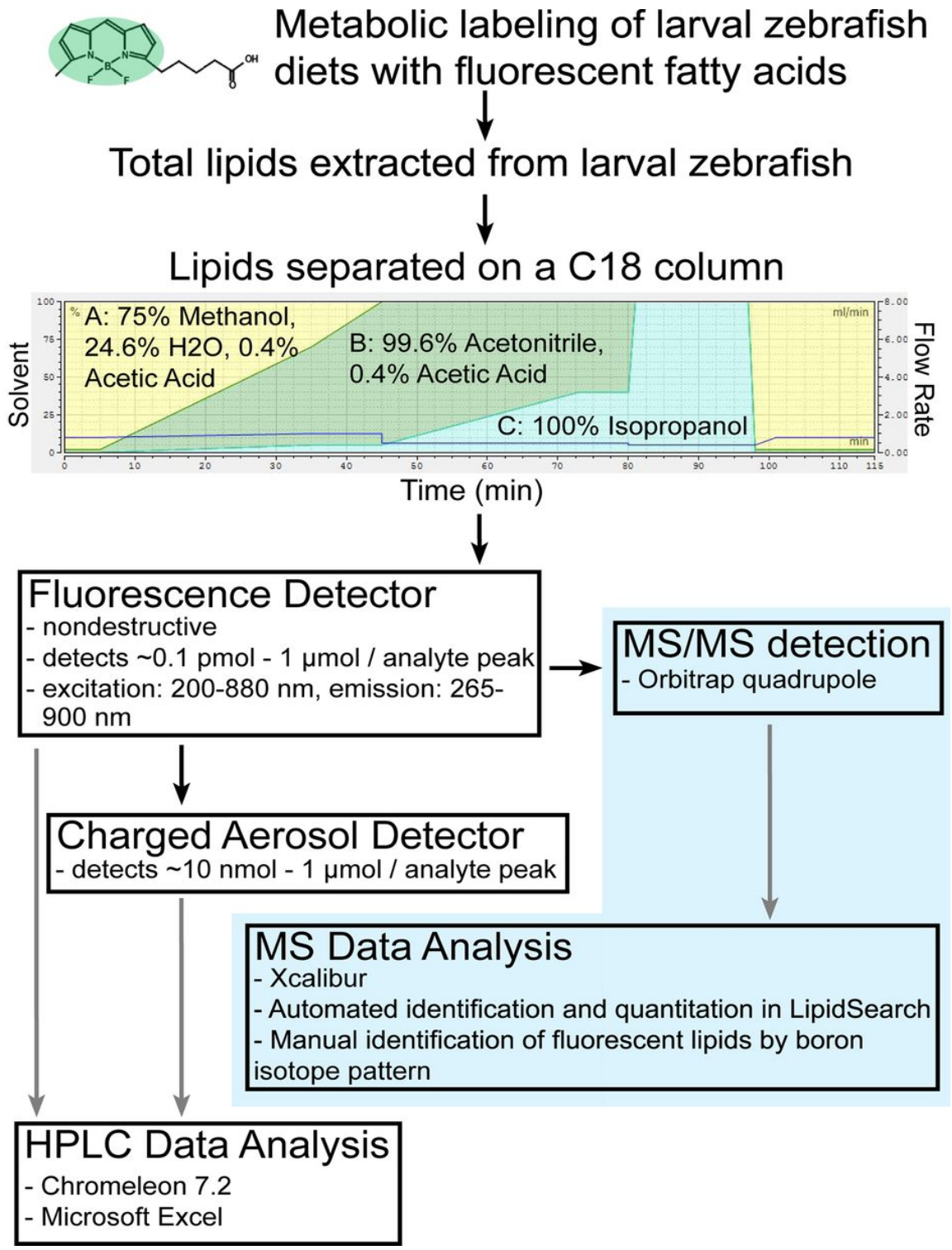
Metabolic labeling of larval zebrafish diets with fluorescent fatty acids
Total lipids extracted from larval zebrafish
Lipids separated on a C18 column
Solvent
A: 75% Methanol, 24.6% H2O, 0.4% Acetic Acid
B: 99.6% Acetonitrile, 0.4% Acetic Acid
C: 100% Isopropanol
ml/min
Flow Rate
Time (min)
Fluorescence Detector
- nondestructive
- detects ~0.1 pmol - 1 µmol / analyte peak
- excitation: 200-880 nm, emission: 265-900 nm
MS/MS detection
- Orbitrap quadrupole
Charged Aerosol Detector
- detects ~10 nmol - 1 µmol / analyte peak
MS Data Analysis
- Xcalibur
- Automated identification and quantitation in LipidSearch
- Manual identification of fluorescent lipids by boron isotope pattern
HPLC Data Analysis
- Chromeleon 7.2
- Microsoft Excel

lipid species are unchanged (Figure 2). The triglyceride content of larval zebrafish fed a HF/HC meal is increased on average 10-fold over larval zebrafish fed a LF/LC meal when calculated from the LC-MS/MS data (n = 3). A similar change in triglyceride levels, plus an increase in cholesterol ester, is observed when HPLC data is processed through the combined HPLC-CAD/LC-MS data analysis workflow (Table 1). The combined workflow is advantageous over simple quantitation of HPLC-CAD data because it allows for analysis of lipid species that were not identified by HPLC-CAD (e.g. ceramides, monoglycerides, and diglycerides), and also allows quantitation of free cholesterol and two more cholesterol ester species than what can be detected in larval zebrafish samples analyzed with MS/MS detection (Table 1, Supplemental Table S1, and Supplemental Table S2).

BODIPY-labeled fatty acids are metabolized by larval zebrafish into different arrays of complex lipids depending on fatty acid chain length

Thin-layer chromatography assays have shown that larval zebrafish fed BODIPY FL-C5, -C12, and -C16 in a HF/HC meal incorporate these fluorescent fatty acids into the three major classes of complex lipids (phospholipids, triglycerides, and cholesterol esters) in different proportions (28). Because HPLC resolves individual lipid species within each class where TLC does not, we repeated the experiments of Carten et al. (2011) in order to investigate the fluorescent lipid product profile of each of these BODIPY-fatty acids at a higher resolution. Larval zebrafish were fed BODIPY FL-fatty acids in a HF/HC meal for two hours, and total lipids were extracted after a 16-hour chase period. The products of each BODIPY FL-fatty acid were analyzed by HPLC with fluorescence detection, which revealed that carbon chain length of fluorescent saturated fatty acids influences their channeling into complex lipids: while BODIPY FL-C12 is incorporated into a wide array of nonpolar lipids and phospholipids, BODIPY FL-C16 and BODIPY FL-C5 are largely incorporated into nonpolar lipids and a smaller amount of phospholipid. A single cholesterol ester product (confirmed through the use of standards and an

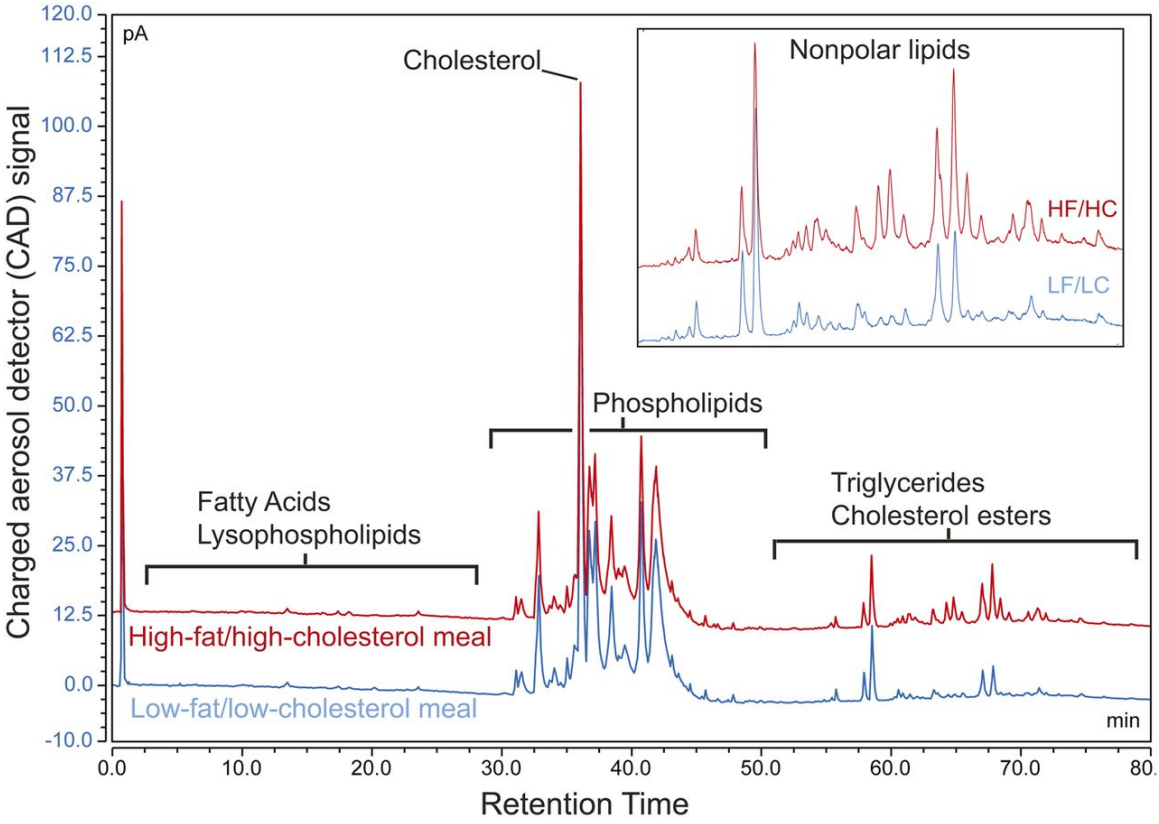

Figure 2. Multistep gradient HPLC-CAD facilitates resolution and quantitation of all classes of lipids in a single underivatized sample. Several triglyceride species are increased in larval zebrafish following a single HF/HC meal while other lipid classes remain unchanged. Similar results are obtained when lipid class distribution is quantitated directly from the mass spectrometry data set using LipidSearch, and when quantitation of HPLC-CAD analyte peaks (identified previously using LC-MS/MS) is performed in Chromeleon (Table 1). The HF/HC trace (red) is offset by 12.5 pA (picoamperes). This chromatogram represents results from 3 independent experiments.

Table 1. Lipid class composition of larval zebrafish fed low-fat/low-cholesterol (LF/LC) or high-fat/high cholesterol (HF/HC) diets; determined by LC-MS/MS, HPLC-CAD, or the combined workflow described in Figure 1.

	Mass Spectrometry		HPLC-CAD		Combined Workflow	
	Percent of total lipid[a]		Percent of total lipid		Percent of total lipid	
Class[b]	LF/LC	HF/HC	LF/LC	HF/HC	LF/LC	HF/HC
Fatty Acid	0.9 ± 0.3	0.8 ± 0.2	1.1 ± 0.8	0.6 ± 0.2	0.2 ± 0.1	0.2 ± 0.1
Phospholipid	94.3 ± 29.9	90.5 ± 30.5	62.1 ± 36.0	62.9 ± 20.8	62.9 ± 34.5	67.5 ± 18.5
Triglyceride	0.5 ± 0.1	4.8 ± 1.1	6.1 ± 3.6	12.6 ± 3.5	0.7 ± 0.3	7.4 ± 1.9
Diglyceride	0.1 ± 0.1	0.1 ± 0.0	-[c]	-[c]	0.8 ± 0.4	0.6 ± 0.2
Monoglyceride	0.2 ± 0.1	0.1 ± 0.1	-[c]	-[c]	13.3 ± 10.5	4.9 ± 2.8
LPL	0.6 ± 0.2	0.6 ± 0.2	1.4 ± 1.1	0.4 ± 0.3	1.2 ± 0.7	0.8 ± 0.3
Ceramide	0.7 ± 0.2	0.6 ± 0.2	-[c]	-[c]	0.7 ± 0.3	0.6 ± 0.2
CE	0.0 ± 0.0	0.0 ± 0.0	3.1 ± 1.2	5.4 ± 1.4	1.7 ± 0.5	2.8 ± 0.8
Cholesterol	-[c]	-[c]	26.3 ± 6.3	17.9 ± 2.4	16.9 ± 1.1	13.9 ± 1.4
Other	2.7 ± 1.0	2.6 ± 0.7	-[c]	-[c]	11.6 ± 0.9	1.4 ± 0.4

[a]Lipids are quantitated by class as a percentage of the total signal ± standard deviation (n = 3).

[b]LPL: lysophospholipid, CE: cholesterol ester

[c]Lipid class could not be identified and/or quantitated by this method.

ACAT inhibitor, data not shown) of each BODIPY FL-fatty acid was observed. No oxidation intermediates of BODIPY FL-fatty acids were found (Figure 3, Table 2).

Though resolution and quantitation of individual complex lipid products of BODIPY FL-FAs was achieved by HPLC-fluorescence, it was not practical to use standards to identify each putative fluorescent phospholipid and triglyceride peak due to the number of possibilities. MS detection identified 31 unlabeled fatty acids in larval zebrafish that could combine with BODIPY FL-FAs to form fluorescent complex lipids with the observed retention times, which gives a total of 273 possible phospholipid products and 496 possible triglyceride products of each BODIPY FL-fatty acid (assuming none are double-labeled, which is unlikely due to the low ratio of labeled to unlabeled dietary fatty acids in these experiments).

Based on retention times of purchased standards and non-fluorescent peaks identified by LC-MS/MS, we hypothesized that fluorescent peaks eluting between 15 and 45 minutes on the HPLC-Fluorescence chromatograms in Figure 3 were phospholipids and fluorescent peaks eluting between 45 and 80 minutes were nonpolar lipids (e.g., triglycerides and sterol esters). To test this hypothesis, total lipid extracts from larval zebrafish fed BODIPY FL-fatty acids in a HF/HC meal were subjected to acetone precipitation to separate polar and nonpolar fractions, each of which was analyzed by HPLC with fluorescent detection (Supplemental Figure S1). These data confirmed that the predicted class of each peak was as expected. For more precise identification of specific fluorescent complex lipids, the products of each BODIPY FL-fatty acid were also analyzed by LC-MS/MS as described above, and the unique isotopic signature of boron was used to identify putative BODIPY-lipids. Five BODIPY FL-C12 phospholipids, two BODIPY FL-C5 phospholipids, a BODIPY FL-C16 triglyceride, and the cholesterol esters of BODIPY-FL C5 and BODIPY FL-C12 were identified by this method (Supplemental Table S4). Fluorescent fatty acids are especially useful metabolic labeling reagents in the larval zebrafish model because biochemical and live imaging assays may be performed in parallel. The fluorescent lipid feeding procedures used in this study are well established as methods to investigate dietary lipid transport

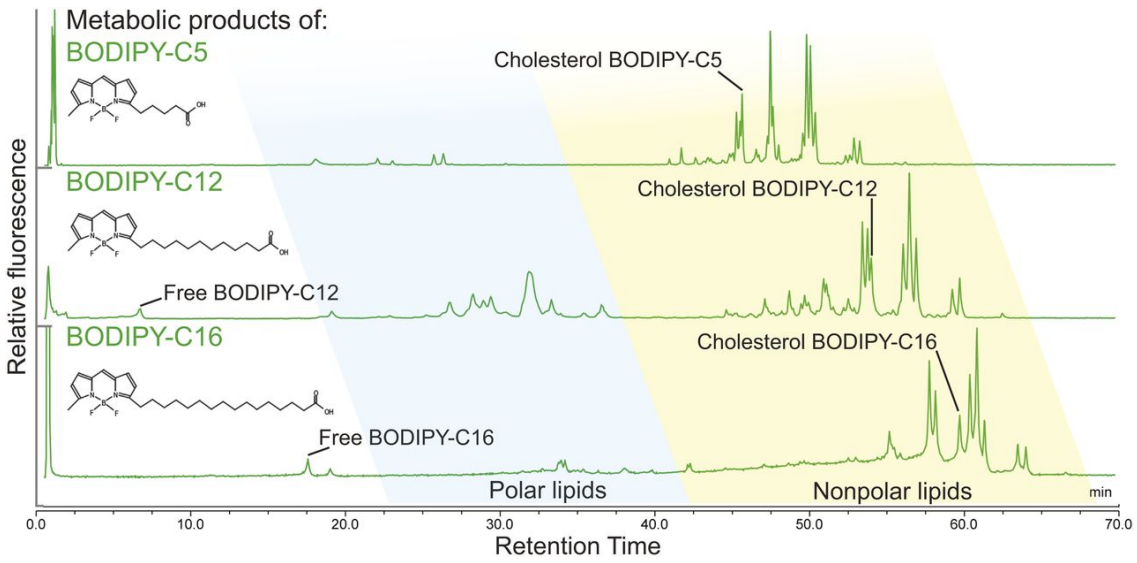

Figure 3. The chain length of BODIPY FL-labeled saturated FAs affects their incorporation into complex lipids. HPLC-fluorescence analysis resolves products of BODIPY FL-C5, -C12, and -C16 synthesized by larval zebrafish that have been given these fluorescent FAs in a HF/HC meal. Results are representative of >10 independent HPLC-fluorescence analyses of total lipid extracts taken from 6 dpf larval zebrafish sampled 16–20h postfeeding.

Table 2. Distribution of fluorescent products of BODIPY-FL fatty acids among the major lipid classes, 16 hours post-feeding.

	Fatty acid	Phospholipids	Cholesterol ester	Triglycerides	Total polar:total nonpolar lipids
BODIPY FL-C5	n/a[a]	7.5 ± 1.3	9.6 ± 0.6	82.9 ± 1.9	0.08
BODIPY FL-C12	1.5 ± 0.7	39.5 ± 1.4	11.0 ± 1.3	48.0 ± 2.0	0.67
BODIPY FL-C16	5.5 ± 1.6	5.6 ± 0.5	3.0 ± 0.5	85.9 ± 2.0	0.06

[a]Free BODIPY FL-C5 could not be quantitated in this assay as it runs in the solvent front. Fluorescent products of BODIPY FL-fatty acids fed to larval zebrafish in a HF/HC meal are quantitated by class as percentage of total fluorescence ± standard deviation (n = 3 for BODIPY FL-C5, n = 6 for BODIPY FL-C12 and -C16).

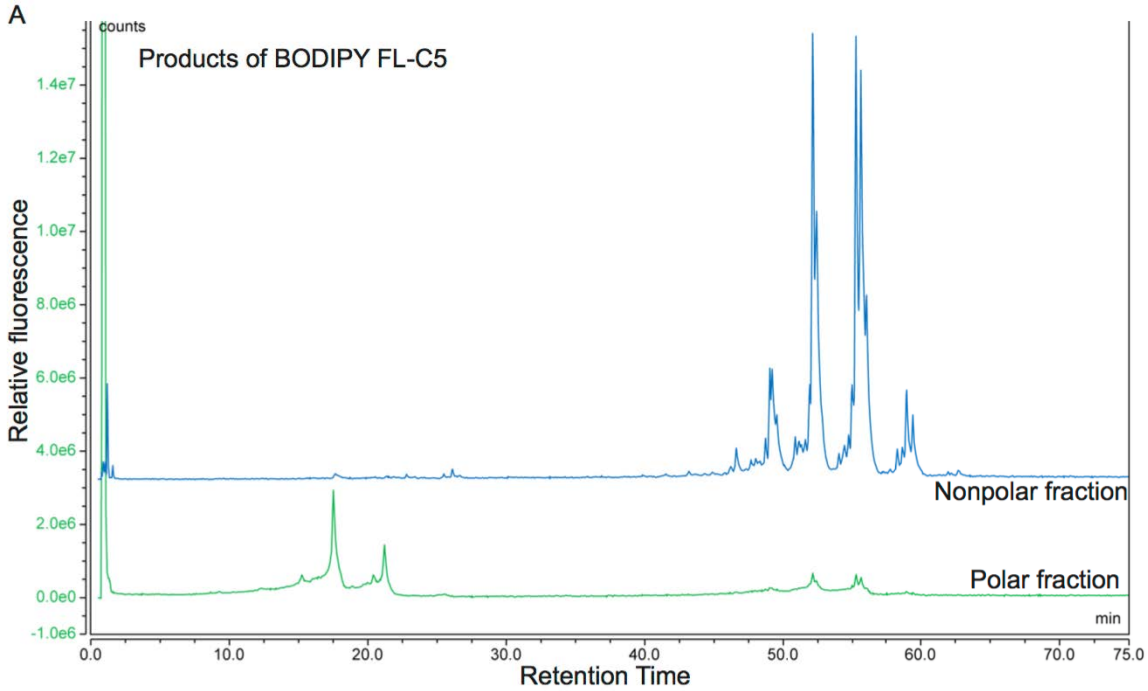

Supplemental Figure S1

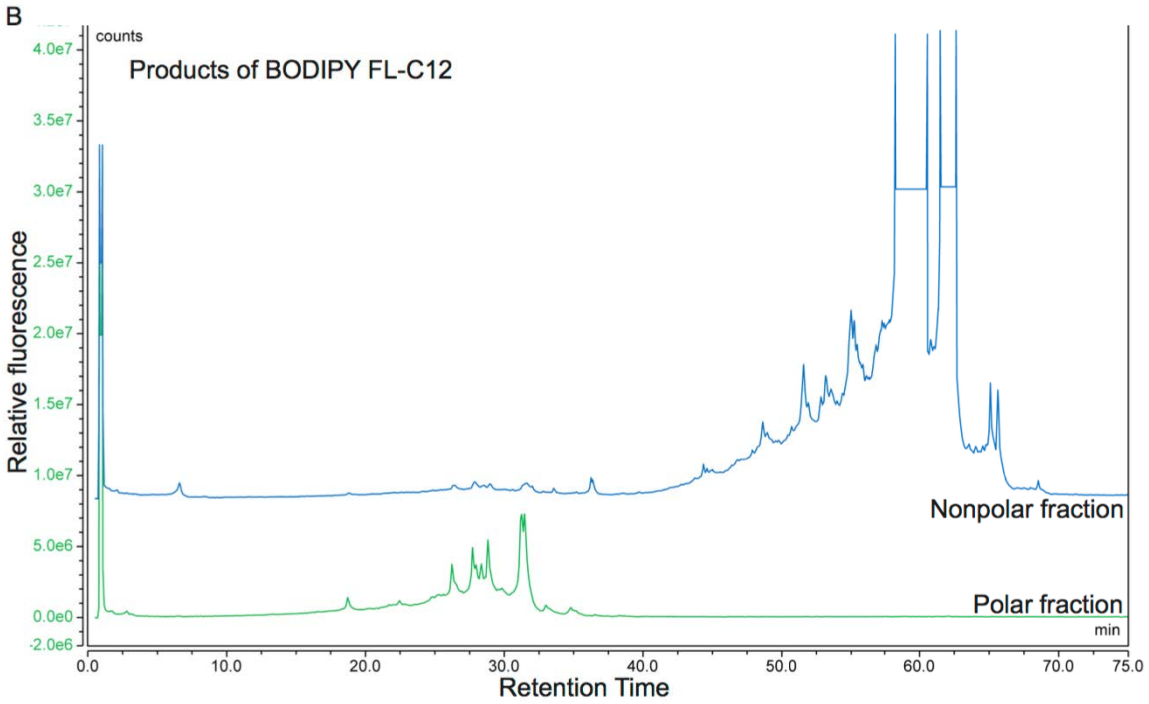

Supplemental Figure S1, continued

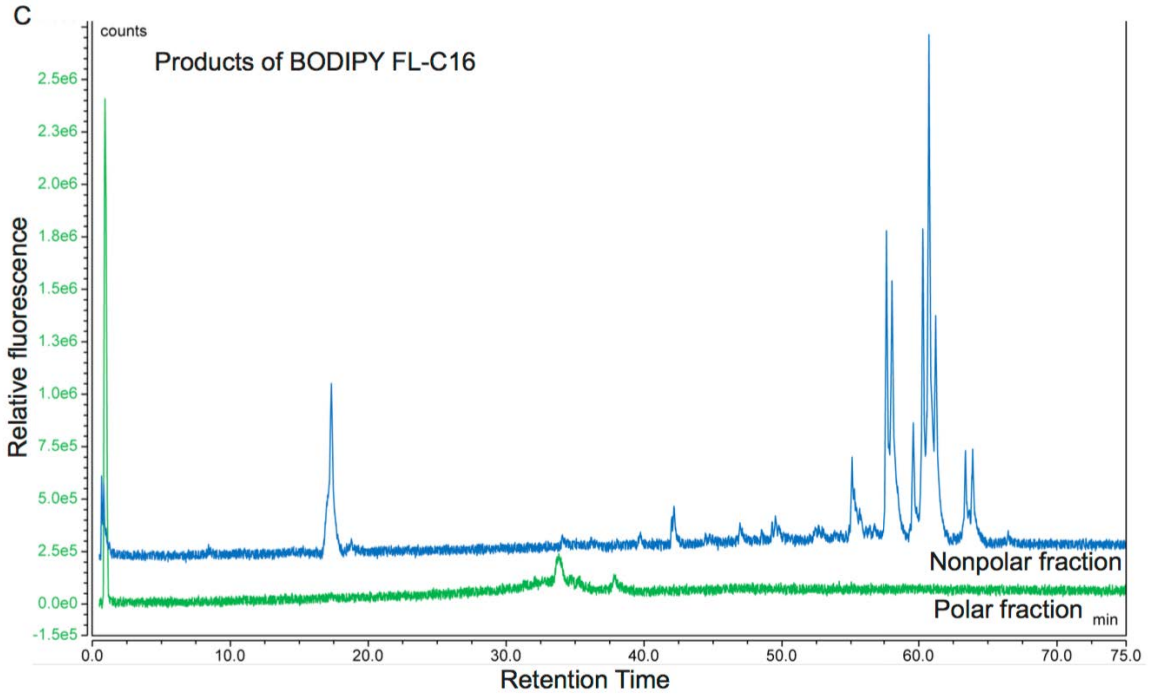

Supplemental Figure S1. Fluorescent products of BODIPY FL-fatty acids were identified as polar or nonpolar lipids by acetone precipitation followed by HPLC.

A) Products of BODIPY FL-C5 running at 15-22.5 minutes are enriched in the polar fraction. Products running between 45 and 65 min are enriched in the nonpolar fraction. B) Products of BODIPY FL-C12 running before 35 minutes are enriched in the polar fraction, and products running after 35 min are enriched in the nonpolar fraction. C) Two polar products of BODIPY FL-C16 elute between 30 and 40 min. All other products are nonpolar. Results on each chromatogram are representative of 3 samples per group.

and deposition in tissues, cells, and subcellular structures in the larval zebrafish as well as other models (5, 88, 104). At 4-8 hours from the start of feeding BODIPY FL-C5 in a HF/HC meal, fluorescence is seen by live confocal microscopy in a variety of subcellular structures and membranes in the larval zebrafish liver, pancreas, and intestinal enterocytes, while BODIPY FL-C16-derived fluorescence in these organs is concentrated in lipid droplets (28). Based on this previously published imaging data, we expected to detect a larger amount of phospholipid products of BODIPY FL-C5 when compared with BODIPY FL-C16. This hypothesis was supported by HPLC-Fluorescence lipid profiles, in which the products of BODIPY FL-C5 in samples taken 8 hours post-feeding are 6.6 ± 1.3% phospholipid (n = 13) and products of BODIPY FL-C16 in samples taken 6-10 hours post-feeding are 2.1 ± 0.5% phospholipid (n = 4, p = 0.000012; Student's T-test).

As all variants of the BODIPY fluorophore are large compared with the labeled fatty acids, we hypothesized that the metabolism of BODIPY-fatty acids would not exactly replicate that of their unlabeled counterparts but would resemble the metabolism of larger fatty acids. Specifically, as the BODIPY FL fluorophore is approximately the length of a 4-carbon chain, we tested the hypothesis that BODIPY FL-C12 and ^{3}H-palmitate would yield similar product profiles. BODIPY FL-C12 and ^{3}H-palmitate were fed to larval zebrafish in equimolar amounts in a HF/HC meal, and products were analyzed 18 hours post-feeding by HPLC. Following fluorescent detection, HPLC eluent was collected in one-minute fractions which were assayed for radioactivity so that the metabolism of both radioactive and fluorescently labeled fatty acids could be characterized simultaneously. The complex lipid product profiles of BODIPY FL-C12 and ^{3}H-palmitate, while not identical, contain similarly high ratios of labeled phospholipid to labeled nonpolar lipid when compared with the products of BODIPY FL-C5 and BODIPY FL-C16 (Tables 2,3). Full product profiles of BODIPY FL-C12 and ^{3}H-palmitate present in larval zebrafish 18 hours post-feeding are shown in Supplemental Figure S2.

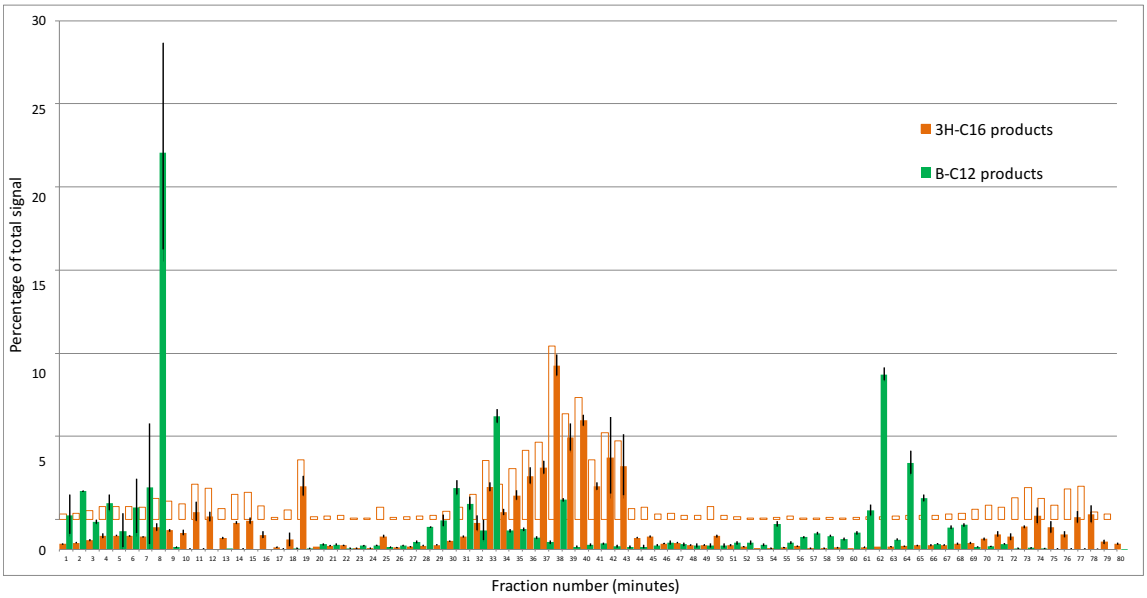

Supplemental Figure S2. BODIPY FL-C12 and ^{3}H-C16 form similar product arrays when fed to larval zebrafish. Larval zebrafish were fed equimolar amounts of BODIPY FL-C12 and palmitic acid in a HF/HC meal, and then sampled for lipid extraction 18 hours post-feeding (n = 4). HPLC analysis of complex lipid products is summarized above. Blue bars represent the percentage of total radioactive signal present in each one-minute fraction (products of ^{3}H-C16), and red bars represent the percentage of total area under the curve of the fluorescent chromatogram present in each one-minute segment (products of BODIPY FL-C12). 8 min = free BODIPY FL-C12, 19 min = free ^{3}H-C16, 1-7 min and 20-40 min = fluorescent polar lipids, 20-50 min = radioactive polar lipids, 41-61 min and 63-80 min = fluorescent triglycerides, 51-77 min and 79-80 min = radioactive triglycerides, 62 min = Cholesterol BODIPY FL-C12, 78 min = Cholesterol ^{3}H-C16. Radioactive lipids eluting before 19 minutes could not be identified as lysophospholipids or fatty acid oxidation intermediates within the scope of this study, and were not included in the data analysis.

Table 3. Distribution of labeled products of BODIPY FL-C12 and ^{3}H-C16 fatty acids among the major lipid classes, 18 hours post-feeding[a].

	Fatty acid	Polar lipids	Cholesterol ester	Triglycerides	Total polar:total nonpolar lipids
BODIPY FL-C12	22.5 ± 6.2[b]	43.4 ± 7.4	9.9 ± 0.4	24.2 ± 1.3	1.27
^{3}H-C16	4.3 ± 0.7	76.8 ± 4.0	2.4 ± 0.6	16.5 ± 2.9	4.06

[a]Larvae were fed and incubated post-feeding at room temperature. For all other experiments, feeding was conducted at 30°C.
[b]Products of labeled fatty acids fed to larval zebrafish in a HF/HC meal are quantitated by class as percentage of total signal ± standard deviation (n = 4).

Fluorescent lipid analogs of similar chain lengths and different fluorescent tags are metabolized by larval zebrafish into different arrays of complex lipid products

As BODIPY FL-C12 is especially physiologically relevant due to its similarity to palmitate and forms a wider array of polar and nonpolar products than the other two BODIPY FL-fatty acids examined, we focused on this chain length for the remaining experiments, which addressed the effects of dietary context and variants of the BODIPY fluorophore on the metabolism of fluorescent fatty acids. In addition to BODIPY FL, lipids labeled with many other variants of BODIPY are commonly used in live fluorescent microscopy. As BODIPY-labeled fatty acids are metabolizable, the fluorescent signal in live imaging experiments is derived not only from the BODIPY-fatty acid but also from its metabolic products. To better understand how differences in BODIPY fluorophores impact the metabolism of labeled fatty acids and possibly the subcellular localization of their products, we set out to explore the effect of varying fluorophore chemistry with constant fatty acid chain length.

BODIPY(558/568)-C12 fluoresces red and is therefore especially useful in fluorescent microscopy experiments involving cells or animals expressing GFP. This red fluorescent tag, at 272 g/mol, is substantially larger than BODIPY FL (218 g/mol) and carries an additional 5-member thienyl ring structure (Figure 4 inset). Previous work comparing the metabolism of the

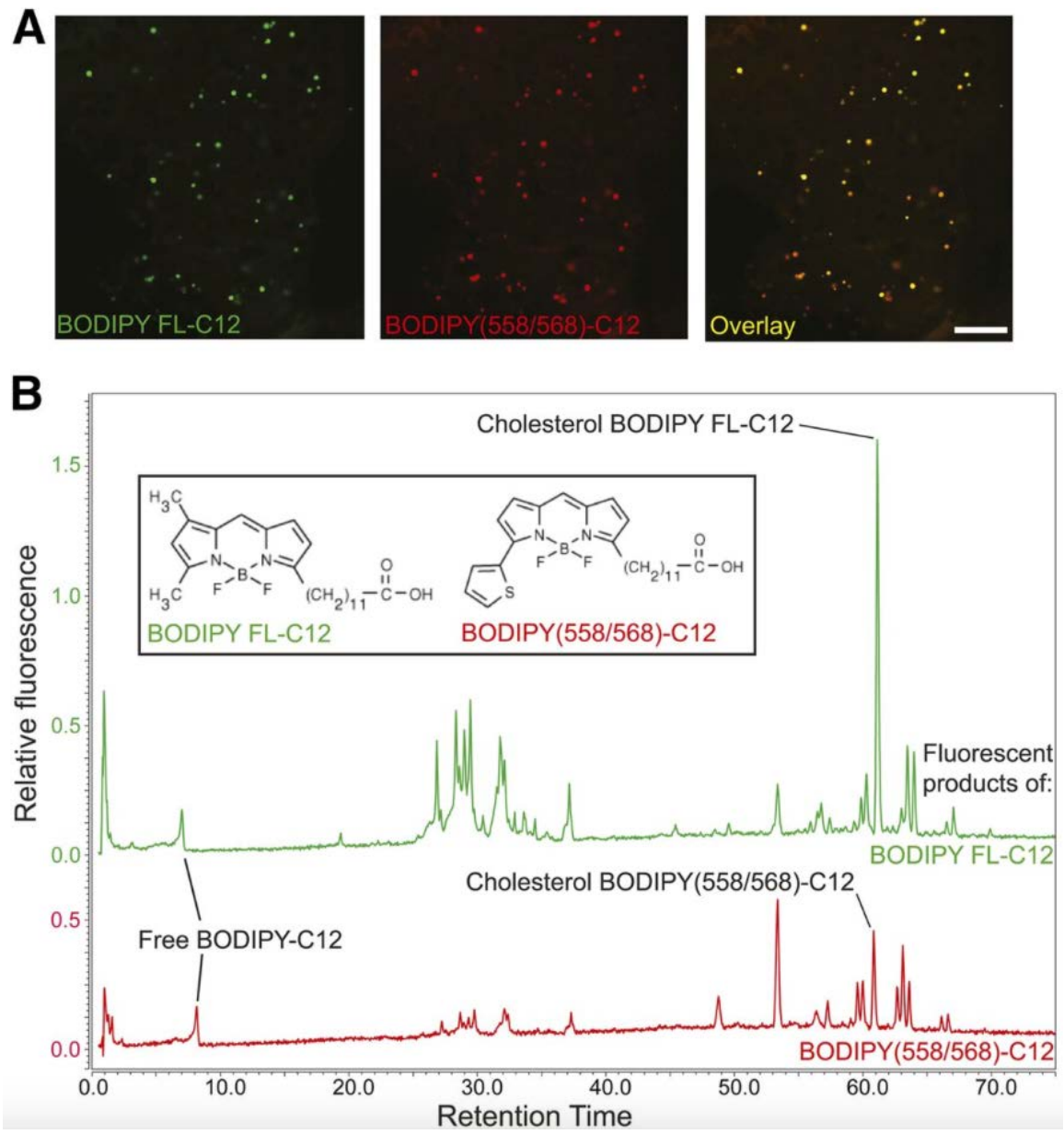

Figure 4. BODIPY FL-C12 and BODIPY(558/568)-C12 are processed similarly to each other when fed to larval zebrafish in a HF/HC meal. A) When BODIPY FL-C12 and BODIPY(558/568)-C12 are fed simultaneously in a HF/HC meal, they label the same subcellular structures in the larval zebrafish liver 8 hours post-feeding. Scale bar: 25 μm. B) Similar arrays of phospholipid, triglyceride, and cholesterol ester products of BODIPY FL-C12 and BODIPY(558/568)-C12 are observed 8 hours post-feeding, though the products form in different proportions to each other. Results are representative of 6 samples per group.

red and green BODIPY-C12 variants by mouse primary hepatocytes showed by qualitative TLC assays that both of these fluorescent fatty acids are incorporated into both nonpolar complex lipids and phospholipids (91). Because the BODIPY tag accounts for over half of the molecular weight and over 25% of the length of the BODIPY-C12 molecule, we hypothesized that structural differences between BODIPY variants would correlate with differences in the metabolism of BODIPY-lipids that could be quantitated by HPLC-fluorescence.

To test this hypothesis, a mixture of BODIPY FL-C12 and BODIPY(558/568)-C12 in a HF/HC meal was fed to larval zebrafish, which were imaged by live confocal microscopy 8 hours post-feeding. Red and green fluorescence, derived from the products of both BODIPY-C12 variants, appear in the same subcellular structures in the larval zebrafish liver (Figure 4A). Additionally, similar arrays of complex lipid products are observed when each of these fluorescent fatty acids is fed individually (also in a HF/HC meal) and HPLC-Fluorescence is performed on samples taken 8 hours post-feeding (Figure 4B). However, the relative amounts of each BODIPY-C12 product vary depending on the type of BODIPY tag: BODIPY FL-C12 is more readily metabolized into complex lipid products than BODIPY(558/568)-C12, and is incorporated mostly into polar lipids, while BODIPY(558/568)-C12 is incorporated mostly into triglycerides (Table 4).

Table 4. BODIPY FL-C12 and BODIPY(558/568)-C12 are incorporated into similar products, but in different proportions.

	Fatty acid	Polar lipids	Cholesterol ester	Triglycerides
BODIPY FL-C12	2.3 ± 0.1[a]	59.7 ± 0.8	14.2 ± 1.5	23.7 ± 0.8
BODIPY(558/568)-C12	6.6 ± 0.2	23.8 ± 1.0	11.9 ± 1.4	60.0 ± 0.8

[a]Fluorescent products of BODIPY FL-fatty acids fed to larval zebrafish in a HF/HC meal and analyzed 8h post-feeding are quantitated by class as percentage of total fluorescence ± standard deviation (n = 2).

To further examine the effect of BODIPY variant on BODIPY-fatty acid partitioning in the larval zebrafish, we carried out similar feeding and HPLC-Fluorescence experiments using the fluorescent fatty acid TopFluor®-C11. TopFluor is a green variant of BODIPY that carries two additional methyl groups and is bonded to its lipid conjugate at carbon 1 of its central ring, forming a T-shaped molecule in contrast with the more linear BODIPY FL-fatty acids (Figure 5 inset). We hypothesized that though the fluorophores are chemically similar, the position at which the labeled lipid is attached may result in variations in metabolism. When fed to larval zebrafish in a HF/HC meal, TopFluor-C11 is processed into an array of products similar in class to the products of BODIPY FL-C12, though the specific fluorescent HPLC peaks that appear are different (compare Figures 3 and 5).

Fluorescent lipid analogs of similar chain lengths are metabolized by larval zebrafish into different arrays of complex lipid products when dietary lipid content is varied

We then set out to explore the effect of dietary lipid content on fluorescent lipid metabolism, again using BODIPY FL-C12, the most widely metabolized BODIPY FL-fatty acid. LF/LC and low-fat/high-cholesterol (LF/HC) diets were investigated as BODIPY-lipid carriers. BODIPY FL-C12 fed in a LF/LC or LF/HC meal is used to make an array of complex lipid products similar to those synthesized when this fluorescent fatty acid is fed in a high-fat/cholesterol meal, but in different proportions (Figure 6 [upper trace], Table 5). (Chromatograms in Figure 6 show the fluorescent lipid products of BODIPY FL-C12 and BODIPY (558/568)-C12 delivered to larval zebrafish in LF/LC meals. Results are similar for these fluorescent fatty acids fed in LF/HC meals [chromatograms not shown; quantitative data is summarized in Table 5].) Specifically, similar amounts of fluorescent phospholipid are synthesized when BODIPY FL-C12 is fed in all three diets, but with the HF/HC diet less fluorescent cholesterol ester (HF/HC-fed larvae: CE = 11.0 ± 1.3 % of total) and more fluorescent

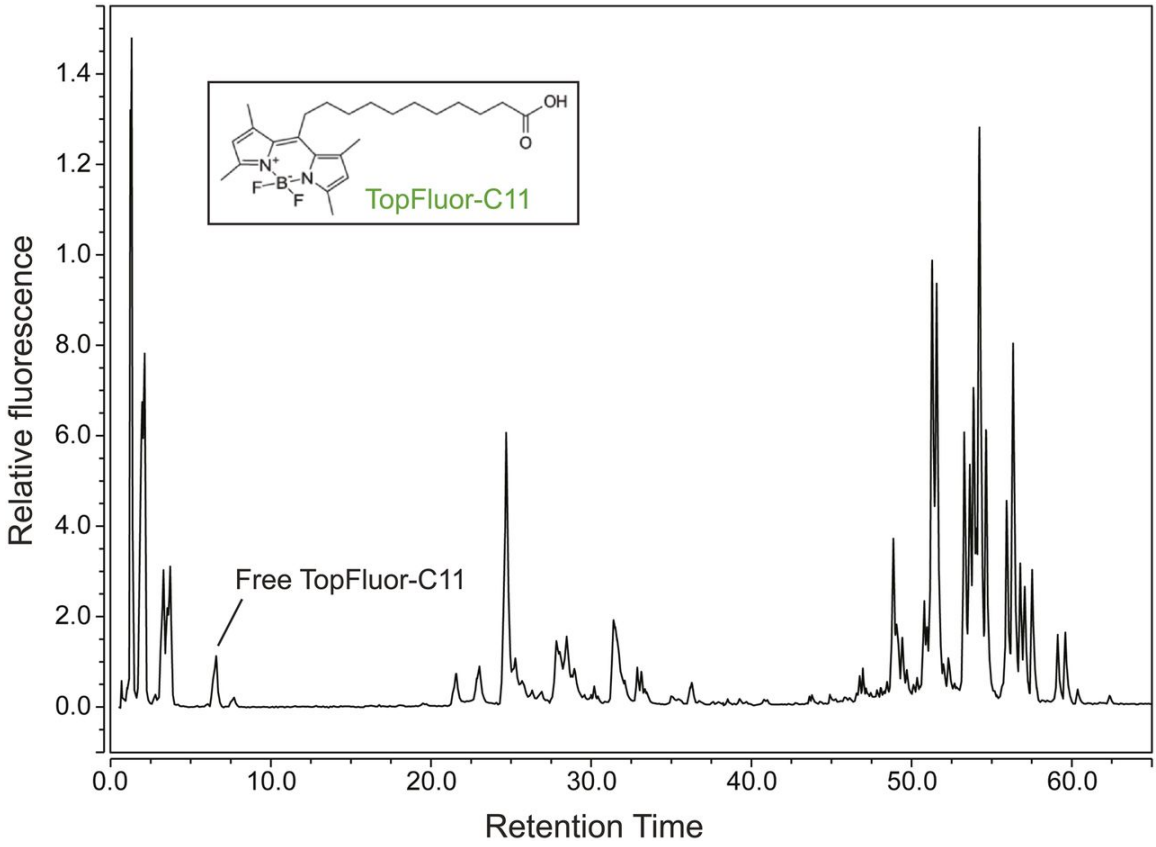

Figure 5. HPLC-Fluorescence product profile of the BODIPY-lipid TopFluor-C11.

Larval zebrafish synthesize a similar array of polar and nonpolar lipids from BODIPY FL-C12 (Figures 3 and 6) and TopFluor-C11 when these fatty acid analogs are delivered in a HF/HC meal. Products of TopFluor-C11 20 hours post-feeding are 1.6 ± 0.1% free TopFluor-C11, 22.1 ± 1.7% polar lipids, and 76.0 ± 1.5% nonpolar lipids (n = 3). Unlike BODIPY FL-C12, some oxidation intermediates of TopFluor-C11 (eluting before 5 min) may be present. No cholesterol ester of TopFluor-C11 was identified.

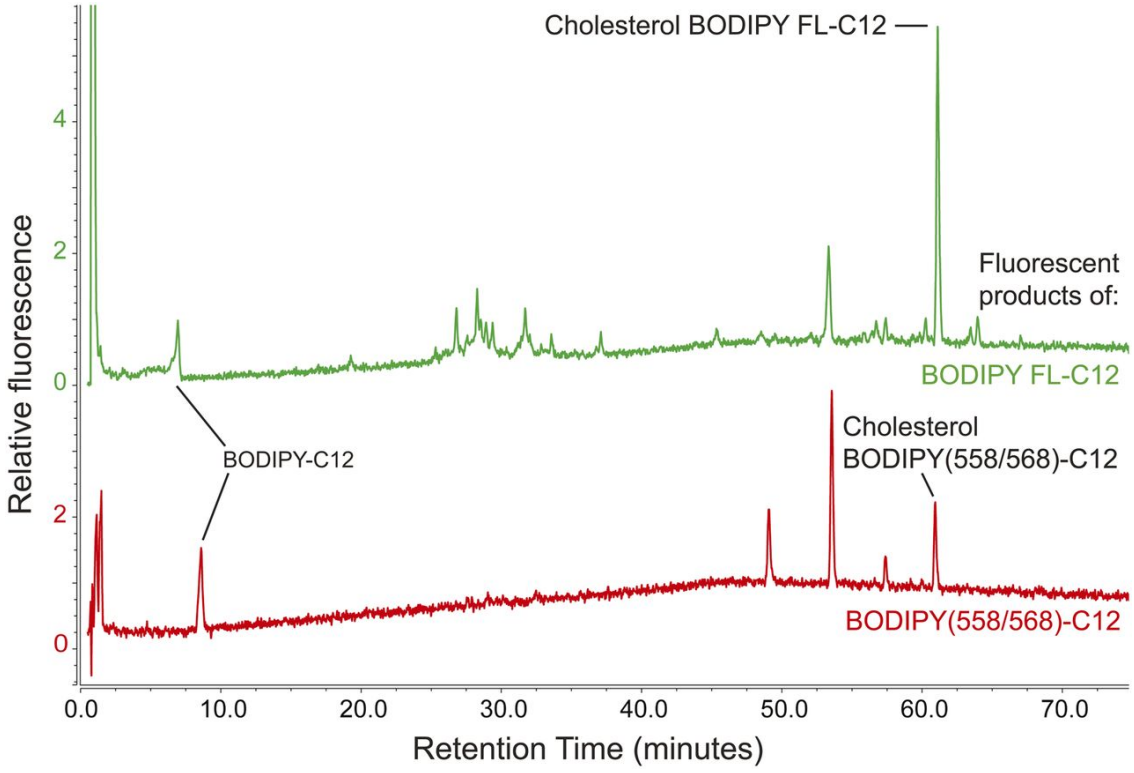

Figure 6. The array of complex lipid products formed when BODIPY-C12 is fed to larval zebrafish in a LF/LC diet varies depending on the type of BODIPY label. BODIPY FL-C12 fed in a LF/LC meal is used to make an array of polar and nonpolar lipid products similar to those synthesized when this fluorescent fatty acid is fed in a HF/HC meal (Figure 4), but in different proportions. In contrast, BODIPY(558/568)-C12 is no longer incorporated into a detectable amount of phospholipid when delivered in a LF/LC diet. Results are representative of 5 samples per group.

Table 5. BODIPY-lipids with similar fatty acid chain lengths are metabolized differently depending on the BODIPY variant, BODIPY-lipid class, and cholesterol content of the diet.

	Products of BODIPY-Lipid Fed in LF/LC Diet				Products of BODIPY-Lipid Fed in LF/HC Diet			
BODIPY-Lipid	%FA[a]	%PL	%TG	%CE	%FA	%PL	%TG	%CE
BODIPY FL-C12	no signal	40.1 ± 5.2*	16.9 ± 1.7	42.9 ± 3.6*	no signal	29.3 ± 0.2*	19.5 ± 2.2	51.2 ± 2.0*
BODIPY(558/568) -C12	15.8 ± 3.0	no signal	52.5 ± 1.2	31.7 ± 3.0	45.9 ± 17.2	no signal	34.1 ± 11.8	20.0 ± 8.9
Cholesterol BODIPY FL-C12	no signal[b]	27.2 ± 0.6[b]	16.8 ± 9.9[b]	56.0 ± 10.5[b]	no signal	30.0 ± 7.7	26.2 ± 7.3	43.7 ± 7.6
Cholesterol BODIPY(576/589) -C11	no signal[b]	no signal[b]	no signal[b]	no signal[b]	no signal	no signal	58.9 ± 3.8	41.1 ± 3.8

[a]Fluorescent products of BODIPY-lipids fed to larval zebrafish in a HF/HC meal are quantitated by class as percentage of total fluorescence ± standard deviation.
[b]n = 2. For all other groups, n = 3.
*$p<0.05$ when LF/LC and LF/HC groups are compared by Student's t-test.

triglyceride is made when compared with the LF/LC (CE = 42.9 ± 3.6 % of total) and LF/HC meals (CE = 51.2 ± 2.0 % of total) (Tables 4 and 5). We hypothesize that the larger amount of fatty acid in the HF/HC diet generally increases triglyceride synthesis and therefore causes more fluorescent fatty acid to be channeled into triglycerides when compared with the LF/LC and LF/HC diets. Addition of cholesterol to a low-fat meal also correlates with increased cholesterol ester synthesis from BODIPY FL-C12, at the expense of incorporation into phospholipid (Table 5, $p<0.05$).

We then sought to determine whether high dietary cholesterol had a similar effect on the metabolism of the red fluorescent fatty acid BODIPY(558/568)-C12. BODIPY(558/568)-C12 contributes fluorescence to all four lipid classes that were measured when delivered in a HF/HC meal (Table 4), but is no longer metabolized into a detectable amount of phospholipid when delivered in a LF/LC or LF/HC meal (Table 5). No significant differences were observed between the fluorescent product profiles of BODIPY(558/568)-C12 delivered in a LF/LC or LF/HC diet

(Table 5). In general, BODIPY(558/568)-C12 appears to be metabolized into complex lipid products to a lesser extent than BODIPY FL-C12.

Metabolism of BODIPY-cholesterol esters by larval zebrafish is responsive to the cholesterol content of the diet and the BODIPY variant

Stoletov *et al* (2009) established the larval zebrafish as a model for hypercholesterolemia in which they observed fluorescent punctae in blood vessels of larval zebrafish fed a red fluorescent cholesterol ester analog (cholesterol BODIPY(576/589)-C11) for several days in a high-cholesterol diet (83). The chemical composition of BODIPY-lipids labeling these punctae, however, was not known. As the fluorescent label of cholesterol BODIPY(576/589)-C11 is located on the acyl chain, we hypothesized that the fluorescent acyl chain would be cleaved from the cholesterol molecule in the intestine by luminal lipases, and that it would subsequently be metabolized like a BODIPY-fatty acid. To test this hypothesis and gain a better understanding of the larval zebrafish as a model of nascent hypercholesterolemia, we repeated the experiments of Stoletov *et al* with HPLC-CAD/Fluorescence analysis, with the addition of larval zebrafish fed cholesterol BODIPY FL-C12 for comparison. Each BODIPY-cholesterol ester was added to LF/LC or LF/HC food, and total lipids were extracted from larval zebrafish after three days of feeding. No fluorescent products of BODIPY(576/589)-C11 were recovered from larval zebrafish fed this fluorescent lipid in the LF/LC diet, suggesting that cholesterol BODIPY(576/589)-C11 is excreted without being digested or absorbed (Table 5, Supplemental Figure S3A). A separate series of HPLC-Fluorescence experiments confirmed that cholesterol BODIPY(576/589)-C11 was present in the food given to this experimental group, and in larvae that still had visible food particles in their intestines (data not shown). When cholesterol BODIPY(576/589)-C11 was delivered in a LF/HC diet, however, fluorescent triglycerides and cholesterol BODIPY(576/589)-C11 were detected. In contrast, fluorescence derived from cholesterol BODIPY FL-C12 delivered in a LF/LC or LF/HC meal appeared in an array of products similar to those produced by feeding

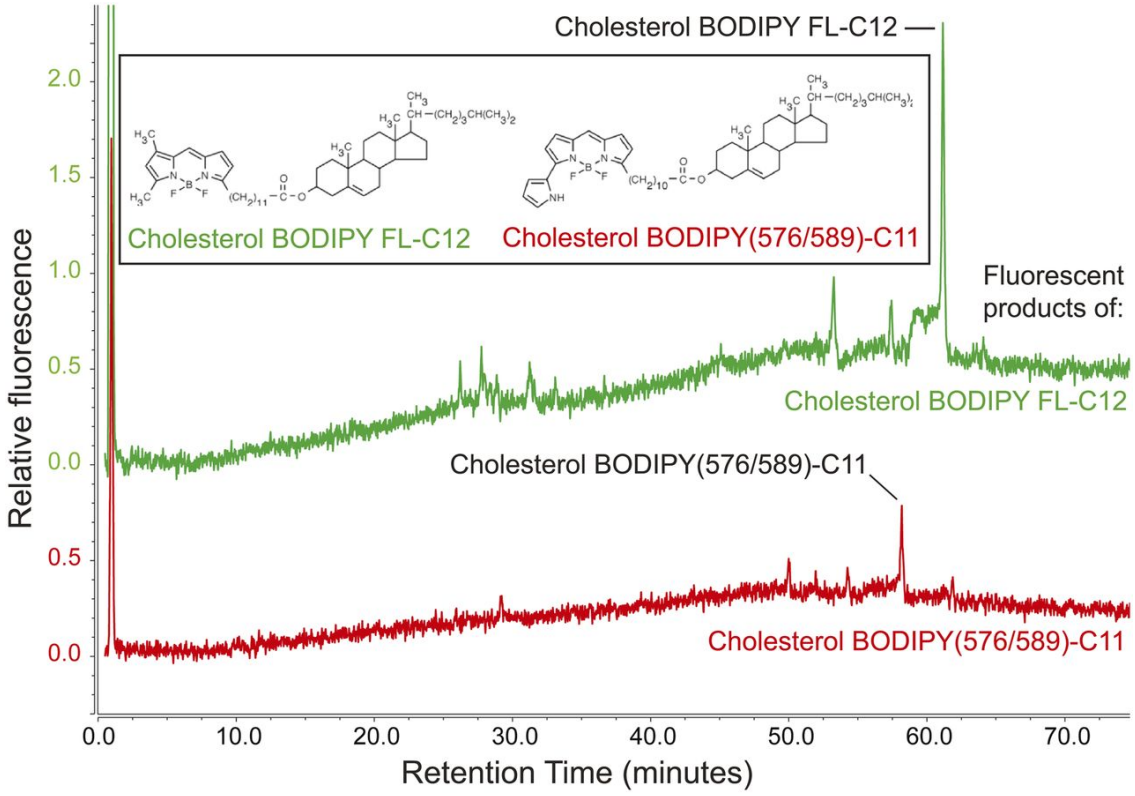

Figure 7. When the fluorescent CE cholesterol BODIPY FL-C12 is fed to larval zebrafish in a LF/HC diet, fluorescent phospholipid, triglyceride, and cholesterol ester products are observed. Cholesterol BODIPY(576/589)-C11 yields fluorescent triglyceride (Supplemental Figure S3B) and cholesterol ester products when delivered in a LF/HC diet. Results are representative of 4 samples per group.

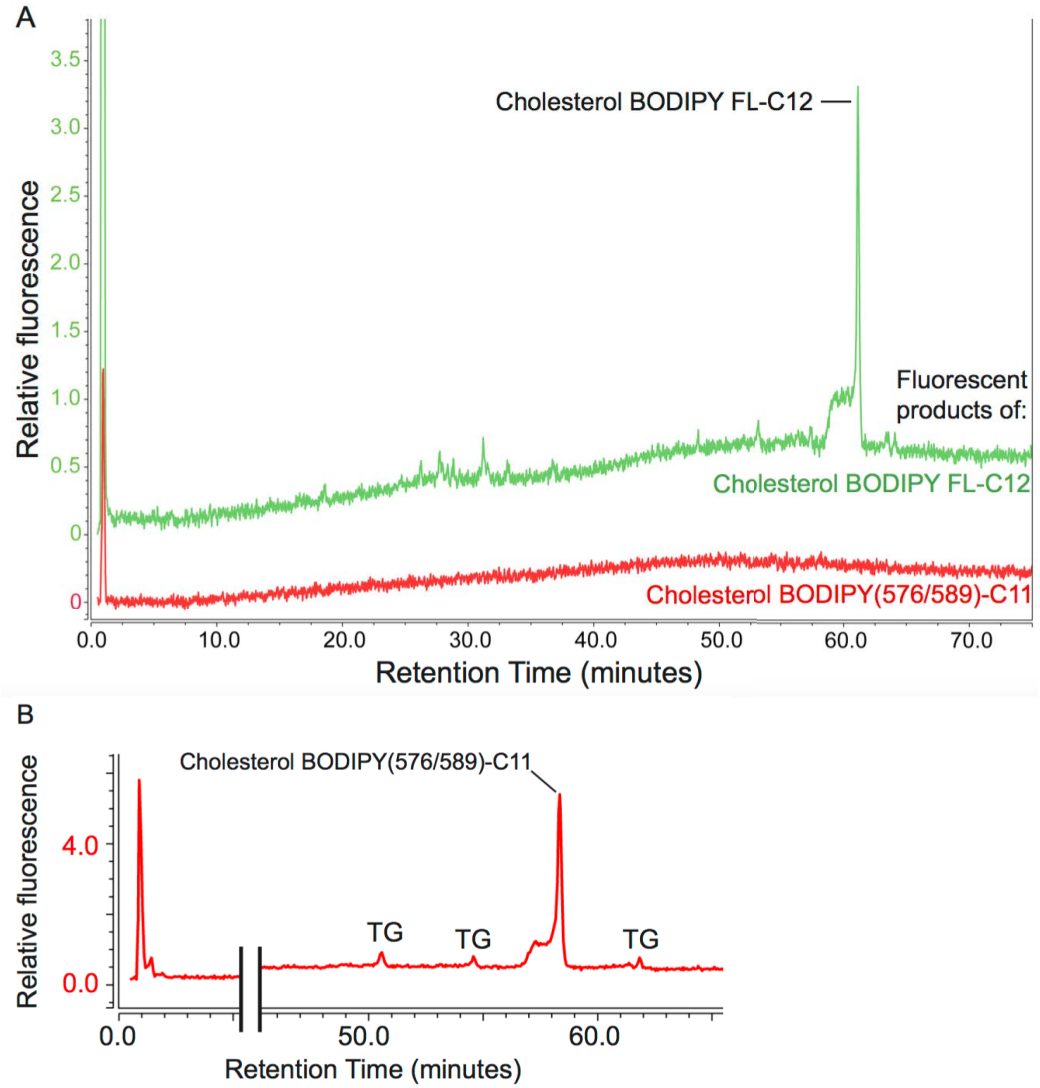

Supplemental Figure S3. Dietary cholesterol is required for metabolism of red BODIPY-labeled CE. A) When cholesterol BODIPY FL-C12 is fed to larval zebrafish in a LF/LC diet, fluorescent cholesterol ester, phospholipid, and triglyceride products are observed. Cholesterol BODIPY(576/589)-C11 yields no fluorescent products when fed in a LF/LC diet. Results are representative of 4 samples per group. B) Cholesterol BODIPY(576/589)-C11 yields a cholesterol ester and three triglyceride products when fed in a LF/HC diet. This sample from the experiment depicted in Figure 7 was overloaded (for the cholesterol ester) in order to allow visualization and quantitation of the fluorescent triglycerides.

the fatty acid BODIPY FL-C12 (Figure 7, Supplemental Figure S3, Table 5). These results suggest that fluorescent lipid punctae observed in larval zebrafish blood vessels may be labeled by a mixture of fluorescent triglycerides and cholesterol esters, and that cholesterol BODIPY FL-C12 is more readily metabolized by larval zebrafish than its red counterpart cholesterol BODIPY(576/589)-C11.

Incorporation of dietary BODIPY-labeled fatty acid analogs into cholesterol esters is responsive to the availability of dietary cholesterol for uptake by enterocytes

To further investigate the role of cholesterol in regulating the metabolism of dietary fatty acids, we sought to understand the effect of the metabolic availability of dietary cholesterol on the partitioning of dietary fluorescent fatty acids among complex lipid classes. Using two pharmaceutical inhibitors of cholesterol absorption and metabolism, we set out to explore the degree to which we could track cholesterol metabolism and its influence on dietary fatty acid partitioning by monitoring fluorescent cholesterol ester synthesis. Ezetimibe is an inhibitor of dietary cholesterol absorption by enterocytes that acts by interfering with the *npc1l1* cholesterol uptake pathway. It has been shown to decrease absorption of dietary radioactive cholesterol or fluorescent cholesterol analogs by 70-80% in humans, other mammals, and larval zebrafish (41, 46, 48, 105). 4-hydroxycinnamic acid (L-phenylalanine methyl ester) amide (CAY10486, Cayman Chemical) is an ACAT inhibitor that has been shown to reduce cholesterol ester synthesis by 70% in mammalian cell culture and by 40% in 3 dpf larval zebrafish (23, 106). We hypothesized that because a high-cholesterol diet increased cholesterol ester synthesis from dietary fluorescent fatty acids, limiting cholesterol absorption would have the opposite effect. Treatment of larval zebrafish with ezetimibe or an ACAT inhibitor before, during, and after a HF/HC meal containing BODIPY-labeled fatty acids resulted in a statistically significant decrease in fluorescent cholesterol ester synthesis (Table 6). The respective decreases in cholesterol ester synthesis resulting from treatment with ezetimibe and the ACAT inhibitor were

Table 6. Cholesterol ester synthesis from dietary fatty acids is decreased by blocking dietary cholesterol absorption.

	5 μM Ezetimibe		100 μM ACAT Inhibitor	
BODIPY-fatty acid	Cholesterol ester (treated:control) [a]	p-value	Cholesterol ester (treated:control) [a]	p-value
BODIPY FL-C5	0.73 ± 0.08	0.02*	0.64 ± 0.07	0.005*
BODIPY FL-C12	0.52 ± 0.16	0.004**	0.44 ± 0.05	0.0007*
BODIPY(558/568)-C12	0.35 ± 0.02	0.002*	0.61 ± 0.12	0.018*
BODIPY FL-C16	0.25 ± 0.10	0.0003**	0.19 ± 0.03	0.00005*

[a]Fold changes are given as the treated:control group ratio of the average CE peak area per larval equivalent in samples taken 18 hours post-feeding, ± standard deviation. All sample groups pass Levene's test for equal variance.

*Student's t-test, unpaired, equal variance, n = 3.

**Nested ANOVA, df = 11 (2 experiments; 2-3 technical replicates per group per experiment).

within one standard deviation of each other in experiments with both BODIPY FL-C12 and BODIPY FL-C16. Neither ezetimibe nor the ACAT inhibitor altered the total cholesterol content of larval zebrafish in a 48-hour drug treatment period with a single HF/HC meal (Supplemental Figure S4B). Changes in cholesterol ester synthesis from fluorescent dietary fatty acids observed in these experiments were determined by dissection to take place in the intestine (Figure 8 and Supplemental Figure S5), suggesting that cholesterol ester synthesis from newly absorbed dietary fatty acids depends primarily on availability of newly absorbed or synthesized cholesterol.

Discussion

Mass spectrometric detection and identification of lipids is an increasingly prevalent approach to lipidomics that provides a wealth of highly detailed information per experimental sample. However, when compared with other biochemical techniques, MS is expensive and time-consuming, which can unnecessarily limit the scope of lipidomic studies. Our combined HPLC-CAD/LC-MS workflow leverages the strengths of both MS and CAD lipidomics by enhancing the depth of information that may be obtained from HPLC-CAD experiments with a lower cost per sample.

The first published metabolic assays using BODIPY FL-C12 showed that in mammalian cell culture this fluorescent fatty acid is incorporated into diglycerides, triglycerides, and three classes of phospholipids identified by HPLC-Fluorescence. However, this analysis was limited in that BODIPY-labeled phospholipids clustered by class and polar and nonpolar fluorescent lipids had to be analyzed separately(87). Our method provides both greater resolution of individual fluorescent complex lipids, and a way to analyze all classes of complex lipids from a single sample. Furthermore, we have built upon earlier work (28) to expand the metabolic labeling toolbox for the larval zebrafish and other model systems by using this method to characterize the complex lipid product profiles of a wider range of fluorescent lipids delivered in a variety of diets (Table 7).

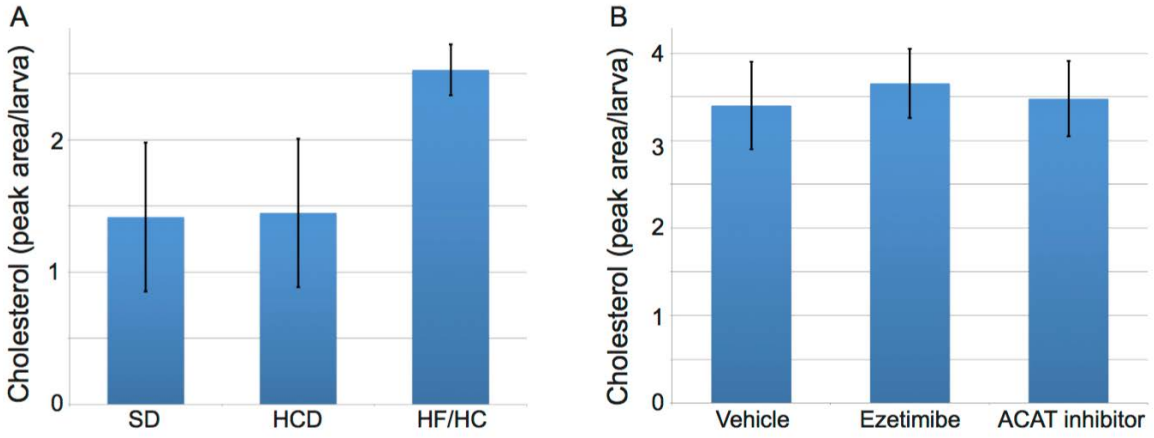

Supplemental Figure S4. Total cholesterol content of larval zebrafish is unchanged by ezetimibe, an ACAT inhibitor, and cholesterol content of the diet. A) There are no statistcally significant differences in cholesterol peak area per larva in larval zebrafish that have been given a single HF/HC meal, or fed LF/LC or LF/HC food for five days and fasted 24 hours before samples were taken (LF/LC-fed larvae: n = 4, LF/HC-fed larvae: n = 3, HF/HC-fed larvae: n = 2). B) There are no statistically significant differences in cholesterol HPLC peak area per larva resulting from treatment of larvae with ACAT inhibitor or ezetimibe prior to feeding BODIPY FL-C12 in an HF/HC meal and subsequent HPLC analysis of samples taken 18 hours post-feeding (n = 3; quantitation performed on HPLC CAD traces from experiments summarized in Table 5; Student's T-tests). Error bars represent 1 SD.

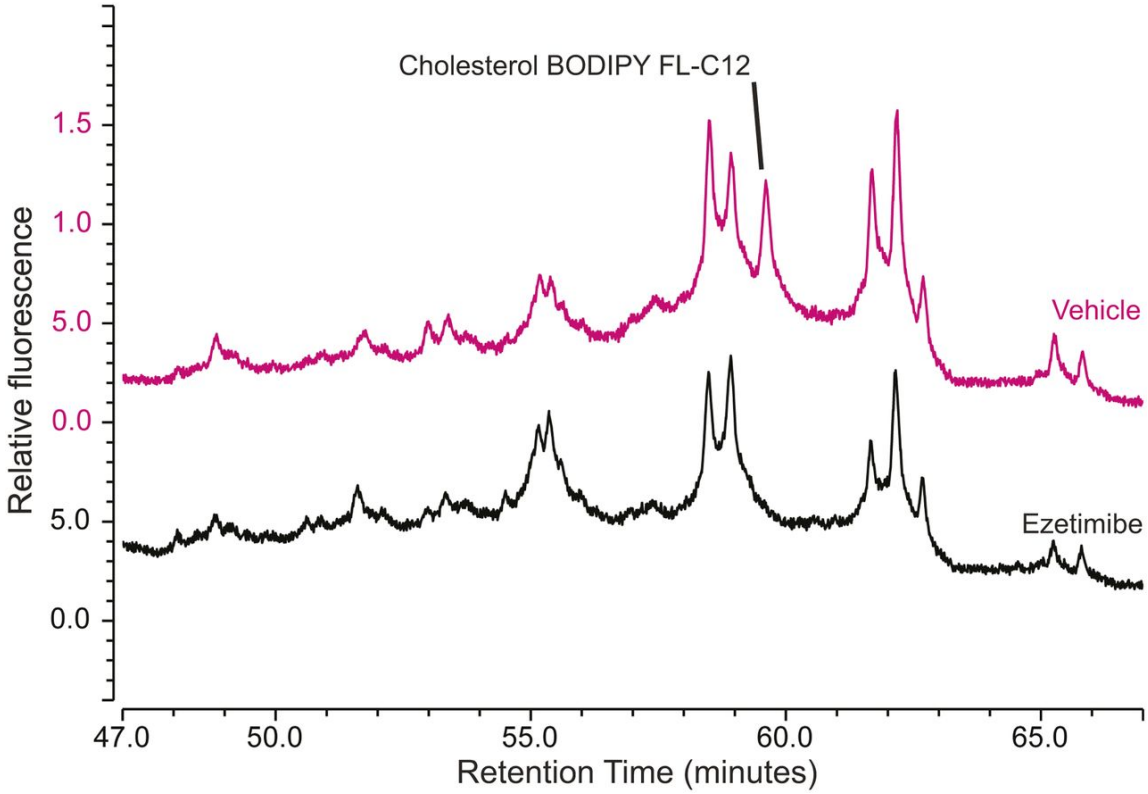

Figure 8. Ezetimibe reduces cholesterol ester synthesis from dietary fatty acids in the intestine. Larval zebrafish (6 dpf) were treated with ezetimibe (or 0.1% ethanol vehicle) and then fed BODIPY FL-C12 in the HF/HC diet. Intestines were dissected from 35 larvae per group 20 hours post-feeding and pooled for lipid extraction. The cholesterol BODIPY FL-C12 peak is present in the HPLC-Fluorescence trace from intestines of larvae in the vehicle control group (upper chromatogram), and absent in the trace from intestines of ezetimibe-treated larvae (lower chromatogram). Results are representative of two samples per group.

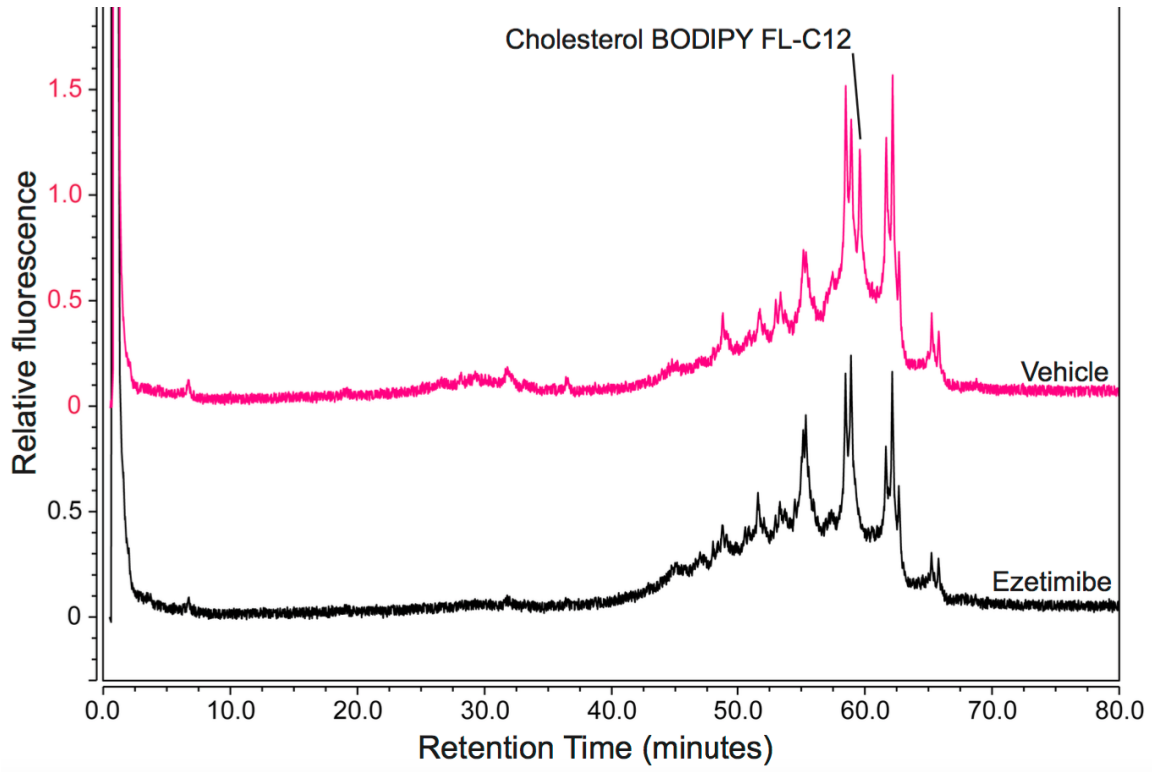

Supplemental Figure S5. Changes in cholesterol ester synthesis associated with ezetimibe treatment occur in the intestine. Full chromatograms from the experiment in Figure 8.

Table 7. Summary of BODIPY lipids, diets and product classes synthesized by larval zebrafish. Each fluorescent HPLC peak is counted as a single product of its corresponding BODIPY-lipid.

BODIPY-lipid	Color	Diet	PL Products	TG Products	CE Products
BODIPY FL-C5	Green	HF/HC	5	26	1
BODIPY FL-C12	Green	HF/HC	10	24	1
BODIPY FL-C12	Green	LF/LC	15	18	1
BODIPY FL-C12	Green	LF/HC	15	18	1
BODIPY(558/568)-C12	Red	HF/HC	7	11	1
BODIPY(558/568)-C12	Red	LF/LC	0	3	1
BODIPY(558/568)-C12	Red	LF/HC	0	3	1
TopFluor-C11	Green	HF/HC	11	22	0
BODIPY FL-C16	Green	HF/HC	5	11	1
Cholesterol BODIPY FL-C12	Green	LF/LC	3	11	1
Cholesterol BODIPY FL-C12	Green	LF/HC	3	11	1
Cholesterol BODIPY(576/589)-C11	Red	LF/LC	0	0	0
Cholesterol BODIPY(576/589)-C11	Red	LF/HC	0	3	1

Our results demonstrate that although all BODIPY-lipids tested were metabolized into multiple fluorescent complex lipid products when fed to larval zebrafish, the resulting product profiles varied with chain length of the labeled fatty acid, BODIPY-lipid class, BODIPY fluorophore variant, and nutritional context (Table 7). Awareness of this variation in distribution of fluorescent signal among lipid classes is not only essential when selecting BODIPY-lipids for metabolic labeling experiments, but is also crucial to understanding and interpreting live imaging experiments using BODIPY-lipids. For example, emission wavelength is a reasonable primary criterion when choosing a BODIPY tag for imaging experiments because it is often necessary to choose a fluorescent lipid color different from that of the fluorescent proteins expressed in transgenic animal models or cell lines.

However, when interpreting results obtained with different BODIPY variants or fluorescent fatty acids of different chain lengths it is important to consider that differences in the distribution of fluorescent signal into lipid classes may have an effect on the distribution of fluorescent signal among subcellular membranes and structures. Additionally, feeding larval zebrafish lipids labeled with the red BODIPY variants generally results in a larger percentage of unincorporated substrate and smaller range of complex lipid products when compared with green BODIPY-lipids. We hypothesize that the larger red BODIPY fluorophore slows uptake of fluorescent fatty acids into enterocytes and/or subsequent enzymatic interactions required for complex lipid synthesis; however, it is also possible that red BODIPY-lipids are more susceptible to lipolysis and that the larger amount of substrate observed is due to faster turnover. Even in experiments where labeling of cellular structures does not vary with the type of BODIPY fluorophore under one set of conditions (e.g., labeling of the same subcellular structures by red and green BODIPY-C12 in Figure 4A despite their different metabolic product profiles in Figure 4B), it cannot be assumed that this will hold true when conditions are varied or that any changes in labeling that occur under different experimental conditions will involve the same mechanisms for different BODIPY-lipids.

Of the BODIPY-lipids examined in this study, the partitioning of BODIPY FL-C12 into complex lipid classes most closely resembles the metabolism of palmitic acid, the most abundant fatty acid in larval zebrafish. Radioactive palmitic acid fed to larval zebrafish is incorporated into complex lipids more quickly than BODIPY FL-fatty acids, but the distribution of signal among polar and nonpolar complex lipids is more similar to that observed with BODIPY FL-C12 than any other fluorescent fatty acid examined (Tables 2 and 3). Furthermore, a similar array of individual complex lipid products are labeled by radioactive palmitate and BODIPY FL-C12, though HPLC retention times are consistently shifted earlier by the BODIPY tag (Supplemental Figure S2). Our results are consistent with a model in which the BODIPY fluorophore delays uptake of labeled lipids by cells, but does not alter the distribution of labeled lipids among complex lipid products.

In contrast to the product profile of BODIPY FL-C12, incorporation of fluorescent lipids into phospholipid occurs at a lower rate with BODIPY FL-fatty acids much larger or smaller than the saturated fatty acids most commonly found in zebrafish phospholipids, 16:0, 18:0, and 18:1 (Supplemental Table S1) (23). BODIPY FL-C5 and –C16, which correspond approximately in total length to nine- and 20-carbon unlabeled fatty acids, are incorporated into less phospholipid than BODIPY FL-C12 or ^{3}H-palmitate. Incorporation of fluorescent fatty acids into phospholipid also appears to be more sensitive to the effects of the larger red fluorophore than incorporation into nonpolar lipids. Multiple mechanisms could account for these metabolic differences, including effects on digestion, uptake by enterocytes, esterification, and turnover of labeled lipids. One possibility is that BODIPY-fatty acids impede diglycerides from interacting with the phospholipid synthesis pathway enzymes, but do not hinder their ability to bind or be esterified by DGAT. As the fatty acid composition of phospholipids is regulated to maintain membrane composition, we expect substrate fatty acid specificity to be more stringent for enzymes involved in phospholipid synthesis and remodeling than for those involved in synthesis of the nonpolar storage lipid classes TAG and CE. Additionally, the relative contributions of *de novo* synthesis

and remodeling of existing phospholipids to the incorporation of fluorescent fatty acids into phospholipid in the larval zebrafish intestine remain to be determined. Future work addressing these issues will clarify the physiological mechanisms underlying differential processing of the various BODIPY-lipids.

Despite early evidence for the synthesis of complex lipids from BODIPY FL-fatty acids in cell culture (87), there have been multiple studies in which metabolism of BODIPY-lipids by cultured mammalian cells was assayed by TLC and complex lipid products were not detected (85, 107, 108). In general, when metabolic products of BODIPY-lipids are observed, they are produced by a whole-animal model given BODIPY-lipids in context of a mixed-lipid diet, primary cultured cells that would already contain lipid droplets (e.g. hepatocytes), or cell culture supplemented with one or more fatty acids (28, 88-91). Our results provide additional evidence supporting the hypothesis that metabolism of BODIPY-lipids is observed in some studies and not others due to differences in the nutritional context in which BODIPY-lipids are delivered. Larval zebrafish preferentially synthesize mixed-acyl triglycerides and phospholipids (Table S1), and the delivery of BODIPY-FL fatty acids to larval zebrafish in a mixed-lipid meal has been shown to promote their metabolism when compared with delivery in embryo media alone (28). To build on this previous work, we have shown that BODIPY-fatty acids are also metabolized to complex lipid products when delivered to larval zebrafish in a standard LF/LC diet, expanding this model for use in experiments where the previously validated HF/HC diet consisting of chicken egg yolk may be impractical or may confound results by delivering too much unlabeled lipid.

The BODIPY-lipid, dietary context, and feeding procedure best suited to an experiment depends on the application. For example, it is apparent from the results of this study that with current HPLC methods the best BODIPY-lipids for monitoring cholesterol ester synthesis in the larval zebrafish are BODIPY FL-C12 and -C16 as their fluorescent cholesterol ester product peaks are well-isolated from neighboring fluorescent triglycerides, which ensures accurate quantitation. The actual effects of both ezetimibe and the ACAT inhibitor on cholesterol ester

synthesis from BODIPY FL-C5 and BODIPY(558/568)-C12 may be larger than what was observable by the HPLC-Fluorescence method used, as unlike their counterparts derived from BODIPY FL-C12 and -C16 the cholesterol BODIPY FL-C5 and cholesterol BODIPY(558/568)-C12 peaks do not fully resolve from neighboring triglyceride peaks (Figures 3 and 4). This would produce a background signal that would increase cholesterol ester peak areas in both control and experimental groups, which would lead to an artificially high treated:control peak area ratio (Table 6). Further HPLC method development will address this issue.

Nutritional context was especially important in experiments investigating the metabolism of BODIPY-cholesterol esters. Addition of a large amount of cholesterol to a low-fat diet appears to promote metabolism of the fluorescent fatty acid group of cholesterol BODIPY(576/589)-C11 into triglyceride and cholesterol ester products, and there is no evidence of intestinal lipolysis of cholesterol BODIPY(576/589)-C11 when it is delivered in a LF/LC diet. (It is not practical to deliver BODIPY-cholesterol esters in a high-fat meal as they are not digested well in this context, likely due to competition with triglycerides and other unlabeled cholesterol esters for intestinal lipases.) We hypothesize that a higher level of cholesterol than that provided by the LF/LC diet is needed to promote release of the enzymes necessary for digestion of BODIPY-cholesterol esters, and that cholesterol BODIPY FL-C12 with its smaller fluorescent tag is more readily hydrolyzed by intestinal lipases than cholesterol BODIPY(576/589)-C11.

Historically, studies of dietary cholesterol metabolism have tracked esterification using radiolabeled cholesterol (92, 93). By using fluorescent fatty acids as metabolic tracers to monitor cholesterol esterification by dietary fatty acids, we are able to build upon the current model for partitioning of dietary cholesterol in enterocytes. Though a number of genes involved in cholesterol channeling have been identified in multiple animal models including the larval zebrafish, the stepwise details of how these processes occur and are regulated in enterocytes are not fully characterized. Sorting of dietary sterols begins upon absorption: after entering the enterocyte through the NPC1L1 transport pathway, dietary cholesterol is largely retained in the

cell while the bulk of absorbed phytosterols are trafficked back to the intestinal lumen through the ABCG5/ABCG8 sterol efflux transporter (109). Once dietary cholesterol is transported to the endoplasmic reticulum (ER), it may be incorporated into enterocyte membranes, or packaged into lipoproteins or lipid droplets with or without being esterified first at the ER membrane by ACAT2 (110).

Though the mechanisms regulating whether or not a newly absorbed dietary cholesterol molecule is esterified are still largely unknown, our results suggest that the amount of cholesterol ester synthesized from newly absorbed dietary fatty acid is primarily responsive to the amount of newly absorbed and metabolically available dietary cholesterol. Cholesterol is abundant in the digestive tissues of the 6 dpf larval zebrafish (determined by dissection and HPLC-CAD analysis; data not shown), but the cholesterol present before feeding appears to be inaccessible to esterification by ACAT, likely due to being located in the plasma membrane (111). There is no statistically significant difference in the whole-body cholesterol content of larval zebrafish that have been fed HF/HC, LF/LC, or LF/HC meals when experimental samples are taken long enough after the withdrawal of food for the contents of the intestinal lumen to clear (Table 1, Supplemental Figure S4A). Additionally, neither ezetimibe nor an ACAT inhibitor produces a detectable change in total cholesterol within the time frame and treatment parameters of the experiments described herein (Supplemental Figure S4B). This illustrates the importance of metabolic labeling in the study of metabolism of a single lipid species, as without the fluorescent marker we employed the signal to noise ratio would have been too low to detect changes in cholesterol ester synthesis from newly absorbed dietary lipids in enterocytes. Physical segregation of ACAT2 from non-ER-located cholesterol pools and/or a lack of transport of cholesterol from other cellular structures to the ER may account for this effect; more work must be done to elucidate how ACAT2 activity is regulated. The method of tracking cholesterol ester synthesis through metabolic labeling with fluorescent fatty acids will be an important complement to radioactive labeling methods in further studies of dietary cholesterol processing.

In summary, the HPLC-CAD/fluorescence lipidomics methods described allow for high-throughput analysis of both total lipids and the products of fluorescent metabolic tracers in a single sample, using equipment that requires a much lower initial investment and smaller support infrastructure when compared with MS methods. The ability to pair this metabolic labeling method with live imaging using the same fluorescent lipid reagents is a major advantage of this approach. Using this platform we provide the most comprehensive analysis of fluorescent fatty acid metabolism to date, new insights into zebrafish models for dyslipidemia, and evidence for coupling between dietary cholesterol uptake and esterification.

Acknowledgments: Marc Plante (formerly of Thermo Fisher Scientific) provided excellent advice on setting up the HPLC method. Isaac Kim provided HPLC assistance. Carmen Tull, Andrew Rock, and Jennifer Anderson maintained fish stocks. This work was supported in part by the National Institute on Alcohol Abuse and Alcoholism (NIAAA) F31AA023142 to VHQ, National Institute of Diabetes and Digestive and Kidney (NIDDK) R01DK093399 to SAF and F32DK109592 to MHW, and National Institute of General Medicine (GM) R01GM63904 to the Zebrafish Functional Genomics Consortium (Stephen Ekker and SAF). The content is solely the responsibility of the authors and does not necessarily represent the official views of the National Institutes of Health (NIH). Additional support for this work was provided by the G. Harold and Leila Y. Mathers Charitable Foundation to the laboratory of SAF.

Conflict of interest: VHQ, MHW and SAF have no affiliations or financial arrangement with any organization that has a financial interest or stake in the material discussed in this manuscript. The Carnegie Institution does hold a patent together with the University of Pennsylvania on the invention of the author (SAF) that describes the use of fluorescent lipids in zebrafish for high-throughput screening Pub. No.: US 2009/0136428 A1. VHQ, MHW and SAF have no current consultancies, honoraria, stock ownership or options, expert testimony or royalties regarding the

material described. JR is currently an employee of Thermo Fisher Scientific, which could benefit from the sale of equipment described in this manuscript.

Author contributions: VHQ wrote the paper, and conceived of and executed the experiments in consultation with SAF. MHW performed confocal imaging experiments and provided editorial assistance. JR designed the mass spectrometry instrument methods; JR and VHQ worked together to perform mass spectrometry experiments and design the boron isotope analysis method. All authors approved the final version of the manuscript.

CHAPTER 3 – HPLC LIPID PROFILING OF MICE REVEALS EFFECTS OF DIET AND A ROLE FOR INTESTINAL CAVEOLIN 1 IN REGULATING PLASMA LIPIDS

Contributions

The paper reproduced below was published in *Disease Models and Mechanisms* (March 1st, 2017). For this study I developed sample preparation and analysis methods for determining lipid profiles of mouse plasma, liver, and adipose tissue samples by HPLC-CAD. I performed all HPLC experiments, quantitated and analyzed the data, performed statistical analyses, wrote the parts of the Methods section on HPLC, interpreted the HPLC data with Jessica Otis, and helped to edit the manuscript.

Intestinal epithelial cell Caveolin 1 regulates fatty acid and lipoprotein cholesterol plasma levels

Jessica P. Otis[1], Meng-Chieh Shen[1], Vanessa Quinlivan[1,2], Jennifer L. Anderson[1], and Steven A. Farber[1,2,*]
[1] Carnegie Institution for Science, Department of Embryology, Baltimore, MD, 21218, USA
[2] Johns Hopkins University, Department of Biology, Baltimore, MD, 21218, USA

Abstract

Caveolae and their structural protein caveolin 1 (CAV1) have roles in cellular lipid processing and systemic lipid metabolism. Global deletion of CAV1 in mice results in insulin resistance and increases in atherogenic plasma lipids and cholesterol, but protects from diet-induced obesity and atherosclerosis. Despite the fundamental role of the intestinal epithelia in the regulation of dietary lipid processing and metabolism, the contributions of CAV1 to lipid metabolism in this tissue have never been directly investigated. In this study the cellular dynamics of intestinal Cav1 were visualized in zebrafish and the metabolic contributions of CAV1 were determined with mice lacking CAV1 in intestinal epithelial cells ($CAV1^{IEC\text{-}KO}$). Live imaging of Cav1-GFP and fluorescently labeled caveolae cargos shows localization to the basolateral and lateral enterocyte PM, suggesting Cav1 mediates transport between enterocytes and the submucosa. $CAV1^{IEC\text{-}KO}$

mice are protected from the elevation in circulating fasted low-density lipoprotein (LDL) cholesterol associated with a high-fat diet, but have increased postprandial LDL cholesterol, total free fatty acids (FA), palmitoleic acid, and palmitic acid. The increase in circulating fatty acids in HFD CAV1^{IEC-KO} mice are mirrored by decreased hepatic fatty acids suggesting a non-cell autonomous role in IEC CAV1 in promoting hepatic fatty acid storage. In conclusion, CAV1 regulates circulating LDL cholesterol and several FA species via the basolateral PM of enterocytes. These results point to intestinal epithelial cell CAV1 as a potential therapeutic target to lower circulating FA and LDL cholesterol, since high levels are associated with development of type II diabetes and cardiovascular disease.

Introduction

Caveolae are flask-shaped pits, 50 to 100 nm in diameter, that form in lipid-rich plasma membrane (PM) regions of most vertebrate cells (112). Caveolae vesicle structure is formed by oligomers of caveolin proteins; approximately 144 caveolin proteins are present in a single caveolae (112). CAV1 is synthesized in the endoplasmic reticulum, transported to the Golgi, and upon exit, oligomerizes and associates with lipid-rich membrane regions (112). A threshold level of membrane cholesterol is required for caveolae to form (113) and CAV1 can directly bind cholesterol (114) and fatty acids (FA) (115).

Historically recognized for their endocytic function, caveolae also regulate cell-signaling pathways, internalization of cell surface receptors and ligands, cell adhesion molecule expression, exocytosis, and transcytosis of caveolae cargos (112). Caveolae are also emerging players in lipid metabolism. Global CAV1 knockout mice (CAV1^{KO}) mice have severe alterations in circulating lipids, including decreased fasting free FA (FFA), increased postprandial FFA (116), increased triglycerides (TG) (116, 117), and increased non-high density lipoprotein (HDL) total, free, and esterified cholesterol (116-119). CAV1^{KO} mice are insulin resistant (120), but are protected from

diet-induced obesity (116) and atherosclerosis (121, 122). The plasma lipid and body mass changes in $CAV1^{KO}$ mice have been proposed to result from a variety of mechanisms including altered lipid droplet architecture, reduced adipocyte lipid droplet formation (123), and impaired adipocyte metabolic flexibility (124), while protection from atherosclerosis is likely due to decreased endothelial adhesion molecule expression.

The cells that line the intestinal epithelia, enterocytes, are highly specialized to bidirectionally absorb, transport, and export large quantities of luminal contents and basolateral plasma components. However, the mechanisms by which dietary lipids are internalized, transported, and externalized by enterocytes, as well as how enterocytes receive adequate lipids from adipose stores during fasting, remain incompletely understood. The close association of CAV1 with cholesterol, FAs, lipid droplets, and lipid-rich PM regions suggests a role for CAV1 and caveolae in intestinal lipid metabolism (125). CAV1 is expressed, and caveolae vesicles form, in the enterocytes of several species including humans and mice (126-132). Although it is known that CAV1 and caveolae are present in enterocytes, several basic aspects of their biology, including subcellular localization and metabolic functions, remain unclear.

Although intestinal cholesterol absorption is not disrupted in mice lacking CAV1 (118), isolated intestinal caveolae contain dietary FA (131) and intestinal lipoprotein cholesterol export influences plasma cholesterol levels, so intestinal CAV1 may significantly impact cholesterol metabolism. Cell culture studies have suggested that CAV1 PM localization may be asymmetric in polarized cells such as intestinal enterocytes; however, reports are conflicting. For example, in human intestinal cells CAV1 localizes asymmetrically, but the pattern varies by cell type: in human T84 colonic adenocarcinoma cells, CAV1 was observed only on lateral membranes (133); in human intestinal biopsies, CAV1 was found only on the basolateral surface (127); and in Caco2 cells, CAV1 localizes to the apical plasma membrane (126). This imprecise understanding of enterocyte CAV1 localization hampers understanding of its functions in health and disease in the intestine.

A shortage of studies in live, intact animal models, has limited our understanding of the contributions of intestinal CAV1 to enterocyte cell biology and global lipid metabolism. Therefore, in this study we harnessed the genetic tractability and optical clarity of the larval zebrafish (*Danio rerio*) to perform live imaging of intestinal Cav1 and caveolae-mediated endocytosis for the first time. The zebrafish digestive system is similar to that of the human, composed of a liver, gallbladder, and intestine (134), and lipid and lipoprotein metabolism are highly conserved (16, 17). Similar to humans and mice, the zebrafish genome contains one *cav1* gene, with two major splice transcripts, and it is expressed in the intestine (135). Zebrafish have previously enabled the elucidation of a role for Cav1 in embryonic organogenesis (135, 136) and live super resolution imaging of Cav1 in the embryonic tail (137). Additionally, we employed the power of the mouse model to generate a tissue-specific C*av1* deletion and determine its contribution to global lipid metabolism. Our transgenic zebrafish and knockout mice, combined with a innovative approach to assay enterocyte endocytosis *in vivo*, allows for an unprecedented understanding of enterocyte CAV1 cell biology, the effects of enterocyte CAV1 on systemic lipid metabolism, and how CAV1 in the intestinal epithelia influence metabolic disease risk through alterations in circulating lipids.

Results

Cav1 localizes to the lateral and basolateral PM of zebrafish enterocytes

We generated *Tg(hsp70l:cav1-eGFP)* zebrafish which express zebrafish Cav1 tagged with GFP and performed live imaging. Cav1 localizes to the basolateral and lateral PM of intestinal epithelial cells, but is excluded from the luminal brush border (Fig. 1A). Mean fluorescence intensity is 7.5-fold greater on the lateral PM (605.5 relative units) than the brush border (80.7 relative units) (one-way ANOVA, $p<0.05$) (Fig. 1B).

Immunofluorescence (IF) confirms that endogenous Cav1 localizes to the lateral and basolateral PM, but not the luminal brush border, of enterocytes in larval and adult zebrafish (Fig. 1C,D). As Cav1 protein can exist as either a monomer or an oligomer structuring caveolae vesicles, we examined EM sections to determine where caveolae vesicles localize. Similar to the localization of Cav1, caveolae vesicles are observed on both the basolateral and lateral membranes, but not on the brush border (Fig. 1E,F).

Caveolae-mediated endocytosis occurs only on the basolateral side of enterocytes

The asymmetric PM localization of zebrafish enterocyte Cav1 suggests that caveolae-mediated endocytosis occurs between the intestinal epithelia and submucosa, but not the intestinal lumen. To test this hypothesis, we developed a technique to visualize endocytosis in live

Figure 1 (next page). Cav1 and caveolae localize to the basolateral and lateral PM of enterocytes. (A) Live imaging of *Tg(hsp70l:cav1-eGFP)* zebrafish larvae shows localization of Cav1-eGFP to the lateral and basolateral plasma membranes (PM) of enterocytes, but not the luminal brush border. One enterocyte is outlined, BB: brush border, L: lateral membrane, B: basolateral membrane, I: intracellular (6 dpf). (**B**) Mean fluorescence intensity, in relative units, of Cav1-eGFP in subcellular regions of larval enterocytes. Data is mean ± s.e.m, n=3: 9 fish per n, 3 areas of each region per fish; groups with different letters are significantly different (one-way ANOVA, $p<0.05$). Representative IF images performed with an antibody to CAV1 confirm the polarized PM localization of endogenous Cav1 in (**C, E**) larval (6 dpf) and (**D, F**) adult zebrafish gut epithelia, scale bars represent 5 μm for C and D and 25 μm for E and F. Representative EM images of caveolae vesicles observed on the basolateral and lateral PMs of larval (6 dpf) (**G**) and adult (**H**) zebrafish enterocytes, scale bars represent 100 nm, c: caveolae.

Figure 1.

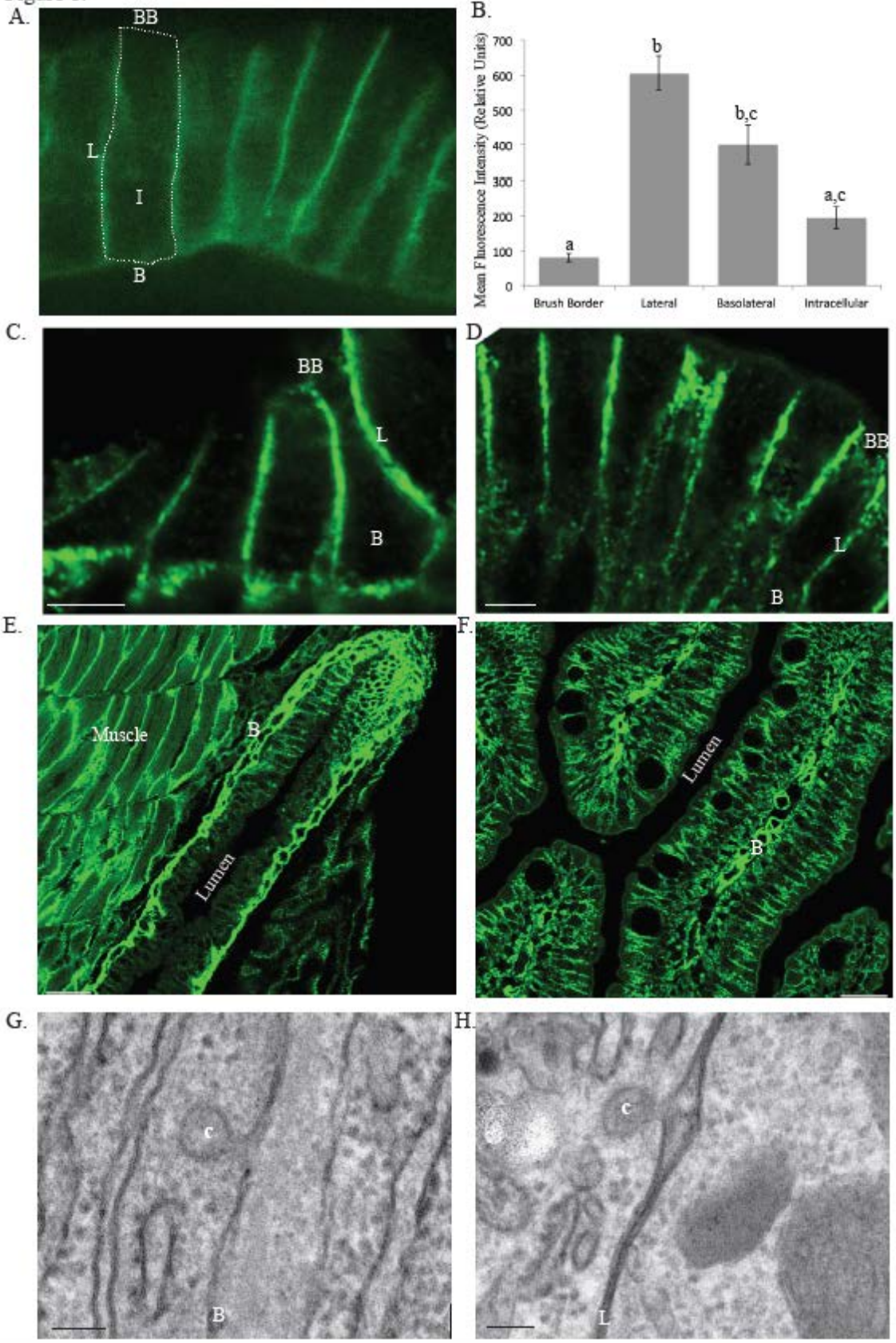
A.
BB
L
I
B
B.
Mean Fluorescence Intensity (Relative Units)
700
600
500
400
300
200
100
0
a
b
b,c
a,c
Brush Border
Lateral
Basolateral
Intracellular
C.
BB
L
B
D.
BB
L
B
E.
Muscle
B
Lumen
F.
Lumen
B
G.
c
B
H.
c
L

zebrafish larvae based on cell culture studies that use fluorescently labeled endocytic cargos (138). We injected fluorescently labeled endocytic cargos that are internalized specifically by caveolae (Alexa Fluor-albumin (139-143) and BODIPY-*d*-LacCer (138, 144)) or clathrin-coated vesicles (BODIPY-*l*-LacCer (138)) to the basolateral or luminal side of enterocytes. Live confocal imaging indicated if endocytosis took place from the basolateral/lateral PM (basolateral injection) or brush border (luminal injection) in the intestinal epithelia. While BODIPY-*l*-LacCer, the cargo transported specifically by clathrin-coated vesicles, is internalized from both enterocyte PM regions, the caveolae-specific cargos Alexa Fluor-albumin and BODIPY-*d*-LacCer are only endocytosed from the basolateral PM (Fig. 2A). The fluorescently labeled caveolae-specific cargos localize to similar cellular locations as endogenous Cav1 and Cav1-GFP (lateral and basolateral PM), while the clathrin-specific cargo localizes to distinct cellular locations (brush border) (Fig. 2A). The mean fluorescence intensity of the lateral PM was 3.45-fold and 11.1-fold greater following basolateral injection of Alexa Fluor-albumin and BODIPY-*d*-LacCer, respectively, relative to luminal injection (Student's t-test, p=0.018 and p=0.003) (Fig. 2B). Two lines of zebrafish with mutations in c*av1* have recently been published (145); we hypothesized that uptake of caveolar cargos would be lost in the enterocytes of the fish. Basolateral albumin injections were repeated in the larvae, however uptake of Alexa Fluor-albumin was not decreased in $cav1^{PD1094}$, likely since total *cav1* mRNA is not decreased in this line, and $cav1^{PD1104}$ larvae were not healthy enough to survive the experiment in our hands (data not shown; fish generously provided by Michel Bagnat). These results suggest that caveolae perform a polarized endocytic function in enterocytes, mediating transport between enterocytes and the submucosa, but not the intestinal lumen.

Figure 2.

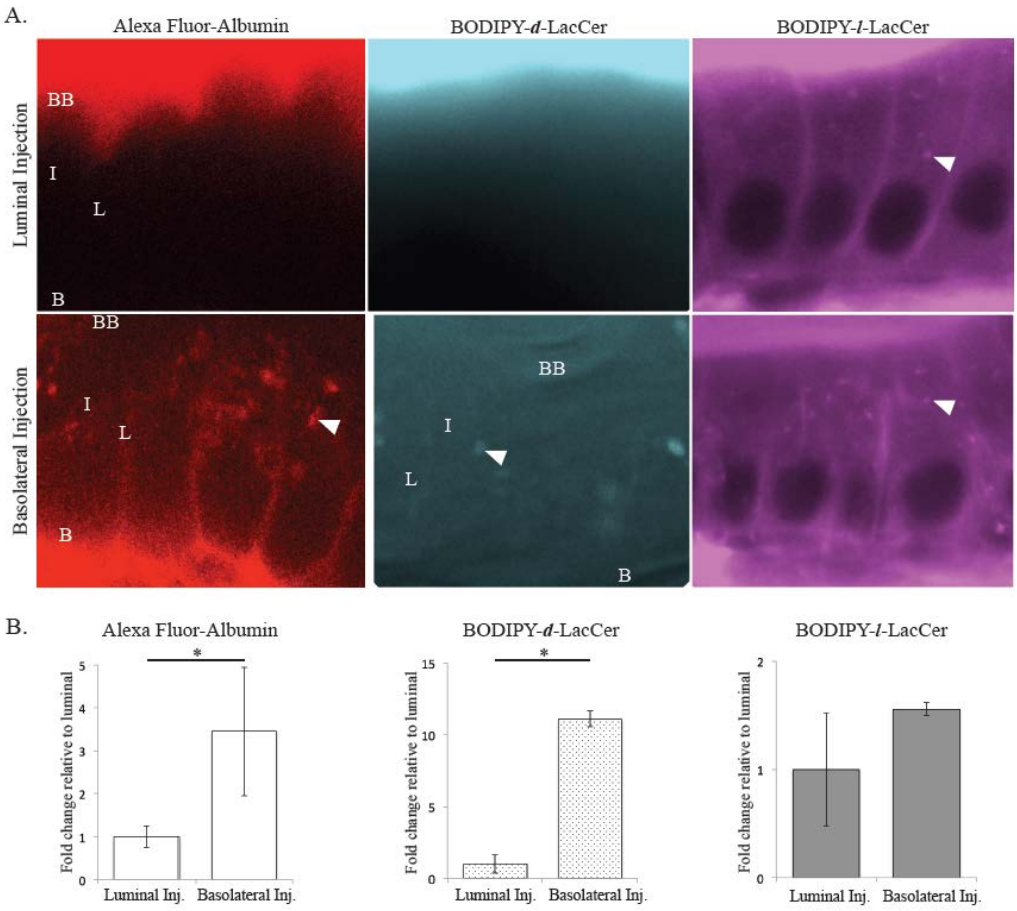

Figure 2. Fluorescently labeled endocytic cargos enable imaging of caveolar endocytosis in the intact zebrafish intestine. (**A**) Representative images show that the caveolar specific cargos Alexa Fluor-albumin and BODIPY-*d*-LacCer are internalized from the basolateral PM of enterocytes, but not the intestinal lumen. In contrast, the cargo transported specifically by clathrin-coated vesicles, BODIPY-*l*-LacCer, is transported into enterocytes from both the basolateral and luminal PMs. BB: brush border, L: lateral membrane, B: basolateral membrane, I: intracellular, N: nucleus, arrowhead: intracellular puncta. (**B**) The mean fluorescence intensity of Alexa Fluor-albumin and BODIPY-*d*-LacCer on the lateral PM of enterocytes is significantly greater following basolateral injection compared to luminal injection. In contrast, the mean fluorescence intensity of BODIPY-*l*-LacCer on the lateral PM of enterocytes is the same following basolateral and luminal injection. Data is presented relative to lateral PM mean fluorescence intensity following luminal injection (mean ± s.e.m, n=3: 9 fish per n, 3 areas of each region per fish, Student's t-test, * signifies $p<0.05$).

Generation of intestinal epithelial cell Cav1 KO mice

While zebrafish are an ideal model to visualize Cav1 and endocytosis, it is extremely challenging to perform tissue-specific gene deletion and measurements of plasma metabolites. To address this challenge mice lacking CAV1 specifically in intestinal epithelial cells ($CAV1^{IEC\text{-}KO}$) were generated by crossing mice with floxed Cav1 ($CAV1^{fl/fl}$) (146) with Villin-Cre mice (147) (Fig. 3A). PCR of gDNA from whole jejunum (a mixed tissue sample containing non-genetically modified smooth muscle and vasculature endothelial cells in addition to intestinal epithelial cells lacking CAV1) shows evidence that Cre recombination occurs in the intestine of $CAV1^{IEC\text{-}KO}$ mice but not in wild type (WT) $CAV1^{fl/fl}$ littermates (Fig. 3B). RT-PCR of jejunum (tissue includes epithelial cells as well as submucosa and muscle) demonstrates that *Cav1* mRNA is decreased ~70% in $CAV1^{IEC\text{-}KO}$ mouse relative to $CAV1^{fl/fl}$ WT (Student's t-test, p=0.01) (Fig.

Figure 3 (next page). Deletion of Cav1 from mouse intestinal epithelial cells ($CAV1^{IEC\text{-}KO}$). (**A**) Schematic representation of deletion of *Cav1* in the intestinal epithelium. (**B**) PCR of genomic DNA from whole mouse jejunum shows that Cre recombination of Cav1 has occurred in $CAV1^{IEC\text{-}KO}$ jejunum but not in $CAV1^{fl/fl}$ WT littermates. (**C**) *Cav1* mRNA is decreased 68% in $CAV1^{IEC\text{-}KO}$ mouse jejunum as evidenced by RT-PCR (mean, Student's t-test, p=0.01, n=10). (**D**) *Cav2* mRNA is decreased 75% in $CAV1^{IEC\text{-}KO}$ mouse jejunum as evidenced by RT-PCR (mean, Student's t-test, p=0.01, n=10). (**E**) CAV1 protein is reduced in the jejunum of $CAV1^{IEC\text{-}KO}$ mice as measured by western blot and normalized to α-tubulin. Data are expressed relative to $CAV1^{fl/fl}$ WT CAV1 protein, n=3 western blots, 5 WT and 5 IKO mice per blot, Student's t-test, * signifies p<0.05. (**F**) Representative western blot. Body mass of male (**G**) and female (**H**) mice; mice were fed a low-fat (10%) or high-fat (60%) diet starting at 10 wk (n=10−15). HFD mice had significantly higher body mass than LFD mice, but loss of intestinal epithelial cell CAV1 did not affect body mass (mean ± s.e.m, linear regression, * signifies p<0.05).

Figure 3.

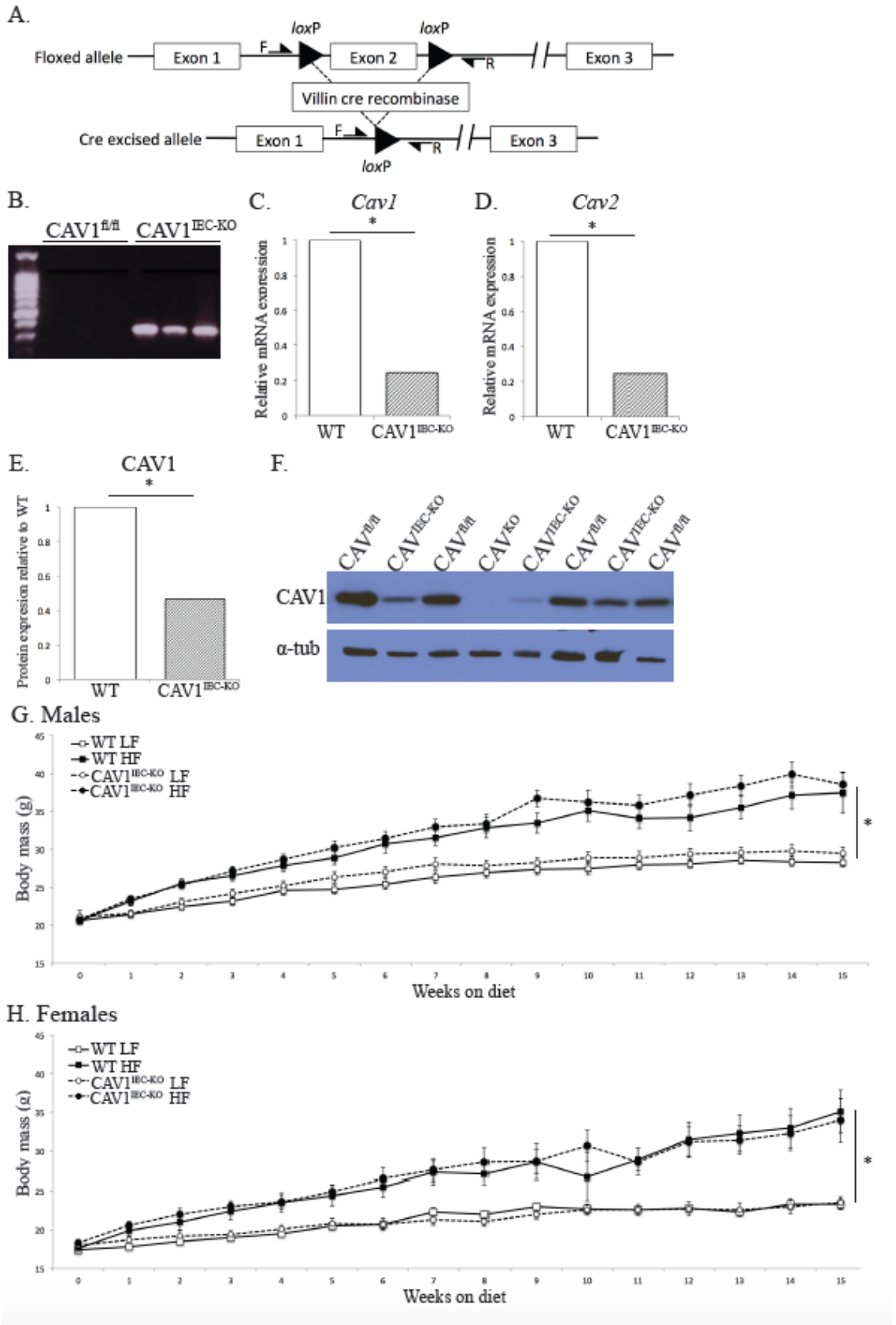
A.
loxP
loxP
Floxed allele
Exon 1
F
Exon 2
R
Exon 3
Villin cre recombinase
Cre excised allele
Exon 1
F
R
Exon 3
loxP
B.
CAV1fl/fl
CAV1IEC-KO
C.
Cav1
*
Relative mRNA expression
WT
CAV1IEC-KO
D.
Cav2
*
Relative mRNA expression
WT
CAV1IEC-KO
E.
CAV1
*
Protein expresion relative to WT
WT
CAV1IEC-KO
F.
CAVfl/fl
CAVIEC-KO
CAVfl/fl
CAVKO
CAVIEC-KO
CAVfl/fl
CAVIEC-KO
CAVfl/fl
CAV1
α-tub
G. Males
WT LF
WT HF
CAV1IEC-KO LF
CAV1IEC-KO HF
Body mass (g)
Weeks on diet
*
H. Females
WT LF
WT HF
CAV1IEC-KO LF
CAV1IEC-KO HF
Body mass (g)
Weeks on diet
*

3C) and not expressed in the jejunum of negative control CAV1^{KO} mice (data not shown). *Cav2* mRNA is also decreased in CAV1^{IEC-KO} mice, which have 75% less *Cav2* mRNA relative to CAV1$^{fl/fl}$ WT mice (Student's t-test, p =0.01) (Fig. 3d)(148, 149). Western blot shows CAV1 protein expression is 55% lower in CAV1^{IEC-KO} mouse jejunum than in CAV1$^{fl/fl}$ WT littermates (Fig. 3E) and that CAV1 is lost in the jejunum of negative control CAV1^{KO} mice (Fig. 3F).

Loss of intestinal epithelial CAV1 does not affect body mass or glucose metabolism

High-fat diet (HFD) increases the body mass of male and female mice relative to mice fed a low-fat diet (LFD), but CAV1^{IEC-KO} does not protect against diet-induced obesity (16 wk on diet, 22 wk old, linear regression, males: F=37.7689, p<0.0001 for diet, females: F=33.8792, p<0.0001 for diet) (Fig. 3G,H). Fasting plasma glucose (Fig. S1A), glucose tolerance (Fig. S1B,C), and insulin tolerance (Fig. S1D) are similarly unaffected by genotype. Thus, neither body mass or glucose metabolism influence the following changes in lipid metabolism.

Deletion of intestinal epithelial CAV1 alters cholesterol levels

Deletion of CAV1 in the intestinal epithelia results in changes in fasting and postprandial circulating total and lipoprotein cholesterol, especially when mice were challenged by 16 wk

Figure S1 (next page). Glucose metabolism is unaltered in CAV1^{IEC-KO} mice. (**A**) Fasting blood glucose is elevated in male and female mice fed HFD relative to mice fed LFD similarly in CAV1^{IEC-KO} (IKO) mice and WT littermates (mean ± s.e.m, n=6−10, two-way ANOVA, p<0.05, groups with different brackets show significant effect of diet, groups with different letters are significantly different by post hoc testing). There were no differences in blood glucose between CAV1^{IEC-KO} (IKO) and WT mice during (**B**) IP or (**C**) oral glucose tolerance tests or (**D**) insulin tolerance test. Data are shown as mean ± s.e.m, n=7−14, one- or two-way repeated measures ANOVA.

Figure S1.

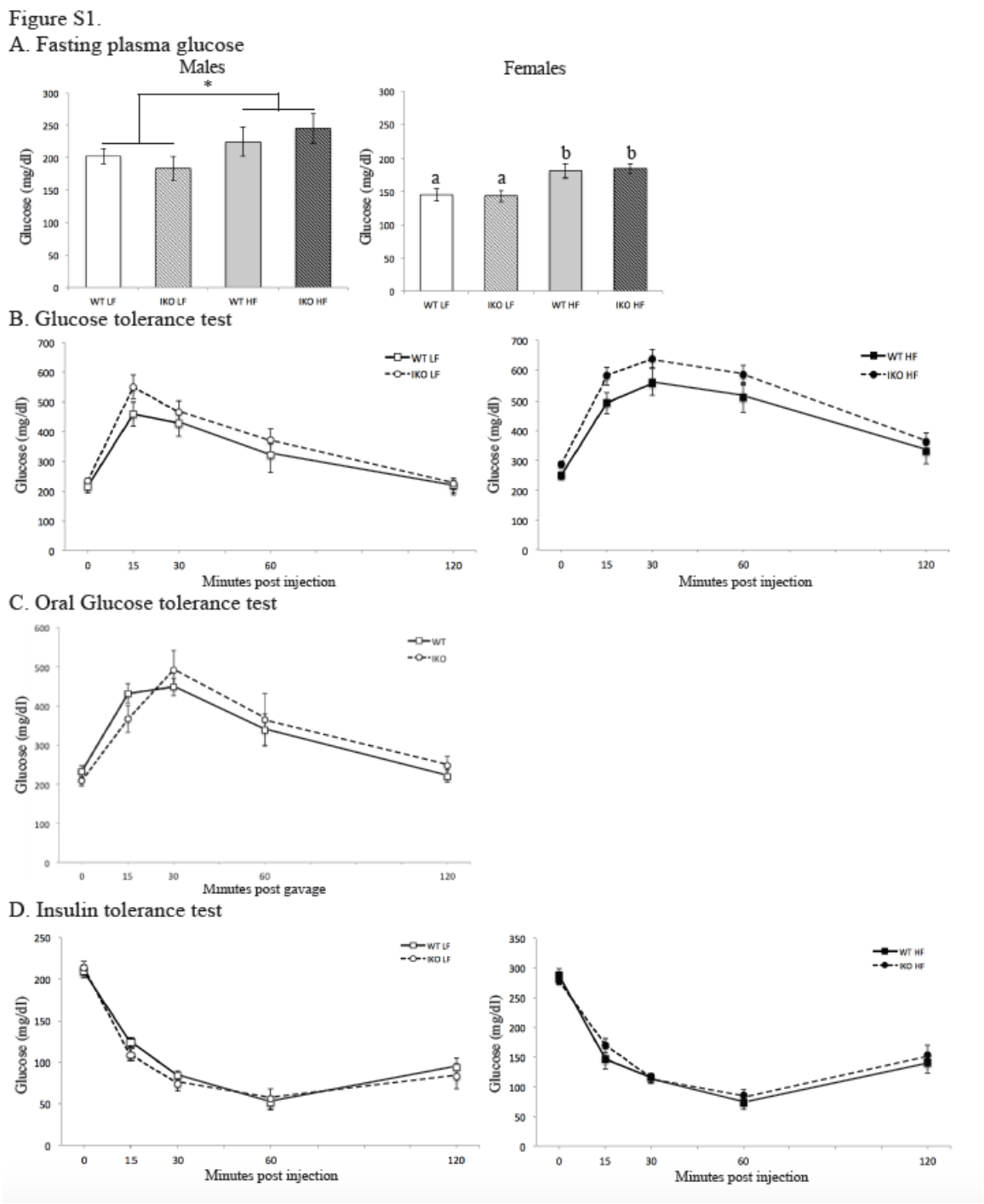
A. Fasting plasma glucose
Males
Females
Glucose (mg/dl)
WT LF
IKO LF
WT HF
IKO HF
a
a
b
b
B. Glucose tolerance test
Minutes post injection
C. Oral Glucose tolerance test
Minutes post gavage
D. Insulin tolerance test

HFD. Compared to CAV1$^{fl/fl}$ WTs, male CAV1^{IEC-KO} mice have a greater increase in total and esterified cholesterol upon HFD treatment relative to LFD controls (increase in total cholesterol: 62.9 mg/dl CAV1^{IEC-KO} vs. 24.3 mg/dl WT, two-way ANOVA, effect of diet: $F(1,24)=8.055$, p=009; increase in esterified cholesterol: 54.4 mg/dl CAV1^{IEC-KO} vs. 19.5 WT mg/dl; two-way ANOVA, effect of diet: $F(1,23)=7.610$, p=.01) (Fig. 4A). A similar trend for greater total cholesterol is observed in postprandial male mice maintained on chow diet (CD), but only free cholesterol is significantly elevated by these conditions (34.6 mg/dl WT vs. 49.1 mg/dl CAV1^{IEC-KO} increase, Student's t-test, $p<0.05$) (Fig. 4C). It is well established that plasma lipids can show sexual dimorphism; here the effects of intestinal CAV1 on plasma cholesterol are sexually dimorphic: CAV1$^{fl/fl}$ WT females have greater HFD-associated elevations in total cholesteroliui8 (WT: 55.1 mg/dl; CAV1^{IEC-KO}: 10.8 mg/dl increase, two-way ANOVA, effect of diet, $F(1,26)=5.881$, p=0.02), free cholesterol (WT: 10.9 mg/dl, CAV1^{IEC-KO}: 1.7 mg/dl increase, two-way ANOVA, effect of diet, $F(1,26)=5.075$, p=0.03), and esterified cholesterol compared to CAV1^{IEC-KO} females (WT: 44.3 mg/dl, IKO: 9.2 mg/dl increase, two-way ANOVA, effect of diet, $F(1,26)=4.707$, p=0.04) (Fig. 4B).

Intestinal epithelial CAV1 deletion protects against HFD-induced LDL cholesterol increase

Male CAV1^{IEC-KO} mice are protected against the HFD-associated increase in fasted (4 hr) plasma low-density lipoprotein cholesterol (LDL-C) seen in CAV1$^{fl/fl}$ WT littermates (HFD WT: 35.5 mg/dl, 5.5 mg/dl greater than LFD; HFD CAV1^{IEC-KO}: 23.7, 6.3 mg/dl less than LFD) (two-way ANOVA, significant interaction between diet and genotype, $F(1,24)=5.261$, p=0.03) (Fig. 5A), though female mice do not exhibit this protection (Fig. 5B). Conversely, postprandial LDL-C is elevated in male CAV1^{IEC-KO} mice (23.4 mg/dl) compared to WT (16.1 mg/dl) (Student's t-test, $p<0.05$) (Fig. 5C). HDL-C is also altered in CAV1^{IEC-KO} mice, as female mice have a greater HFD-induced increase in HDL-C relative to LFD in CAV1^{IEC-KO} mice (13.3 mg/dl for males, 17.1 mg/dl females) compared to WT (9.6 mg/dl for males, 0.2 mg/dl for females) (two-way ANOVA,

Figure 4.
A. Males

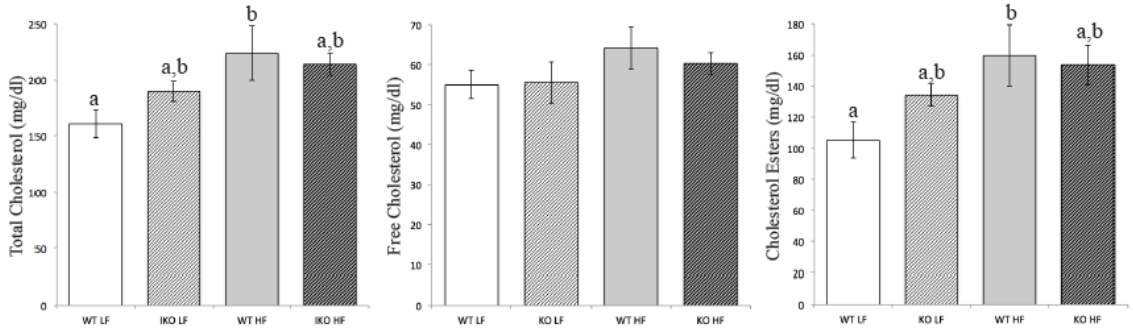

B. Females

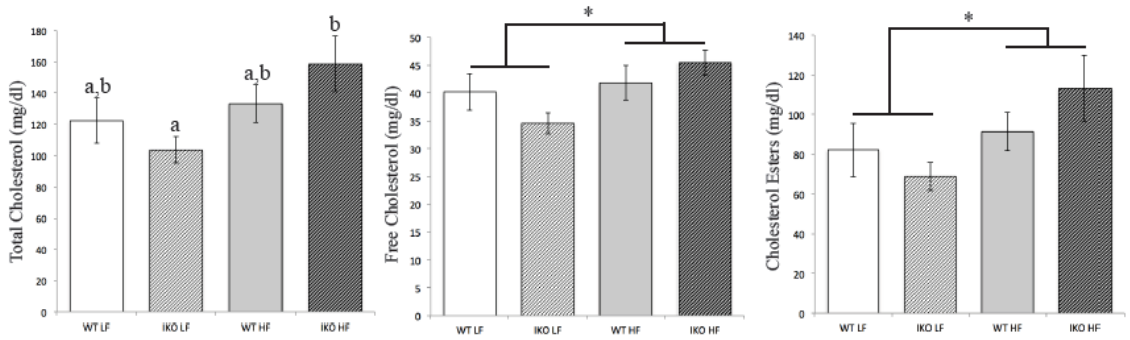

C. CD Males

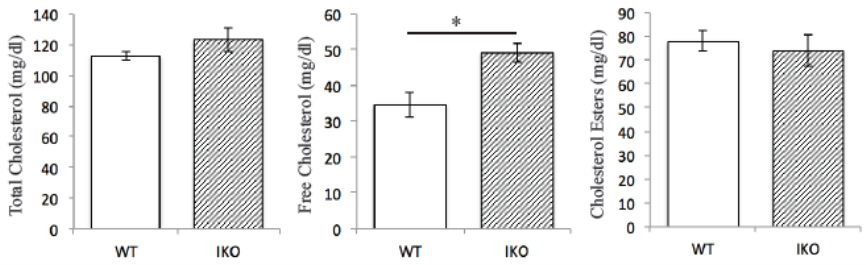

Figure 4. Loss of CAV1 in the intestinal epithelia alters plasma cholesterol levels. (**A**) In male mice, total and esterified plasma cholesterol are elevated by HFD in WT, but not CAV1$^{IEC\text{-}KO}$ (IKO), mice following a 4 hr fast (n=5−8). (**B**) Conversely, for female mice, total, free, and esterified plasma cholesterol are elevated by HFD in 4 hr fasted CAV1$^{IEC\text{-}KO}$, but not WT, mice (n=8−9). (**C**) Post-prandial male CAV1$^{IEC\text{-}KO}$ mice fed CD have greater plasma free cholesterol mice than WT (n=6−8). Data are mean ± s.e.m, two-way ANOVA, * signifies $p<0.05$, groups with different brackets show an effect of diet, groups with different letters are significantly different by post hoc testing.

Figure 5.

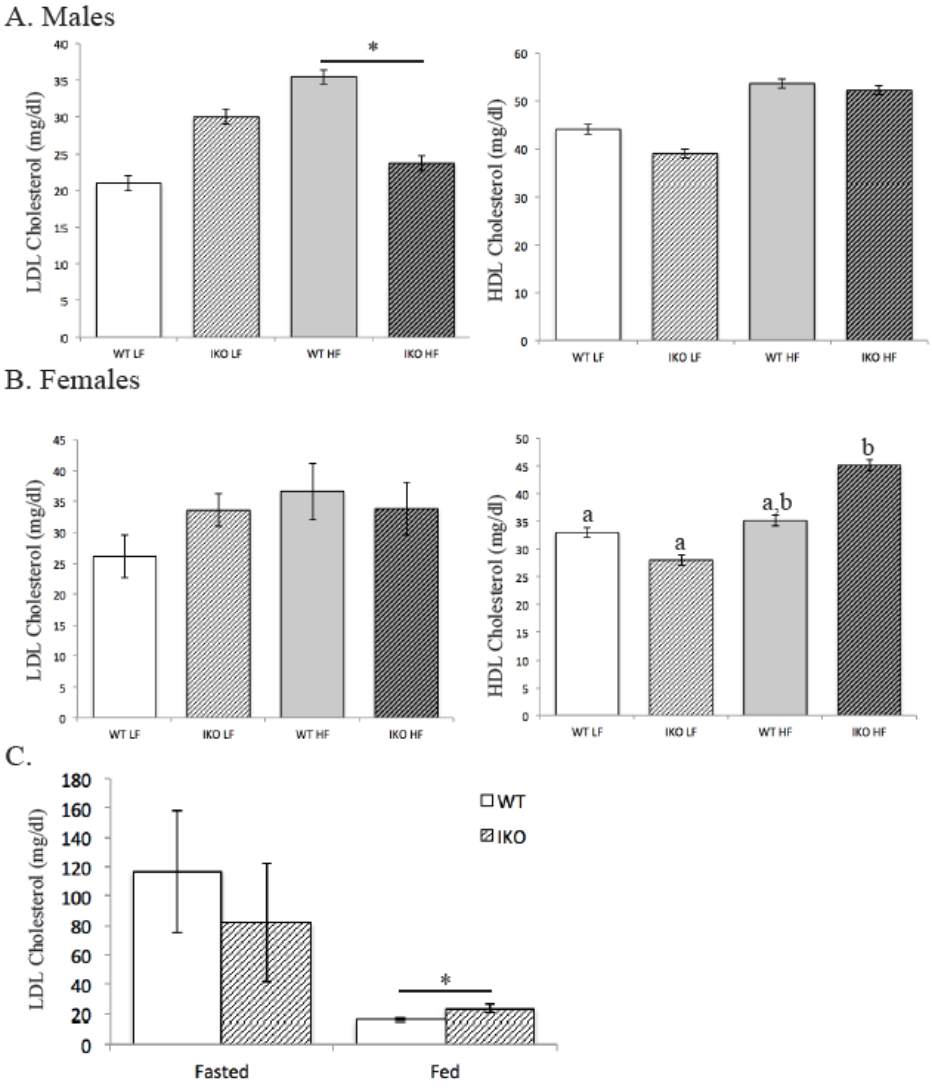

Figure 5. Lipoprotein cholesterol levels are affected by loss of CAV1 in the intestinal epithelia. Male CAV1^{IEC-KO} (IKO) mice are protected from HFD-induced increase in fasted plasma LDL cholesterol (n=6−10, mean ± s.e.m, two-way ANOVA, significant interaction between diet and genotype) (**A**), but female mice are not (n=8−9) (**B**). Female IKO, but not WT, mice have higher fasted plasma HDL cholesterol on HFD than LFD (mean ± s.e.m, two-way ANOVA, groups with different letters are significantly different by post hoc testing). (**C**) CAV1^{IEC-KO} mice on CD have higher post-prandial plasma LDL cholesterol than WT mice (mean ± s.e.m, Student's t-test, * signifies $p<0.05$, n=6−9).

significant effect of diet F(1,28)=9.516, p=0.005, and interaction between diet and genotype F(1,28)=5.684, p=0.024) (Fig. 5A,B).

Intestinal epithelial CAV1 deletion increases plasma free fatty acids

Loss of intestinal epithelial CAV1 increases plasma non-esterified fatty acids (NEFA) in fasted male HFD CAV1$^{IEC\text{-}KO}$ mice (1.43 mmol/L) compared to HFD CAV1$^{fl/fl}$ WT littermates (0.94 mmol/L) (two-way ANOVA, effect of diet, F(1,23)=13.15, p=0.0014) (Fig. 6A). NEFA are also greater in postprandial CD-fed male CAV1$^{IEC\text{-}KO}$ mice (0.42 mmol/L) than WT mice (0.27 mmol/L) (Student's t-test, p<0.05)(Fig. 6C). Moreover, serum NEFA decreases less in CD-fed male CAV1$^{IEC\text{-}KO}$ mice upon feeding (0.44 fold-decrease) than WT male mice (0.83 fold-decrease) (Student's t-test, p<0.05).

Figure 6 (next page). Intestinal CAV1 deletion alters circulating FFA but not TG. (**A**) In male mice, plasma NEFA are higher in HFD fed CAV1$^{IEC\text{-}KO}$ (IKO) mice than WT mice (means with different letters are significantly different by post hoc testing, 4 hr fast, n=5−8, mean ± s.e.m, two-way ANOVA, * signifies p<0.05). (**B**) Female mice showed no changes in fasted plasma TG or NEFA (n=8−9). (**C**) NEFA are also higher in postprandial plasma of male CD CAV1$^{IEC\text{-}KO}$ mice compared to WT controls and (**D**) show a greater fold decrease upon feeding relative to fasting (n=6−8, mean ± s.e.m, student's t-test, * signifies p<0.05). (**E**) Lipids measured by HPLC in plasma of male mice fasted 4 hr. There are significant effects of diet for all and, for palmitoleic and palmitic acid, the interaction between diet and genotype (n=6, mean ± s.e.m, two-way ANOVA, means with different letters are significantly different by post hoc testing, means with different brackets show only a diet effect). (**F**) Lipids measured by HPLC in liver of male mice fasted 4 hr (n=5, mean ± s.e.m, student's t-test, * signifies p<0.05). (**G**) Cholesterol oleate measured by HPLC in white adipose tissue of male mice fasted 4 hr (n=5, mean ± s.e.m, student's t-test, * signifies p<0.05).

Figure 6.

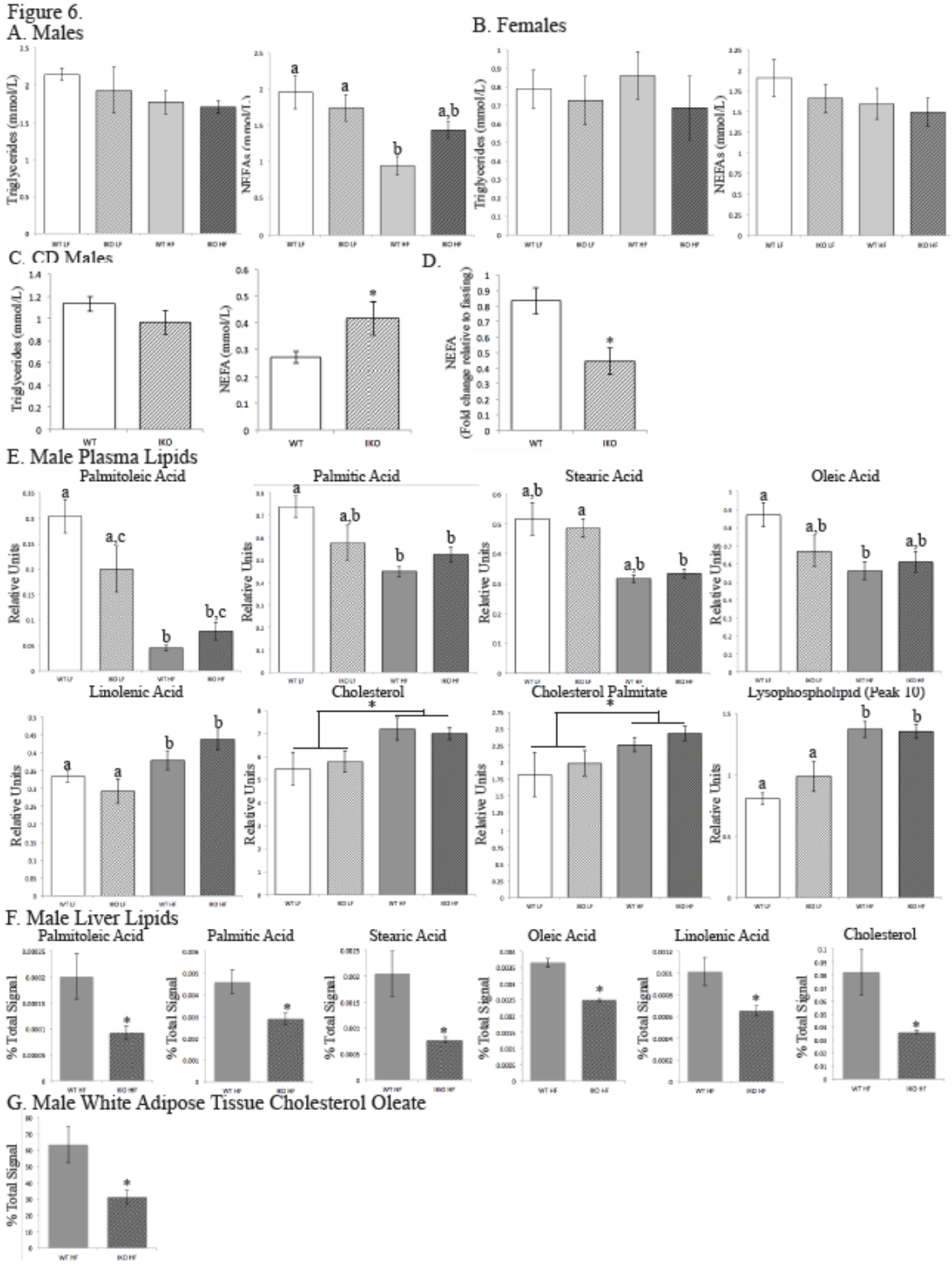
A. Males
B. Females
Triglycerides (mmol/L)
NEFAs (mmol/L)
C. CD Males
D.
NEFA (mmol/L)
NEFA (Fold change relative to fasting)
WT
IKD
E. Male Plasma Lipids
Palmitoleic Acid
Palmitic Acid
Stearic Acid
Oleic Acid
Linolenic Acid
Cholesterol
Cholesterol Palmitate
Lysophospholipid (Peak 10)
Relative Units
F. Male Liver Lipids
% Total Signal
G. Male White Adipose Tissue Cholesterol Oleate

HPLC Lipidomics

To investigate changes in the levels of specific species of plasma NEFA and cholesterol esters we performed a lipidomics study. Using HPLC, we measured the relative levels of several major plasma lipids including 8 FA species, free cholesterol, two cholesterol esters (-oleate and -palmitate), and 5 putative lysophospholipids in the plasma of $CAV1^{IEC\text{-}KO}$ and $CAV1^{fl/fl}$ WT male mice (16 wk HFD or LFD, 26 wk old, 4 hr fast). Strikingly, palmitoleic acid (16:1) is altered in the same pattern by diet and genotype as total NEFA (two-way ANOVA, effect of diet, $F(1,20)=41.70$, $p<0.0001$, effect of genotype, $F(1,20)=5.438$, $p=0.03$) (Fig. 6E). Similarly, palmitic acid (16:0) is significantly affected by both diet and the interaction between diet and genotype (two-way ANOVA, diet effect: $F(1,20)=10.77$, $p=0.0037$; interaction effect $F(1,20)=5.388$, $p=0.031$) (Fig. 6E). Stearic acid (18:0) is significantly elevated by HFD, compared to LFD, in $CAV1^{IEC\text{-}KO}$ mice (two-way-ANOVA, $F(1,20)=11.95$, $p=0.0025$) (Fig. 6E). Oleic acid (18:1) and linolenic acid (18:3) are both higher in LFD than HFD fed mice (diet effect found by two-way-ANOVA, oleic acid: $F(1,20)=7.664$, $p=0.0119$, linolenic acid: $F(1,20)=28.72$, $p<0.0001$) (Fig. 6E). Neither diet nor genotype affects any of the other FA measured (22:6, 20:4, and 18:2). In sum, palmitoleic, palmitic, stearic, and oleic acid may contribute to the observed elevation of total NEFA in LFD mice compared to HFD mice.

As described above, cholesterol assay kits found that diet affects total and esterified plasma cholesterol in $CAV1^{IEC\text{-}KO}$ mice (Fig. 4). HPLC analysis identified a direct contribution of free cholesterol (two-way ANOVA, effect of diet, $F(1,20)=8.693$, $p=0.008$) and cholesterol palmitate (two-way ANOVA, effect of diet, $F(1,20)=4.800$, $p=0.04$), which are both increased by HFD (Fig. 6E). Finally, one putative lysophospholipid (peak 10) which could not be identified with standards is also increased by HFD (two-way ANOVA, effect of diet, $F(1,20)=33.25$, $p<0.0001$) (Fig. 6E).

To investigate the mechanism underlying the elevation in plasma NEFAs in male HFD CAV1^{IEC-KO} relative to male HFD WT mice, liver and white adipose lipids were also measured by HPLC in male HFD mice. Four of the fatty acids that were decreased in CAV1^{IEC-KO} plasma, palmitoleic, palmitic, stearic, oleic, and linolenic acids, were also significantly decreased in the liver (Fig. 6F). It is striking that all of the fatty acids that are decreased in the liver of CAV1^{IEC-KO} mice, with the exception of stearic acid, have a trend to be increased in the plasma where total NEFAs are increased. Additionally, hepatic cholesterol is lower in HFD CAV1^{IEC-KO} mice (Fig. 6F). No differences were observed in triglycerides, cholesterol esters, or, similar to plasma, 22:6, 20:4, or 18:2 in the liver of HFD mice (data not shown). Of all these lipids, only cholesterol oleate varied in the white adipose tissue, showing a decrease in CAV1^{IEC-KO} mice (Fig. 6G; data for other lipids not shown).

Discussion

The global obesity epidemic has caused an explosion in the prevalence of metabolic diseases such as type II diabetes and cardiovascular disease. Intensive efforts have focused on the identification of therapeutic targets to better prevent and treat metabolic syndrome. Previous work had identified functional roles of adipocyte and endothelial CAV1 in susceptibility to diet-induced obesity (116), insulin resistance (120), and atherosclerosis (121). In this study we expanded upon these findings by visualizing the localization of enterocyte Cav1 and caveolar endocytosis and identifying a role for CAV1 in the intestinal epithelia in the regulation of plasma FA and LDL cholesterol, lipids that contribute to the development of several metabolic diseases.

Although it is known that CAV1 is expressed in the intestinal epithelium (126), the intracellular localization of this protein has remained ambiguous: lateral PM localization in Caco-2 colon-derived cells (150); either the brush border or lateral and basolateral PM localization in Caco-2 cells depending on the fix, permeabilization method, and antibody used (126); lateral

membrane of T84 colon derived cells (127); cytoplasmic vesicles and lateral PM at adherens and tight junctions in mouse jejunum (129); low levels on the mouse small intestine brush border (130); cytoplasmic vesicles in mouse colon (132); deep apical tubules in pig small intestine (151); human small intestine cytoplasmic vesicles (128); and apical PM and cytoplasmic vesicles in *C. elegans* intestine (152). Here our *in vivo* study reveals that Cav1 localizes asymmetrically to lateral and basolateral enterocyte PM in larval zebrafish. CAV1 is a FA- and cholesterol-binding protein and caveolae can only form in lipid-rich PM regions. Although these lipid-rich regions do form on the enterocyte brush border (153), this membrane has a lipid composition distinct from the lateral and basolateral PM, with more glycolipids and less cholesterol and sphigomyelin (154). It is possible that the relative scarcity of cholesterol in the brush border excludes CAV1 and caveolae from this PM. Unfortunately, the cellular localization of mouse CAV1 in the intestinal epithelia could not be determined due to non-specific antibody binding which we observed in enterocytes.

Fluorescently labeled endocytic cargos are valuable tools to visualize various types of endocytosis in cultured cells (138, 155). Here, we extended this technology to image the enterocyte PM regions that likely perform caveolae-mediated endocytosis *in vivo*. The results suggesting that caveolae-mediated endocytic activity in enterocytes is asymmetric points to a role for caveolae in vesicular transport between enterocytes and the body, but not the intestinal lumen. The optical clarity of larval zebrafish and advances in mouse vital imaging present the opportunity to extend this technique to investigations of caveolae- and clathrin-mediated endocytosis in a multitude of tissues in the context of health or disease.

Prior studies have reported increased fasting plasma cholesterol in male $CAV1^{KO}$ mice, largely consisting of elevations in VLDL and LDL cholesterol resulting from adipocyte lipid storage defects and decreased aortic and hepatic LDL uptake (117, 118). Our studies find that the intestinal epithelium does not mediate these changes, as we did not observe differences in plasma cholesterol or cholesterol palmitate in $CAV1^{IEC\text{-}KO}$ mice. However, we did find that LDL

cholesterol levels were increased postprandially and decreased during fasting (when hepatic cholesterol is also decreased) in male HFD CAV1^{IEC-KO} mice; this is opposite of the pattern observed in CAV1^{KO} mice. Another striking observations is that male CAV1^{IEC-KO} mice have increased fasting plasma NEFA (HFD), mirrored by decreases in several hepatic fatty acids, and decreased postprandial NEFA (CD). The literature regarding the effect of total body CAV1 deletion on circulating FFA is conflicting, with reports of higher fasting and postprandial FFA (116, 124), decreased fasting FFA (123), or no changes (118).

First, we hypothesized that the changes in LDL cholesterol and FFA could be mediated by the cluster of differentiation 36 scavenger receptor (CD36). CD36 delays LDL clearance (156), so impairment of its function in CAV1^{IEC-KO} mice could accelerate LDL clearance, causing the observed decrease in fasting LDL cholesterol. Increased postprandial LDL cholesterol could also be explained, as CD36 facilitates cellular cholesterol uptake (157). Additionally, FFA could be increased due to impaired CD36 localization and function, since CD36 facilitates FA uptake (157, 158) and its deletion increases serum FFA (159). CD36 is highly expressed in the proximal intestine (160) and CAV1 is necessary for CD36 to properly localize to the PM of mouse

Figure S2 (next page). (A) Deletion of CAV1 does not affect CD36 localization in the intestinal epithelia. Representative images of CD36 immunofluorescence in the jejunum of HFD treated CAV1^{IEC-KO} and WT littermate mice show localization to the brush border and small, apical punctae of enterocytes. Mice were fasted 4 hr, jejunum was fixed in 4% PFA overnight at 4°C, imbedded in OCT, cut into 10 μ cryosections, treated with Diva Decloaker antigen retrieval, probed with primary anti-CD36 (AF2519, R&D Systems) and secondary donkey-anti-goat (A-11055, Life Technologies), and imaged on a Leica SP-5 confocal microscope with a 63x oil immersion objective. **(B)** Plasma albumin is not affected by diet or genotype in male CAV1^{IEC-KO} (IKO) and WT littermates fed LFD or HFD. Mice were fasted 4 hr, plasma was collected by cardiac puncture, and albumin was measured in duplicate with a BCG albumin assay kit from Sigma-Aldrich (mean ± s.e.m, n=7−9).

Figure S2.

B. Intestinal CD36 localizaiton

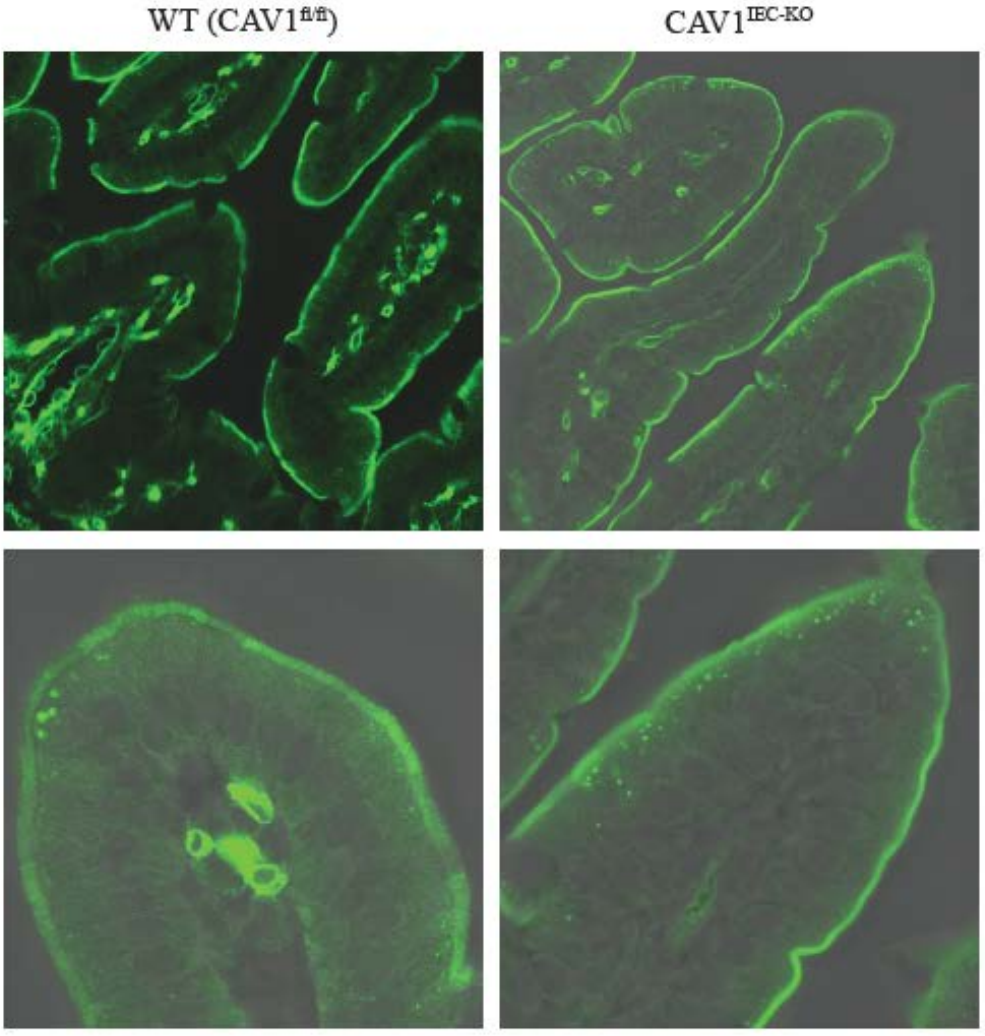

B. Plasma albumin

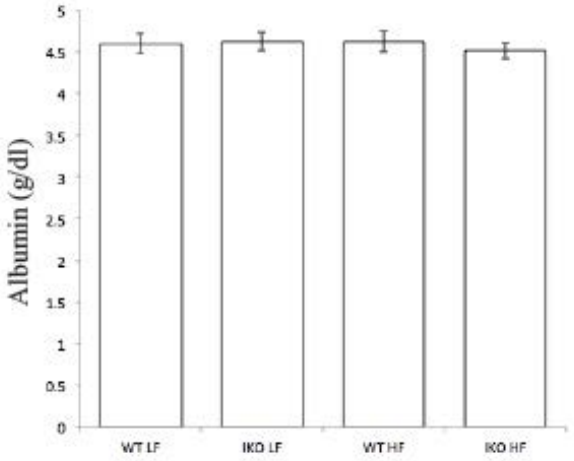

embryonic fibroblasts (161). Therefore, we speculated that CD36 PM localization and or expression may be dysregulated in CAV1^{IEC-KO} mice. However, contrary to the previous findings in mouse embryonic fibroblasts, no change in CD3 localization was observed in the intestinal epithelia of HFD treated CAV1^{IEC-KO} mice (Fig. S2A) and no decrease in mRNA or protein expression were observed (data not shown). In support of this conclusion, it would be expected that hepatic cholesterol would increase if the CD36-medated LDL clearance delay was perturbed, but instead HPLC analysis found a decrease in hepatic cholesterol.

Second, changes in circulating FFA in CAV1^{IEC-KO} mice could be mediated by changes in intestinal albumin uptake. Circulating FFA are transported by albumin, as much as 18% of which is absorbed and catabolized by the intestine (162). Indeed, we showed that Alexa Fluor-albumin is internalized by caveolae on the basolateral PM of enterocytes. If this were true a concomitant increase in plasma albumin would be expected, however this was not observed (Fig. S2B). As circulating albumin levels are tightly regulated, this hypothesis cannot be ruled out lacking direct measurement of albumin flux from the liver. Nonetheless, in further support of our conclusion, increased postprandial plasma lipids likely do not result from altered intestinal processing because no changes in serum NEFA or TG were observed by an oral lipid tolerance test (Fig. S3).

Third, we hypothesized that CAV1^{IEC-KO} mice may have decreased intestinal insulin signaling, and thus insulin stimulated plasma FA uptake, underlying the observed increase in circulating NEFA. This hypothesis is supported by the fact that insulin signaling is present in the intestine (163), the insulin receptor localizes to caveolae (164), and that global CAV1 knockout mice are insulin resistant (120). Substantiating this hypothesis insulin receptor mRNA is significantly decreased in the jejunum of CAV1^{IEC-KO} mice compared to controls (Fig. S4), but no change in insulin receptor subunit β protein was observed by Western blot (data not shown). Importantly, there may be a non-IEC autonomous mechanism (insulin signaling or otherwise) by which hepatic fatty acid uptake is decreased or secretion is increased leading to the observed

Figure S3.

A. Males

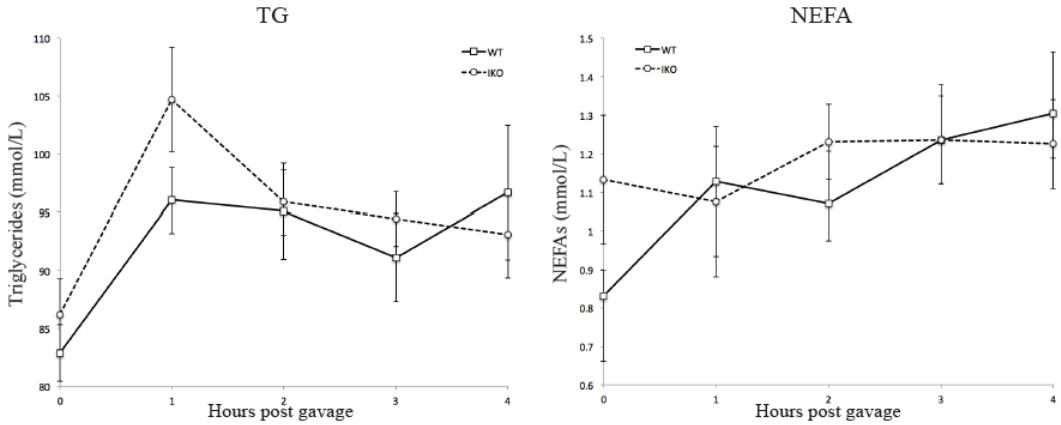

B. Females

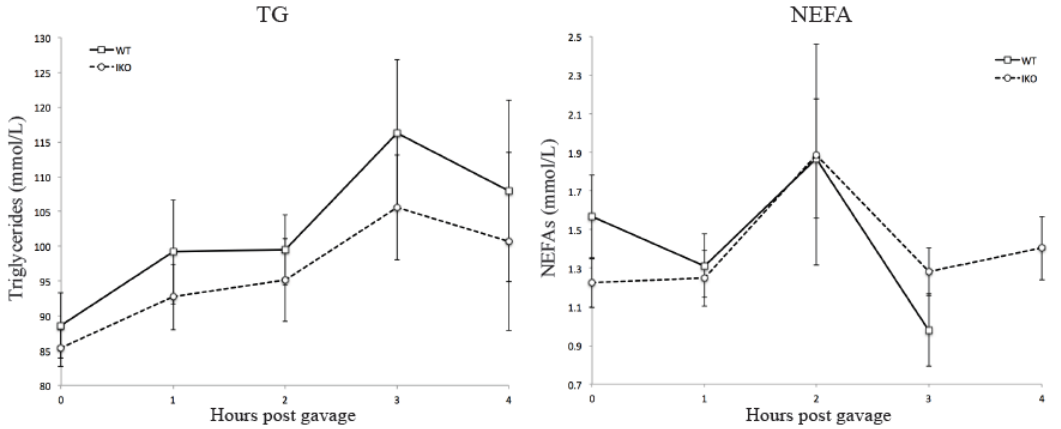

Figure S4.

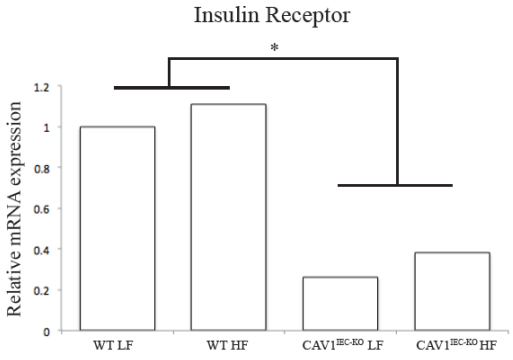

Figure S3. Lipid tolerance test show no change in serum TG or NEFA in CAV1^{IEC-KO} mice following emulsified lipid gavage. Male and female CAV1^{IEC-KO} (IKO) and WT littermates were fed CD and fasted 16 hr prior to gavage (n=7−9).

Figure S4. Deletion of Cav1 from the mouse intestinal epithelium (CAV1^{IEC-KO}) decreases insulin receptor expression. Insulin rector mRNA is decreased in the jejunum of CAV1^{IEC-KO} mice compared to wild type (WT) littermates. Means, 2-way ANOVA, significant effect of genotype p=0.0106, F(1,26)=7.595), n=6-9.

decrease in several hepatic fatty acids and corresponding increase in circulating NEFA. Similarly, loss of CAV1 in IEC may underlie a non-cell autonomous mechanism by which hepatic cholesterol is decreased, limiting the amount of LDL that can be secreted, causing the decrease in LDL-C observed in CAV1^{IEC-KO} mice.

HPLC determined that palmitoleic and palmitic acid contribute to the overall increase in fasting NEFA observed in HFD CAV1^{IEC-KO} mice. Palmitoleic acid is an omega-7 mono-unsaturated FA that is enriched in endothelial caveolae (165). If palmitoleic acid is also preferentially carried in enterocyte caveolae, it follows that loss of CAV1 could result in decreased palmitoleic acid uptake, and the observed plasma elevation. Further investigation of the detailed mechanism would be of interest since palmitoleic acid is a bioactive lipid: dietary supplementation has plasma lipid lowering, anti-diabetic, and anti-inflammatory activity (166), but elevated plasma palmitoleic acid is correlated with increased heart failure (167) and non-alcoholic fatty liver disease (168). It is possible that no influence of genotype on plasma palmitoleic acid levels in LFD mice was found simply because it comprises a much smaller proportion of the diet (0.04% of total LFD vs. 0.44% of total HFD by mass). Caveolae are also enriched in palmitic acid (169) so plasma palmitic acid may in higher in CAV1^{IEC-KO} than WT mice due to the mechanism proposed above. Since CAV1 is palmitoylated (170), decreased activity in this pathway may contribute to the plasma palmitic acid elevation.

Finally, the sexual dimorphism observed in the changes in plasma lipids in CAV1^{IEC-KO} mice must be addressed. It is well established that male and female animals have metabolic differences; in C57BL/6J mice, this includes differences in lipid and fatty acid metabolism gene expression in multiple tissues (171). Moreover, sex-specific metabolic differences have been observed previously in global CAV1 KO mice: decreased body mass on chow diet compared to WT in male, but not female, mice and increased food intake relative to WT in female, but not male, mice (116). However, neither sex had increased circulating free fatty acids compared to WT, and LDL cholesterol was only measured in male mice, where it was increased compared to

WT (116). In contrast to this previous study, we report that CAV1^{IEC-KO} male, but not female, mice were protected from the HFD-induced increase in plasma LDL cholesterol observed in WT. Although the mechanism for this difference is unknown, it is possible that sexually dimorphism in estrogen receptor signaling underlies this difference. When estrogen binds the estrogen receptor α (ERα) transcription factor, ERα activates transcription of the LDL receptor (LDLR), which takes up LDL from the circulation (172). CAV1 has been shown to potentiate the action of ERα in cultured cells (173). Additionally, female mice of mixed genetic background (129/Pas x C57BL/6J, ~90% C57BL/6J) have higher *Ldlr* and *Cd36* hepatic gene expression compared to males (174). Therefore, since estrogen levels are higher in females, differences in estrogen-stimulated LDLR transcription and subsequent cellular uptake may underlie the observed sex-specific differences in LDL cholesterol in CAV1^{IEC-KO} mice. Furthermore, female CAV1^{IEC-KO} mice had significantly increased HDL cholesterol on HFD compared to LFD; this difference was not observed in WT females, and the trend was non-significant in males. These findings are consistent with Link et al.'s report that mice with two X chromosomes have higher HDL cholesterol levels than XY mice (175). The observed sexual dimorphism does not preclude intestinal epithelial CAV1 as a potential therapeutic target for metabolic disease as many pharmaceuticals currently in use have sexually dimorphic actions, including the LDL cholesterol lowering drug fenofibrate (176). Nor does the modest decrease in LDL cholesterol preclude intestinal epithelial CAV1 as a therapeutic target, since even a 1% reduction in LDL cholesterol leads to a 1% decrease in cardiovascular disease risk (177).

In conclusion, this study demonstrated that CAV1 localizes to, and caveolar endocytosis occurs on, the lateral and basolateral PM of intestinal enterocytes. Although the detailed cellular mechanism remains to be elucidated, it is clear that CAV1 on enterocyte basolateral membranes influences circulating levels of LDL cholesterol and NEFA, specifically palmitoleic and palmitic acid. Elevated plasma FA and LDL cholesterol are associated with metabolic disease, including type II diabetes and cardiovascular disease. The results of this study indicate that CAV1 in the

intestinal epithelium may serve as a therapeutic target to lower circulating FA and LDL cholesterol and prevent disease in males.

Experimental Procedures

Generation of transgenic zebrafish

Zebrafish research was approved by the Carnegie Institution Department of Embryology IACUC Committee (protocol #139). Zebrafish were housed at 28°C with a 14:10 light:dark cycle. *Tg(hsp70l:cav1-eGFP)* zebrafish were created with the tol2-Gateway system (178). Zebrafish *cav1* was cloned from Image Consortium plasmid #3719638 (fb95c12) and Gateway cloning constructed *hsp70l:cav1-eGFP*: the zebrafish heat shock cognate 70-kd protein, like (*hsp70l*) promoter driving *cav1* tagged with eGFP (provided by Chi-bin Chien). This plasmid was injected with tol2 transposase for genome integration with a microforged glass needle (P-97 Flaming/Brown micropipette puller, Stutter Instruments, Novato, CA) connected to a nitrogen gas pressure injector (PLI 100, Harvard Apparatus, Cambridge, MA) into 1−2 cell zebrafish embryos (AB background). F0 larvae were heat shocked (45 min, 37°C, in 15 ml embryo media (EM)) at 6 day post-fertilization (6 dpf) and screened for mosaic Cav1-eGFP expression 4−6 hours later. Three independent stable lines were established and all further experimentation was undertaken in stable transgenic animals.

Live imaging of zebrafish larvae and quantification of fluorescence

Approximately 24 hr prior to imaging larvae were heat shocked as described above to induce Cav1-eGFP expression. Larvae were anesthetized with tricaine (Sigma-Aldrich, St. Louis, MO) and mounted in 3% methyl cellulose (Sigma-Aldrich, St. Louis, MO) under a coverslip (28). Live *Tg(hsp70:cav1-eGFP)* larvae were imaged on a SP-2 confocal microscope (Leica

Microsytems, Deerfield, IL) with an argon laser under a 63x oil immersion objective. Images were collected as 12 bit and analyzed with Metamorph software (Molecular Devices, Sunnyvale, CA). Regions of the brush border, lateral, and basolateral PM, as well as intracellular regions, were outlined for quantification of mean fluorescence intensity (3 regions of interest for each cellular area, 3 images per fish, 3 fish per experiment, for a total of 3 experiments or 9 fish).

Immunofluorescence and Electron Microscopy

Larval (6 dpf) zebrafish and intestines from adult zebrafish and were collected for IF and EM. Prior to euthanasia adult fish were fed shellfree *Artemia* (decapsulated, non-hatching; INVE Aquaculture, Ogden, UT) and Hikari Micropellets (Aquatic Eco-systems, Apopka, FL) twice daily; adults used for EM fed on a lipid-rich, hard-boiled chicken egg yolk for 1 hr *ad lib*; larvae studied were lecithotrophic (6 dpf) and thus were not provided exogenous food. IF samples were fixed in 4% paraformaldehyde in PBS overnight at 4°C, embedded in paraffin and 10 µ slices were mounted on positively charged slides. IF was carried out on zebrafish using an antibody to CAV1 (#610059, BD Transduction Labs, Lexington, KY) and Alexa Fluor 488 goat-anti-rabbit IgG (#A-11008, Invitrogen, Carlsbad, CA). Completed IF sections were mounted with Fluoromount-G (SouthernBiotech, Birmingham, AL) and imaged with a 63x oil immersion objective and an argon laser on an SP-5 confocal microscope (Leica Microsytems). EM samples were fixed in 3% glutaraldehyde (Electron Microscopy Sciences, Hatfield, PA) and 1% formaldehyde, post-fixed in reduced osmium (Electron Microscopy Sciences), stained with uranyl acetate (Fisher Scientific), embedded in Epon 812 resin (Ladd Research Industries, Williston, VT), and imaged on a Technai-12 electron microscope (FEI, Hillsboro, OR) with a 794 multiscan camera (Gatan, Pleasanton, CA). Mouse CAV1 IF was attempted on paraffin sections and cryosections of jejunum collected after a 4 hr fast, but non-specific fluorescence was observed in enterocytes, even in the negative control, global CAV1 KO mice. The antibodies tested were: BD Biosciences/Transduction labs #610059, 610057 and 610406, Santa Cruz Biotechnology #sc-894,

Abcam #ab2910, and Cell Signaling # 3238s. The antigen retrieval methods tested were Tris-EDTA buffer, sodium-citrate buffer, and Diva Decloaker (Biocare Medical, Concord, CA).

Imaging fluorescently labeled endocytic cargos *in vivo*

WT Larvae (6 dpf) were anesthetized in tricaine and mounted in 1.2% low melt agarose (Sigma-Aldrich) in EM. A microforged glass needle was loaded with (4,4-difluoro-4-bora-3a, 4a-diaza-S-indacene)-*l*-threo-lactosylceramide (BODIPY-*l*-LacCer)) (provided by David Marks) or BODIPY-*d*-erythro-LacCer (#895279, Invitrogen) at a concentration of 2.5 µg/µl in 30% ethanol and 70% embryo media, or Alexa Fluor-594-albumin (#A13101, Fisher Scientific, Pittsburgh, PA) at a concentration of 5 µg/µl in PBS. A nitrogen-pressured injection rig was used to inject 2 nl to the basolateral side of the intestine or into the intestinal lumen. Larvae were freed from the agarose, allowed to recover for 30 min (LacCer) or 1 hr (albumin) while swimming freely, re-anesthetized, mounted in 3% methyl cellulose under a coverslip, placed on ice to stop endocytosis (179), imaged, and the same sample size was analyzed with Metamorph software as described above.

Breeding *CAV1*$^{IEC\text{-}KO}$ mice

Mouse research was approved by the Carnegie Institution Department of Embryology IACUC Committee (protocol #156). Mice were housed at 20-21°C with a 12:12 light cycle. Mice with a floxed *Cav1* allele (provided by Michael Elliot) (146) were crossed with Tg(Vil-cre)997Gum/J mice (#004586, Jackson Labs, Bar Harbor, ME) which express Cre recombinase specifically in the intestinal epithelium, producing mice lacking *Cav1* specifically in the intestinal epithelium (CAV1$^{IEC\text{-}KO}$)(back crossed to C57BL/6 6 times) (Fig. 1A). All experiments were performed with CAV1$^{IEC\text{-}KO}$ vs. Cav1$^{fl/fl}$ (WT) littermates.

Mice were genotyped for floxed *Cav1* (350 bp band following PCR with F1:TTC TGT GTG CAA GCC TTT CC and R1:GTG TGC GCG TCA TAC ACT TG) and Vil-Cre PCR (1,100

bp band following PCR with F: GTG TGG GAC AGA GAA CAA ACC and R:ACA TCT TCA GGT TCT GCG GG). The occurrence of Cre recombination in the intestine of $CAV1^{IEC\text{-}KO}$ mice was verified by the presence of a 350 bp band (F1 primer above, R2: GGG GAG GAG TAG AAG GTG GC) (146) on genomic DNA isolated from whole jejunum segments by NaOH extraction (180). *Cav1*^{tm1Mls} ($CAV1^{IEC\text{-}KO}$) mice lacking functional *Cav1* in all tissues were used as controls (#007083, Jackson Labs, Bar Harbor, ME).

RT-PCR

Cav1 and *Cav2* mRNA levels were measured in whole jejunum by RT-PCR: mRNA was isolated with Trizol (Invitrogen), cDNA was synthesized with AMV reverse transcriptase (New England Biolabs, Ipswich, MA), and RT-PCR was run with the PrimePCR SYBR Green assay for mouse *Cav1* and *Cav2* according to the manufacturer's instructions (#100-25636, BioRad Laboratories, Hercules, CA).

Western Blot

CAV1 protein was measured by Western blot as previously described (181). Briefly, cytosolic fractions of jejunum were run on denaturing SDS-Page gels with a Mini-Protean system (BioRad Laboratories), transferred to nitrocellulose, blocked with blocking grade blocker (BioRad Laboratories), and probed with antibodies to CAV1 (#610059, BD Transduction Labs, Lexington, KY), α-tubulin (#T6199, Sigma-Aldrich), goat-anti-rabbit IgG-HRP (#170-6515, BioRad Laboatoris), and goat-anti-mouse IgG-HRP (#170-6516, BioRad Laboratories). Protein expression was imaged by chemiluminescence (SuperSignal West Pico Chemiluminescent Substrate, Pierce, Rockford, IL). Data from 3 western blots, with 5 WT and 5 IKO mice each, was analyzed with ImageJ software (NIH, Bethesda, MD).

Experimental diets

Upon weaning, mice were fed CD *ad lib* (#7012, Harlan Teklad, Fredrick, MD). At 10 wk of age, mice were either continued on CD, or fed a 60% HFD or 10% fat, nutrient-matched LFD (#D12492 and #D12450J respectively, Research Diets, New Bruswick, NJ) *ad lib*. Mice fed HFD and LFD were massed weekly until euthanasia at 26 wk; n=10−15 mice per diet.

Plasma cholesterol and lipid analysis

Mice were euthanized by CO_2 inhalation and blood was collected by cardiac puncture. Serum was collected by centrifugation (15 min, 2,000 x g, 4°C) after allowing blood to clot on ice. Plasma was collected by centrifugation (15 min, 2,000 x g, 4°C) in EDTA-treated tubes (Sarstedt, Numbrecht, Germany). All serum and plasma samples were snap frozen and stored at -80°C. Kits were used to measure total cholesterol (Infinity Total Cholesterol, Fisher Scientific), free cholesterol (Free Cholesterol E, Wako Diagnostics, Richmond, VA), HDL cholesterol (HDL-C E, Wako Diagnostics), LDL cholesterol (LDL-C Reagent L-type, Wako Diagnostics), NEFA (HR Series NEFA-HR(2), Wako Diagnostics), and TGs (Infinity Triglycerides, Fisher Scientific) according to the manufacture's directions. For HFD and LFD male mice n=5−8, for HFD and LFD female mice n=8−9; and for CD male mice, n=6−8.

HPLC

HPLC was implemented to measure levels of specific plasma lipids. Lipids were extracted from plasma (50 µl), liver (10-50 mg), and white adipose tissue (15-40 mg) using a modified Bligh-Dyer procedure (28), dried under vacuum, and resuspended in the injection solvent HPLC-grade 2-propanol.

HPLC was performed using a LPG-3400RS quaternary pump, WPS-3000TRS autosampler, TCC-3000RS column oven, Accucore C18 column (150 x 3.0 mm, 2.1 µm particle size) and Dionex Corona Veo charged aerosol detector (all from Thermo Scientific). Lipids were

separated over 80 min in a multistep gradient as follows: 0-5 min at 0.8 mL/min in 98.0% mobile phase A (methanol-water-acetic acid, 750:250:4) and 2.0% mobile phase B (acetonitrile-acetic acid, 1000:4), 5-35 min at 0.8-1.0 mL/min, 98.0-30% A, 2.0-65.0% B, and 0-5.0% mobile phase C (2-propanol), 35-45 min at 1.0 mL/min, 30%-0% A, 65.0%-95.0% B, and 5.0% C, 45-73 min at 1.0 mL/min, 95.0-60.0% B and 5.0-40.0% C, and 73-80 min at 1.0 mL/min, 60.0% B, and 40.0% C (adapted from pers. corr. with Marc Plante, Thermo Scientific). Following the analytical portion of the gradient, the column was washed for 20 min with 100% mobile phase C at 0.4 mL/min, then returned to 98% A and 2% B at 0.8 mL/min for re-equilibration. Injection volume was between 5 and 25 μL and was adjusted for each sample to produce optimum peak shape for quantitation. The autosampler tray was maintained at 20.0^{o}C and the column oven temperature at 40.0^{o}C.

Chromatographic peaks were identified by comparison with standards (Sigma-Aldrich). Early-eluting peaks not identified as FA were confirmed as polar lipids by acetone precipitation (adapted from (95)), and based on their retention times when compared with those of polar lipid standards, were determined to most likely be lysophospholipids (data not shown). Quantitative comparison of the relative amounts of lipid species of interest was performed blinded using Chromeleon 7.2 (Dionex, Sunnyvale, CA). Peak baselines were drawn manually and areas (in picoamperes (pA)*min) were determined automatically. For plasma samples, all peak areas were divided by the area of the second lysophospholipid peak in the same sample. This lipid was chosen as it varied the least among all of the samples after accounting for injection volume. For comparison between samples, lipid amounts are expressed as [peak area (pA*min)]/[area of peak 2 (pA*min)]. For liver and white adipose samples, all peak areas were normalized to percent of total signal to control for unequal extraction efficiencies and differences in starting tissue mass between samples.

Glucose metabolism

Blood glucose was measured in mice fasted 4 hr by tail bleed using a glucometer (AlphaTRAK glucose meter, VWR, Radnor, PA) just prior to euthanasia (n=6−10). For IP GTT, mice fasted 4 hr were administered 2 g/kg sterilized glucose in water IP and blood glucose was measured from the tail vein by glucometer at 0, 15, 30, 60, and 120 min (n=9−14). For OGTT, the same dose of sterile glucose was administered by gavage and blood glucose was monitored as described (n=7−9). ITT was performed by administering mice IP insulin (#12585-014, Gibco, Gaithersburg, MD) at a dose of 0.76 U/kg for LFD mice and 1 U/kg for HFD mice; blood glucose was measured as described for GTT (n=7−13). GTT and ITT results were analyzed by two-way, and OGTT by one-way repeated measures ANOVA followed by Tukey's post hoc test.

Lipid tolerance test

Male and female CAV1^{IEC-KO} and WT littermates were housed on CD until 12 wk old, fasted 16 hr, and gavaged with 10 µl/g body mass 20% emulsified Intralipid (soybean oil) (Sigma). Serum was collected from tail bleed at 0, 1, 2, 3, and 4 hours post gavage. TGs and NEFA were assayed as described above.

Statistics

Differences in Cav1-eGFP fluorescence intensities were compared with a one-way ANOVA followed by Tukey's post hoc test. Student's t-test was used to compare endocytic cargo membrane fluorescence and RT-PCR measurements of jejunal mRNA. Western blot data from each of 3 blots were adjusted by expression of the loading control and expressed relative to WT levels, averaged together, and compared by Student's t-test. Differences in BM were compared by linear regression. Plasma lipids identified by HPLC were compared by two-way ANOVA followed by Tukey's post hoc test. Liver and white adipose lipids measured by HPLC were compared by Student's t-test. All data analyzed by ANOVA were first confirmed for

homogeneity of variance by Bartlett's or Brown-Forsythe tests. Statistics were performed with Prism software (GraphPad, La Jolla, Ca).

Acknowledgements

The authors are grateful to Michael Elliot, David Marks, Michel Bagnat, and the late Chi-bin Chien for experimental reagents and animals, to Michael Wolfgang, Guang William Wong, and Alex Bortvin for consultation on experimental design, to Blake Caldwell, Eugenia Dikovsky, Amy Kowalski, Mike Sepanski, and Erin Zeituni for technical assistance, and to Nada Abumrad for IF advice. This study was funded by NIDDK-NIH F32DK096786 (J.P.O.), RO1DK093399 (S.A.F.), and RO1GM63904 (The Zebrafish Functional Genomics Consortium: PI Stephen Ekker and Co-PI S.A.F). This content is solely the responsibility of the authors and does not necessarily represent the official views of NIH. Additional support for this work was provided by the Carnegie Institution for Science endowment and the G. Harold and Leila Y. Mathers Charitable Foundation (S.A.F).

Competing Interests

The authors have no financial or non-financial competing interests to declare.

Author Contributions

Conceptualization, J.P.O and S.A.F.; Methodology, J.P.O., V.Q.R., and S.A.F.; Formal Analysis, J.P.O, J.L.A., and V.Q.R.; Investigation, J.P.O., M.C.S., and V.Q.R.; Writing − Original Draft, J.P.O. and V.Q.R.; Writing − Review & Editing, J.P.O., J.L.A., S.A.F, M.C.S., and V.Q.R.; Funding Acquisition, J.P.O. and S.A.F.

CHAPTER 4 – ETHANOL ALTERS DIETARY LIPID METABOLISM IN LARVAL ZEBRAFISH

Introduction

Potential crosstalk between ethanol metabolism and dietary fatty acid metabolism

Cirrhosis is characterized by advanced steatosis, fibrosis, and inflammation of the liver that often leads to liver failure, can progress to hepatocellular carcinoma, and is the twelfth leading cause of death in the United States (182). Cirrhosis and the progressively worse conditions that lead to it are known collectively as Alcoholic Fatty Liver Disease (AFLD), and the progression from simple steatosis (triglycerides as > 5% of the liver mass) to steatohepatitis (steatosis with inflammation) to cirrhosis (largely irreversible fibrosis of the liver) is driven in part by the accumulation of damage from repeated acute alcohol-induced injuries: Metabolism of alcohol in hepatocytes releases toxic byproducts such as acetaldehyde and reactive oxygen species, causing inflammation. Ethanol is also associated with mitochondrial stress and reduced catabolic capacity – this combined with the fact that ethanol itself can be used to synthesize saturated fatty acids leads to hepatic steatosis (183). Prolonged hepatic inflammation can result in fibrosis, which occurs when hepatic stellate cells secrete extracellular matrix components into the liver in response to tissue damage (184). In studies performed by Lieber et al, hepatic steatosis and inflammation were significantly increased in human subjects given large amounts of ethanol for just two days (185). Although the role of alcohol overconsumption alone in both acute and long-term liver injury has been studied extensively, progression of AFLD does not correlate perfectly with the amount or duration of ethanol exposure. Furthermore, the effect of light to moderate regular drinking and/or infrequent binge drinking on the progression of non-alcoholic fatty liver disease (NAFLD) is poorly understood: it is known that even in a healthy liver ethanol promotes storage of dietary fatty acids in hepatocyte lipid droplets over oxidation, but potential variations in the effect of ethanol on different fatty acids both in terms of catabolism and

partitioning into complex lipids have not been characterized. Since 70% of adults drink at least occasionally (NIAAA, 2012), it is important to understand how light and/or infrequent ethanol intake may influence both fatty acid metabolism in the absence of chronic disease, and the progression of non-alcoholic fatty liver disease.

The zebrafish is an established model system for ethanol research

Both adult and larval zebrafish metabolize ethanol and can develop hepatic steatosis, inflammation, and fibrosis as a result of ethanol exposure (186, 187). They express analogs of genes important in ethanol metabolism including *adh1* (alcohol dehydrogenase), *aldh* (aldehyde dehydrogenase), and *cyp2e1* (a cytochrome P450 family member involved in xenobiotic metabolism) (186). Adult male zebrafish raised continuously in a 1% ethanol solution developed steatosis or steatohepatitis at 2 weeks, and hepatic fibrosis (collagen accumulation) occurred by 12 weeks of treatment (188). Larvae also exhibit acute alcohol-associated hepatic steatosis when treated with 2% ethanol for >18 hours during the last day of yolk absorption (starting at 4 dpf): neutral lipid accumulates in the liver (revealed by Oil red O staining of fixed larvae) and hepatomegaly occurs (186). In the three days following this single exposure to ethanol, larvae develop liver inflammation (e.g., expression of inflammatory cytokines is increased), oxidative stress (shown with the H2CDF ROS reporter and increased expression of *sodB* and other associated genes), hepatic stellate cell proliferation, and increased deposition of the ECM components collagen and laminin (186, 187).

Outstanding questions about the influence of ethanol on nutrient metabolism

Though it has long been known that ethanol influences lipid metabolism by driving accumulation of triglyceride in the liver, the specific details of potential interactions between ethanol metabolism and lipid metabolism are currently unknown. For example, though it is known that ethanol promotes fatty acid synthesis in the liver by activating SREBP-1c (189), the

potential role of specific dietary lipids in alcoholic hepatic steatosis has not been examined. Furthermore, as the byproducts of ethanol metabolism globally disrupt function, it is plausible that fatty acid metabolism would be disrupted in tissues that metabolize both ethanol and dietary nutrients. As described in Chapter 2, a strength of the larval zebrafish model is the ability to use the same fluorescent fatty acid reagents as metabolic labels for both live imaging and biochemical experiments. Here I have employed this technique to examine the influence of ethanol on both the deposition of dietary fatty acids and their products in the liver, and the partitioning of dietary fatty acids into complex lipids.

Methods

Zebrafish

Adult zebrafish and larvae were maintained as described in Chapter 2.

Ethanol treatment

Larval zebrafish were raised to 5 days post-fertilization when their yolk supplies were depleted. For all HPLC experiments, larvae were soaked in a solution of 1% ethanol (v/v) in embryo media for 20 hours at 25^{o}C (adapted from (186)). Ethanol concentrations were varied for confocal imaging experiments.

Fluorescent lipid feeding

For HPLC, larvae were fed BODIPY FL, -C5, -C12, or –C16 in a 5% chicken egg yolk emulsion as described in Chapter 2. In the most recent experiment (Figure 2), TopFluor-Cholesterol was added to the feed solution as a control for amount eaten and lipid extraction efficiency. (TopFluor-Cholesterol is not esterified during the first 18 hours after feeding; later time points were not examined (with Jessica Otis)).

Confocal microscopy

For live confocal imaging of the liver, larvae were fed BODIPY FL-C5 in a 5% chicken egg yolk emulsion as described in (28). Imaging was performed as described in Chapter 2.

HPLC-Fluorescence/CAD

HPLC-Fluorescence/CAD including sample preparation and data analysis was performed using the "B-C12" chromatography methods as described in Chapter 2.

Results

Larval zebrafish exhibit acute alcohol-induced hepatic steatosis

In previously published work, the standard ethanol dosage given to larval zebrafish to induce the hepatic injury response is immersion in 2% ethanol from 96 to 120 hpf (hours post-fertilization) (186, 190-192). This treatment has been useful for some applications such as detecting subtle ethanol-associated changes in gene expression (186, 187). However, overnight treatment of zebrafish larvae with 2% ethanol also causes gross morphological defects and impaired swimming behavior (186), which is a concern in nutritional experiments as the ability of the larvae to eat could be affected. Larval zebrafish were immersed overnight (20 hours) in a range of ethanol concentrations to identify the lowest ethanol dose that would consistently produce acute hepatic steatosis without altering feeding behavior. Following ethanol treatment, larvae were given a high-fat meal of chicken egg yolk emulsified with a fluorescently labeled fatty acid BODIPY FL-C5), and their livers were imaged by live confocal microscopy. Pretreatment with 1-1.5% ethanol resulted in significantly increased liver fluorescence, indicating an ethanol-associated increase in hepatic deposition of the fluorescent metabolic products of BODIPY FL-C5 (Figure 1). Pretreatment with 1% ethanol did not increase or decrease food

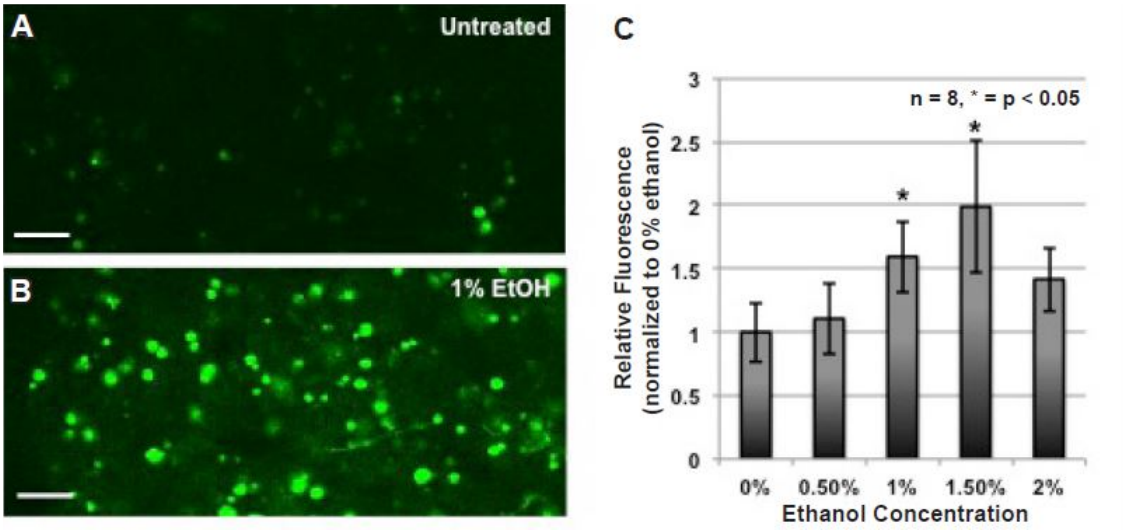

Figure 1. Acute hepatic steatosis is observed in the larval zebrafish after a single ethanol treatment. A) and B) Zebrafish larvae were raised to 6 dpf and then treated overnight with a range of ethanol concentrations. They were then fed an emulsion of fluorescent fatty acid (BODIPY FL-C5). After a 20 hour chase, hepatic steatosis was evaluated by live confocal imaging. 400x magnification, scale bars = 10μm. C) The extent of hepatic steatosis following ethanol treatment was quantitated by total liver fluorescence. Overnight immersion in a 1% or 1.5% ethanol solution before a meal containing fluorescent fatty acid resulted in a significant increase in hepatic BODIPY fluorescence (Student's T-test).

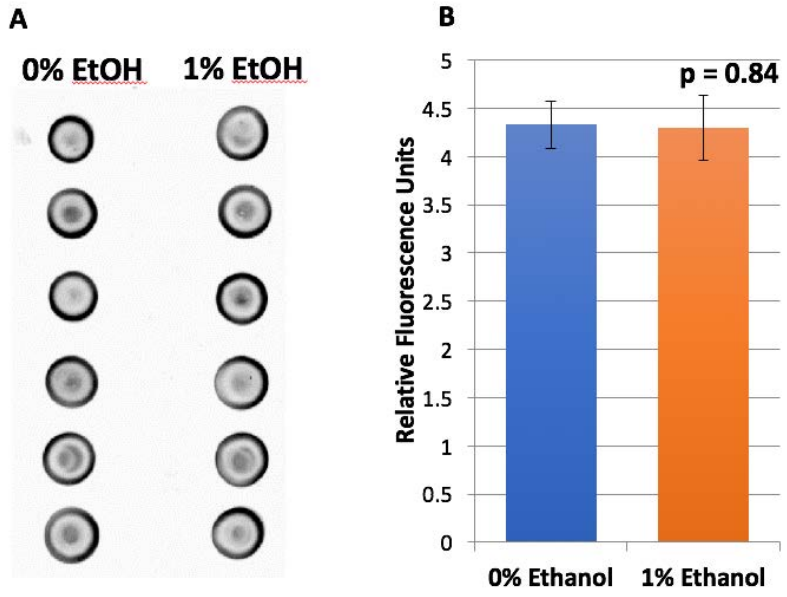

Figure 2. Overnight treatment with 1% ethanol does not significantly affect feeding. A) Zebrafish larvae were raised to 6 dpf, immersed in 1% ethanol for 20 hours, and fed an emulsion of BODIPY FL-C5 in a HF/HC meal. Total lipids (including intestinal contents) were extracted from groups of 15 larvae and spotted on a TLC plate. B) Total fluorescence of each spot in A) was quantitated. There was not a significant difference between ethanol-treated and untreated groups (Student's T-test, n = 6).

consumption (Figure 2).

Additionally, previous work by the Sadler Laboratory has shown that exposure of zebrafish larvae to 1% ethanol for 8 hours resulted in a tissue ethanol content of 0.20%, which is consistent with the average blood ethanol concentration of a human who has consumed three to four servings of alcohol (193, 194). Taken together, these results suggest that acute hepatic steatosis (and therefore, alcoholic liver injury) can be modeled in larval zebrafish by treatment with ethanol at a dose that does not alter feeding behavior and is physiologically comparable to ethanol consumption by humans. Furthermore, these results are the first to demonstrate that dietary fatty acids contribute to acute alcohol-induced steatosis.

Preprandial ethanol promotes channeling of dietary fatty acids into phospholipids

Treatment of 5 dpf larval zebrafish with 1% ethanol overnight before feeding fluorescent fatty acids in a HF/HC meal is associated with increased incorporation of BODIPY FL-C5 and BODIPY FL-C12 into one or more fluorescent phospholipid species each (Figures 3, 4). The specific identities of some of these phospholipids were determined through the LC-MS/MS experiments described in chapter 2: significant increases in PC(22:6, BODIPY FL-C5), PC(BODIPY FL-C12, 18:1), and PE(BODIPY FL-C12, 16:0) occur in larvae treated with ethanol before being fed BODIPY FL-fatty acids. Other BODIPY FL-C12 lipids quantitated in these experiments were identified as phospholipids or nonpolar lipids by acetone precipitation followed by HPLC, and Cholesteryl BODIPY FL-C12 (which did not change in response to ethanol) was identified using a standard (see Chapter 2). A time course experiment in which larvae were treated with ethanol, fed BODIPY FL-C12, and then sampled at intervals 6-22h post-feeding revealed that preprandial ethanol exposure is associated with a significant shift toward synthesis of phospholipid from dietary fluorescent fatty acids up to 16 hours post-feeding, with an average of 1.23-fold more fluorescent phospholipid (quantitated as a percentage of total fluorescence) in ethanol-treated larvae with a comparable decrease in triglyceride ($n = 3$, $p<0.05$, Student's T-test)

(Figure 4). Ethanol-treated larvae contained an average of 25% more PC(BODIPY FL-C12, 18:1) at 6, 9.5, and 16 hours; 39% more PE(BODIPY FL-C12, 16:0) at 6 and 16 hours, and 22% less PC(BODIPY FL-C12, 16:0) at 6 and 22 hours ($n = 3$, $p<0.05$, Student's T-test). Similar experiments performed with BODIPY FL-C16 showed no ethanol-associated changes in fatty acid partitioning, which is consistent with results obtained from BODIPY FL-C5 and –C12 as BODIPY FL-C16 contributes to a minimal amount of phospholipid. In the experiment in Figure 4, larvae were fed TopFluor-Cholesterol as a feeding control. This BODIPY-lipid is not degraded or esterified by larval zebrafish, and may be detected and quantitated by HPLC-Fluorescence in the same sample and experiment as the complex lipid products of BODIPY FL-C12. At 6 hours post feeding, ethanol-pretreated larvae contain 34% more TF-Chol and 35% more BODIPY FL-C12 per larva than controls ($p = 0.05$), while the total BODIPY FL signal does not vary between the two groups. At 9.5 hours post-feeding, the ethanol treated group contains 24% more BODIPY FL-C12 per larva ($p = 0.04$) and the total BODIPY FL signal per larva is 20% higher ($p = 0.003$). One possible explanation is that for both of these fluorescent lipids, a saturation point is reached and some is excreted without being absorbed. If ethanol slows intestinal peristalsis, then unabsorbed substrate in the intestinal lumen would result in a larger HPLC peak for either of these analytes. At later time points when the intestine is emptying, unabsorbed substrate would no longer be present in larval lipid extracts. It is also possible that ethanol pretreatment results in faster uptake of one or both of these fluorescent lipids into enterocytes. While the potential effects of preprandial ethanol on feeding, lipid absorption, and excretion require further study, the effect of ethanol on channeling of dietary fatty acids into phospholipid is evident no matter which quantitation method is used. Planned experiments in which I will investigate potential mechanisms for the effects of ethanol on fatty acid metabolism are discussed in the concluding chapter.

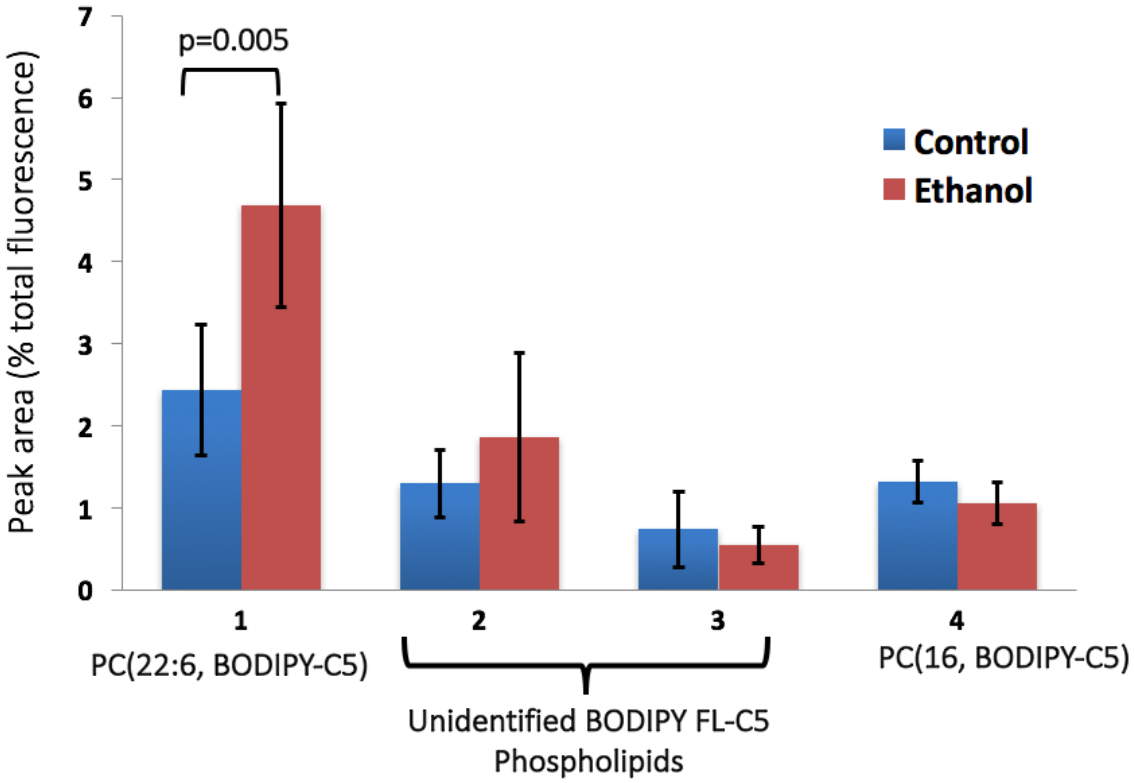

Figure 3. One of four BODIPY FL-C5 phospholipid products increases 1.9-fold with preprandial ethanol treatment. Larval zebrafish were treated overnight with 1% ethanol and then fed BODIPY FL-C5 in a HF/HC meal. Samples were taken for HPLC-Fluorescence 8 hours post-feeding, and all complex lipid products of BODIPY FL-C5 were quantitated. The amount of PC(22:6, BODIPY-C5) synthesized increased significantly with ethanol treatment but the other fluorescent phospholipids and all nonpolar BODIPY FL-C5 products did not change. (Nested ANOVA, df = 13)

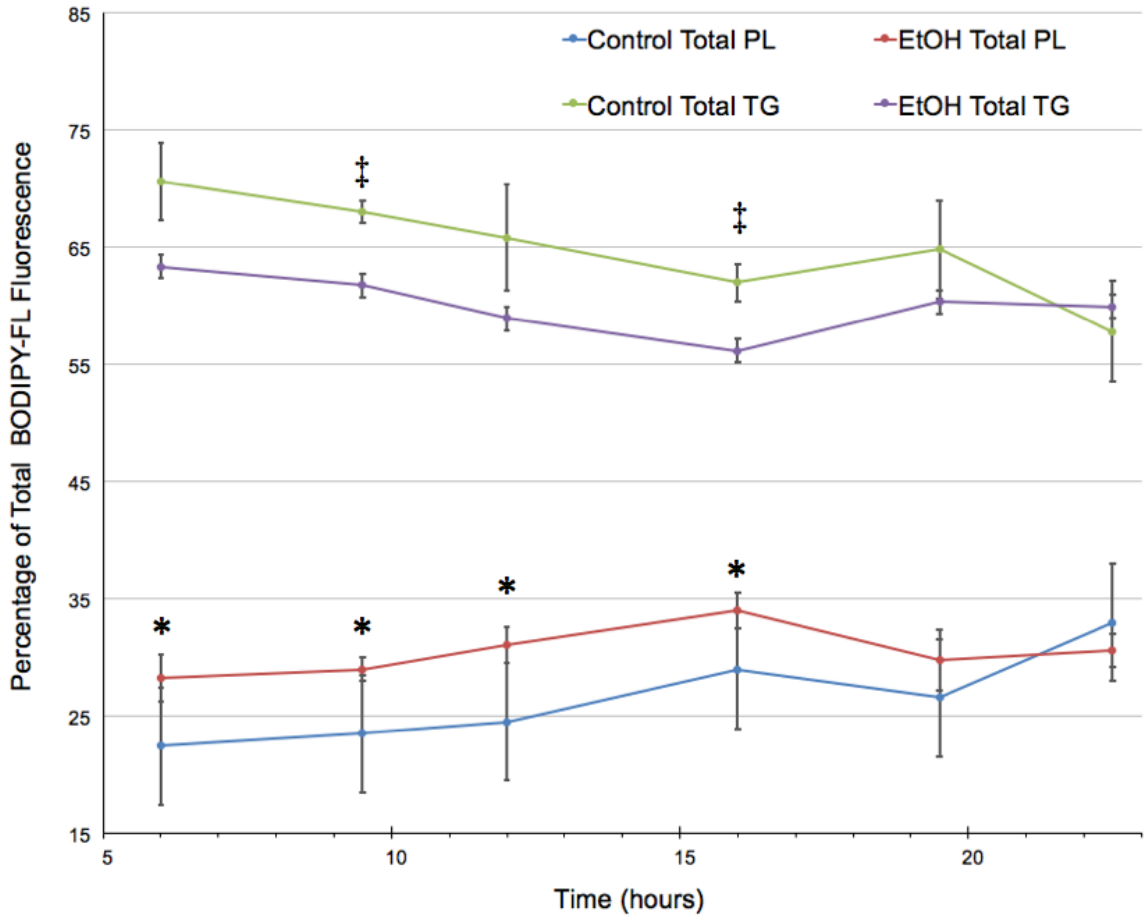

Figure 4. Preprandial ethanol treatment is associated with increased phospholipid synthesis from dietary fluorescent fatty acids. Larval zebrafish were treated overnight with ethanol, fed BODIPY FL-C12 in a HF/HC meal, and samples were taken for HPLC-Fluorescence over a 22-hour time course. * = Time points at which total phospholipids are significantly different between control and ethanol-treated groups. ‡ = Time points at which total triglycerides are significantly different between control and ethanol-treated groups. (Cholesterol BODIPY FL-C12 was measured as well and did not change with ethanol treatment.) (n = 3, Student's T-test, */‡: $p<0.05$)

FUTURE DIRECTIONS

LC-MS lipidomics and the zebrafish yolk as lipid metabolism model

Advances in the precision of LC-MS lipidomics have allowed quantitation of the changes in thousands of lipid species in the yolk and body of the developing zebrafish as the yolk is absorbed over the first five days of life. This model of lipid transport in a closed system presents an opportunity for investigation of roles of specific lipids in development. For example, there is a large increase in the molar amount of PC(18:2/20:4) in the yolk over the first 5 days of development. Phospholipids carrying 20:4 (arachidonic acid) are the precursor of eicosanoids, which are important signaling molecules. Potential roles for eicosanoids in yolk utilization could be investigated in this model. A larger question in the MS lipidomics field is the physiological significance of changes in rare lipid species; specifically what degree of variability is normal and what degree of change would merit follow-up to look for a biological effect.

Global changes in lipid classes over the course of yolk absorption also suggest avenues of future research. For example, the maternally-deposited yolk contains free cholesterol as well as cholesterol ester. As cholesterol esterification in cholesterol-absorbing cells such as enterocytes is a mechanism for detoxification of excess free cholesterol, the role of cholesterol ester in the yolk is unclear. From fertilization to 5 dpf CE moves from the yolk to the body but is not depleted. I hypothesize that when the yolk is fully absorbed at 5 dpf, an initial supply of free cholesterol is needed until *de novo* cholesterol synthesis can fulfill demand, and that this need is met by breakdown of CE absorbed from the yolk. Potential regulation of the relative amounts of triglyceride and cholesterol ester in lipid droplets and lipoproteins is not well-studied. As a larger structure rich in netural lipid the embryonic zebrafish yolk would be a good system in which to address the relative roles of these two classes of "energy storage" lipids.

Characterization of apolipoprotein expression and function in the zebrafish yolk has also raised questions that could be investigated further, such as what types of lipoproteins are secreted by the yolk and how closely they resemble lipoproteins produced by adult animals. This would be important for understanding the range and limitations of the yolk as a model of lipoprotein trafficking. Finally, the spatial expression patterns of apolipoprotein genes within the yolk suggest a functional regionalization of the yolk that is currently uncharacterized. It is possible that variation in apolipoproteins in the yolk is linked to regionalization of the developing intestine (195).

Dietary lipid processing in the larval zebrafish intestine

Although several families of transporters and lipid-binding proteins have been found to play a role in dietary lipid uptake and processing by intestinal enterocytes, their relative contributions to lipid absorption, the regulation of their activity, and how they may interact with each other have not been determined. For example, results presented in Chapter 2 suggest that cholesterol ester synthesis from dietary fatty acids is primarily regulated in response to availability of incoming free cholesterol, but the mechanism is unknown. It is also not clear whether the cholesterol transport protein NPLC1L1 is directly involved in interactions between fatty acid metabolism and cholesterol metabolism. There are multiple membrane-associated fatty acid transporters in enterocytes as well, including FATP4, CD36, and Cav1. The relative contributions of each of these proteins, non-caveolar endocytosis, and simple diffusion to dietary fatty acid uptake are not understood. Furthermore, unlike in the mammalian intestine where it localizes to the brush border, Cav1 is expressed only at the basolateral side of the enterocytes of larval zebrafish (62). The functional significance of this difference remains to be determined – palmitoleic acid is an important signaling lipid but it is not known whether the change in plasma palmitoleic acid concentration observed in Cav1 mutants is physiologically significant. Also, due to its subcellular location, I would not expect Cav1 to participate directly in dietary lipid uptake.

The mechanism for the effect of Cav1 deletion on plasma and tissue lipid composition is also unknown. I hypothesize that changes in albumin trafficking via Cav1 account for changes in lipid composition, as albumin is both a caveolar cargo and a fatty acid carrier.

Additionally, the functional role for specialization of proteins in the ACS and FABP (fatty acid-binding protein) families for different subclasses of fatty acids is also not fully understood. The ACSs that activate different fatty acids localize to different areas within the cell in mammals, but it is unknown whether this applies in zebrafish. As zebrafish express multiple paralogs of each ACS it would be interesting to see whether further functional and/or spatial specialization occurs.

Finally, the biology of lipid droplets in enterocytes is an area that lends itself to further exploration in the larval zebrafish. Zeituni and colleagues (2016) observed that just after feeding a large number of small lipid droplets form in the enterocytes of larval zebrafish and then fuse as they mature. Potential consequences of differences in lipid droplet size and number (vs. total volume of neutral lipid in the cell) are unknown. One way that ethanol could increase synthesis of phospholipid from newly absorbed dietary fatty acids in the intestine is by increasing lipid droplet number and decreasing average lipid droplet size. The physiological effects of variation in lipid droplet size in the intestine remain to be explored and will be important to consider during ongoing work with ethanol.

Remaining questions and technical challenges arising from experiments with ethanol

Both the live imaging and HPLC-Fluorescence experiments described in Chapter 4 are ongoing, and additional method development is required. Initial confocal imaging of larval zebrafish livers for the contribution of dietary fatty acids to acute alcoholic steatosis did not allow automated quantitation of lipid droplet size, so these experiments should be repeated to obtain higher-quality images. Also, these experiments did not show whether all of the fluorescent lipid-rich structures that accumulated in larval zebrafish undergoing acute alcoholic steatosis were lipid

droplets, or if some were other subcellular structures such as endosomes. Transgenic zebrafish lines with fluorescently labeled perilipins are now available (Meredith Wilson, unpublished data) and will be used to identify lipid droplets in future live imaging experiments. The potential for physiological effects from variations in lipid droplet size is a topic of current interest, and whether lipid droplet size, number, or both are increased in the larval zebrafish model of acute alcoholic steatosis is unknown. Also, the "B-C12" HPLC-Fluorescence instrument method was designed primarily with nonpolar lipid resolution in mind, but requires further optimization to aid exploration of ethanol's effect on phospholipid synthesis. Specifically, it is necessary to increase separation between the PC(BODIPY FL-C12, 16:0) and PC(BODIPY FL-C12, 18:1) peaks so that they can be accurately quantitated. Finally, not all of the fluorescent phospholipid species that change with ethanol treatment could be identified by LC-MS/MS, and their phospholipid classes (e.g., PC, PS, or PE) should be determined by thin layer chromatography.

Investigating a mechanism for the effect of ethanol on phospholipid synthesis

I hypothesize that ethanol drives incorporation of dietary fatty acids into phospholipids by damaging membranes in enterocytes, resulting in increased phospholipid synthesis using available fatty acids. Of the two major ethanol metabolism pathways, *adh1* and *cyp2e1,* both produce aldehydes which can cause cellular damage through protein adduct formation, but the *cyp2e1* pathway also results in oxidative stress when it is active. Ethanol may damage enterocyte membranes in larval zebrafish by increasing ROS production as it is metabolized. Although zebrafish possess both the *adh1* and *cyp2e1* pathways for ethanol metabolism, *adh1* is expressed in larvae at <1% of adult levels whereas *cyp2e1* expression is equivalent to adult levels by 5 dpf (184). A lack of *adh1* activity in larval zebrafish is a possible explanation for the occurrence of acute alcoholic steatosis and metabolic changes at levels of ethanol that do not visibly alter behavior. This sensitivity of the larval zebrafish liver to ethanol is a strength of the model

compared with mice, which require treatment with amounts of ethanol that result in severe intoxication to develop acute alcoholic steatosis. Larval dissections followed by HPLC (described in Chapter 2, Figures 8 and S5) showed that the partitioning of BODIPY FL-fatty acids into complex lipids occurs in the intestine of the larval zebrafish. I hypothesize that ethanol-associated changes in dietary lipid metabolism occur in the intestine as well. To test this hypothesis, HPLC-fluorescence analysis should be performed on intestines dissected from larvae treated with ethanol and fed BODIPY-FL fatty acids as described above. Cellular fractionation followed by HPLC-fluorescence should also be performed to determine the subcellular location of the BODIPY-FL phospholipids that change with ethanol exposure.

Investigating ethanol-associated changes in hepatic lipid composition in adult zebrafish

Preprandial ethanol induces accumulation of dietary lipid in hepatocytes, in structures that appear to be lipid droplets and therefore would consist primarily of neutral lipids. This finding seems to contradict the biochemical results which show that dietary fatty acids are being channeled toward phospholipid synthesis. However, it is possible that neutral lipids are being directed away from other tissues and into storage in the liver, which would not show up in HPLC-Fluorescence of whole-body lipid extracts. Also, experiments in which intestines, livers, and the remainder of the larval body were dissected and separately subjected to HPLC-CAD/Fluorescence analysis showed that the amount of total lipid in the liver for the sample sizes used in these experiments is so low that only cholesterol, which produces a relatively large HPLC peak, yields a detectable signal. Because of this, if there are changes in the abundance of individual fluorescent or nonfluorescent neutral lipid species in the liver, I would not expect them to be detectable against the background of total neutral lipid in whole-larvae extracts.

In order to obtain larger volumes of liver tissue for lipid analysis, adult or juvenile zebrafish should be fed BODIPY FL-fatty acids mixed into cooked chicken egg yolk following ethanol exposure. The lipid content of dissected livers can then be analyzed by HPLC-

CAD/Fluorescence. Although adults do not exhibit the acute alcoholic steatosis seen in larvae (188), the effects of ethanol on dietary lipid partitioning and dietary lipid deposition in hepatocytes are not necessarily interdependent. The effect of long-term ethanol exposure on dietary lipid metabolism in the intestine and liver of adult zebrafish will also be examined using the ethanol treatment procedure designed by Lin and colleagues (188).

Potential tissue-specific ethanol-associated changes in neutral lipid composition should also be investigated in adult zebrafish. A possible driver of the progression from hepatic steatosis to steatohepatitis is lipotoxicity, a process in which lipids stored in non-adipose tissues promote cell dysfunction and death (196). As some fatty acids are more likely to promote lipotoxicity than others, potential interactions between ethanol and diet that could drive changes in the fatty acid composition of the neutral lipid that accumulates in hepatic steatosis could contribute to diet-dependent variation in the severity of alcoholic liver injury. Lipotoxicity was first demonstrated through the observation of impaired beta cell function associated with free fatty acids (196). In 2001, Schaffer and colleagues published evidence that saturated free fatty acids may promote lipotoxicity more than unsaturated free fatty acids, showing that CHO cells underwent apoptosis following treatment with the saturated fatty acid palmitate, but not with oleate (a monounsaturated fatty acid of similar chain length) (197). Consistent with these cultured cell studies, observational studies of humans with cardiac disease and experiments conducted in rats have both shown that dietary polyunsaturated fatty acids (PUFAs) protect against lipotoxicity-induced cell death in the heart when compared with dietary saturated fatty acids(198, 199).

Lipotoxic effects have been documented in multiple human organ systems and tissues, but are not well characterized in the liver (200). The observed effects of dietary saturated fatty acids and PUFAs on lipotoxicity in the context of cardiac disease may seem to contradict what is known about the reactive properties of ω-3 PUFAs: unsaturated fatty acids can undergo lipid peroxidation, which causes inflammation through chain reactions that release reactive oxygen species. Fatty liver disease in rodents is improved by diets supplemented with ω-3 PUFAs or

tallow (consisting primarily of saturated fats) but worsened by diets supplemented with corn and soybean oils (composed primarily of ω-6 PUFAs) (201, 202). Conversely, feeding extremely large amounts of ω-3 PUFAs exacerbates fatty liver disease in rodent models. To explain this apparent contradiction, I propose a mechanism in which ω-3 PUFAs exacerbate ethanol-induced inflammation by undergoing lipid peroxidation when they are released from storage in hepatocyte lipid droplets. However, when they are incorporated into hepatocyte membrane phospholipids, I hypothesize that ω-3 PUFAs suppress ethanol-induced inflammation by interfering with innate immune signaling. Recent evidence from a rodent model suggests that hepatic inflammation resulting from ischemia/reperfusion injury depends on localization of the TLR4 receptor in lipid rafts, which is inhibited by dietary ω-3 PUFAs (203) . I predict that dietary ω-3 PUFAs that are incorporated into membrane phospholipids will suppress inflammation by the same mechanism in the context of acute alcoholic liver injury. Under this model, the pro- or anti-inflammatory effect of ω-3 PUFAs would be determined by their subcellular localization and incorporation into phospholipids or triglycerides.

Potential physiological effects of increased channeling of dietary fatty acids into phospholipids

If it is correct that ethanol channels more dietary fatty acids into membrane phospholipids when it is being metabolized concurrently with a meal, then ethanol would amplify the effect of diet on membrane composition. This suggests a possible interaction between ethanol and diet that could influence cellular signaling, as the fatty acid composition of membrane phospholipids has the potential to influence the behavior of membrane-resident proteins (199). This could contribute to an explanation of the Mediterranean diet effect, in which a combination of moderate ethanol consumption and a diet high in unsaturated fats is associated with lower rates of heart disease (204). However, the overall physiological importance of dietary fatty acid partitioning in enterocytes for membrane composition in other organs and tissues has yet to be determined. In

larval zebrafish, complex lipid profiles of BODIPY FL-C12 products were the same in the intestine and the remainder of the body 18 hours post-feeding, but due to the dissipation of fluorescent signal after 24 hours it is unknown how long this effect persists. Experiments in adult zebrafish, which have more complex lipid regulation pathways due to the presence of adipose tissue among other processes, should be performed to address the question of persistence and relevance to whole-body membrane lipid composition. Furthermore, all experiments so far have been performed using saturated fatty acids as metabolic labels, but the Mediterranean diet hypothesis would require ethanol to have similar effects on the channeling of dietary unsaturated fatty acids. Metabolic labeling experiments (likely radioactive thin-layer chromatography assays) using unsaturated fatty acid substrates would be an important first step toward understanding possible mechanisms by which ethanol may interact with diets rich in unsaturated fatty acids to promote cardiovascular health.

REFERENCES

1. Ng, A. N., T. A. de Jong-Curtain, D. J. Mawdsley, S. J. White, J. Shin, B. Appel, P. D. Dong, D. Y. Stainier, and J. K. Heath. 2005. Formation of the digestive system in zebrafish: III. Intestinal epithelium morphogenesis. *Dev Biol* **286**: 114-135.

2. Farber, S. A., M. Pack, S. Y. Ho, I. D. Johnson, D. S. Wagner, R. Dosch, M. C. Mullins, H. S. Hendrickson, E. K. Hendrickson, and M. E. Halpern. 2001. Genetic analysis of digestive physiology using fluorescent phospholipid reporters. *Science* **292**: 1385-1388.

3. Wallace, K., and M. Pack. 2003. Unique and conserved aspects of gut development in zebrafish. *Dev Biol* **255**: 12-29.

4. Rawls, J. F., B. S. Samuel, and J. I. Gordon. 2004. Gnotobiotic zebrafish reveal evolutionarily conserved responses to the gut microbiota. *Proc Natl Acad Sci U S A* **101**: 4596-4601.

5. Ho, S. Y., K. Lorent, M. Pack, and S. A. Farber. 2006. Zebrafish fat-free is required for intestinal lipid absorption and Golgi apparatus structure. *Cell Metab* **3**: 289-300.

6. Song, Y., and R. D. Cone. 2007. Creation of a genetic model of obesity in a teleost. *FASEB J* **21**: 2042-2049.

7. Flynn, E. J., 3rd, C. M. Trent, and J. F. Rawls. 2009. Ontogeny and nutritional control of adipogenesis in zebrafish (Danio rerio). *J Lipid Res*.

8. Sander, J. D., L. Cade, C. Khayter, D. Reyon, R. T. Peterson, J. K. Joung, and J. R. Yeh. 2011. Targeted gene disruption in somatic zebrafish cells using engineered TALENs. *Nat Biotechnol* **29**: 697-698.

9. Huang, P., A. Xiao, M. Zhou, Z. Zhu, S. Lin, and B. Zhang. 2011. Heritable gene targeting in zebrafish using customized TALENs. *Nat Biotechnol* **29**: 699-700.

10. Hwang, W. Y., Y. Fu, D. Reyon, M. L. Maeder, S. Q. Tsai, J. D. Sander, R. T. Peterson, J. R. Yeh, and J. K. Joung. 2013. Efficient genome editing in zebrafish using a CRISPR-Cas system. *Nat Biotechnol* **31**: 227-229.

11. Haffter, P., M. Granato, M. Brand, M. C. Mullins, M. Hammerschmidt, D. A. Kane, J. Odenthal, F. J. van Eeden, Y. J. Jiang, C. P. Heisenberg, R. N. Kelsh, M. Furutani-Seiki, E. Vogelsang, D. Beuchle, U. Schach, C. Fabian, and C. Nusslein-Volhard. 1996. The identification of genes with unique and essential functions in the development of the zebrafish, Danio rerio. *Development* **123**: 1-36.

12. Pham, L. N., M. Kanther, I. Semova, and J. F. Rawls. 2008. Methods for generating and colonizing gnotobiotic zebrafish. *Nat Protoc* **3**: 1862-1875.

13. Kimmel, C. B., and R. D. Law. 1985. Cell lineage of zebrafish blastomeres. III. Clonal analyses of the blastula and gastrula stages. *Dev Biol* **108**: 94-101.

14. Bates, J. M., E. Mittge, J. Kuhlman, K. N. Baden, S. E. Cheesman, and K. Guillemin. 2006. Distinct signals from the microbiota promote different aspects of zebrafish gut differentiation. *Dev Biol* **297**: 374-386.

15. Wong, S., W. Z. Stephens, A. R. Burns, K. Stagaman, L. A. David, B. J. Bohannan, K. Guillemin, and J. F. Rawls. 2015. Ontogenetic Differences in Dietary Fat Influence Microbiota Assembly in the Zebrafish Gut. *MBio* **6**: e00687-00615.

16. Otis, J. P., E. M. Zeituni, J. H. Thierer, J. L. Anderson, A. C. Brown, E. D. Boehm, D. M. Cerchione, A. M. Ceasrine, I. Avraham-Davidi, H. Tempelhof, K. Yaniv, and S. A. Farber. 2015. Zebrafish as a model for apolipoprotein biology: comprehensive expression analysis and a role for ApoA-IV in regulating food intake. *Dis Model Mech* **8**: 295-309.

17. Babin, P. J., and J. M. Vernier. 1989. Plasma lipoproteins in fish. *J Lipid Res* **30**: 467-489.

18. Walzer, C., and N. Schonenberger. 1979. Ultrastructure and cytochemistry of the yolk syncytial layer in the alevin of trout (Salmo fario trutta L. and Salmo gairdneri R.) after hatching. II. The cytoplasmic zone. *Cell Tissue Res* **196**: 75-93.

19. Mani-Ponset, L., E. Guyot, J. P. Diaz, and R. Connes. 1996. Utilization of yolk reserves during post-embryonic development in three teleostean species: the sea bream Sparus aurata, the sea bass Dicentrarchus labrax, and the pike-perch Stizostedion lucioperca. *Marine Biology*: 539-547.

20. Thisse, B., Pflumio, S., Fürthauer, M., Loppin, B., Heyer, V., Degrave, A., Woehl, R., Lux, A., Steffan, T., Charbonnier, X.Q. and Thisse, C. 2001. Expression of the zebrafish genome during embryogenesis (NIH R01 RR15402). *In*, ZFIN Direct Data Submission (http://zfin.org/).

21. Iqbal, J., K. Dai, T. Seimon, R. Jungreis, M. Oyadomari, G. Kuriakose, D. Ron, I. Tabas, and M. M. Hussain. 2008. IRE1beta inhibits chylomicron production by selectively degrading MTP mRNA. *Cell Metab* **7**: 445-455.

22. Avraham-Davidi, I., Y. Ely, V. N. Pham, D. Castranova, M. Grunspan, G. Malkinson, L. Gibbs-Bar, O. Mayseless, G. Allmog, B. Lo, C. M. Warren, T. T. Chen, J. Ungos, K. Kidd, K. Shaw, I. Rogachev, W. Wan, P. M. Murphy, S. A. Farber, L. Carmel, G. S. Shelness, M. L. Iruela-Arispe, B. M. Weinstein, and K. Yaniv. 2012. ApoB-containing lipoproteins regulate angiogenesis by modulating expression of VEGF receptor 1. *Nat Med*.

23. Miyares, R. L., V. B. de Rezende, and S. A. Farber. 2014. Zebrafish yolk lipid processing: a tractable tool for the study of vertebrate lipid transport and metabolism. *Dis Model Mech* **7**: 915-927.

24. Fraher, D., A. Sanigorski, N. A. Mellett, P. J. Meikle, A. J. Sinclair, and Y. Gibert. 2016. Zebrafish Embryonic Lipidomic Analysis Reveals that the Yolk Cell Is Metabolically Active in Processing Lipid. *Cell Rep* **14**: 1317-1329.

25. van der Wulp, M. Y., H. J. Verkade, and A. K. Groen. 2013. Regulation of cholesterol homeostasis. *Mol Cell Endocrinol* **368**: 1-16.

26. Berry, E., Y. Liu, L. Chen, and A. M. Guo. 2016. Eicosanoids: Emerging contributors in stem cell-mediated wound healing. *Prostaglandins Other Lipid Mediat*.

27. North, T. E., W. Goessling, C. R. Walkley, C. Lengerke, K. R. Kopani, A. M. Lord, G. J. Weber, T. V. Bowman, I. H. Jang, T. Grosser, G. A. Fitzgerald, G. Q. Daley, S. H. Orkin, and L. I. Zon. 2007. Prostaglandin E2 regulates vertebrate haematopoietic stem cell homeostasis. *Nature* **447**: 1007-1011.

28. Carten, J. D., M. K. Bradford, and S. A. Farber. 2011. Visualizing digestive organ morphology and function using differential fatty acid metabolism in live zebrafish. *Dev Biol* **360**: 276-285.

29. Hama, K., E. Provost, T. C. Baranowski, A. L. Rubinstein, J. L. Anderson, S. D. Leach, and S. A. Farber. 2009. In vivo imaging of zebrafish digestive organ function using multiple quenched fluorescent reporters. *Am J Physiol Gastrointest Liver Physiol* **296**: G445-453.

30. Moschetta, A., F. Xu, L. R. Hagey, G. P. van Berge-Henegouwen, K. J. van Erpecum, J. F. Brouwers, J. C. Cohen, M. Bierman, H. H. Hobbs, J. H. Steinbach, and A. F. Hofmann. 2005. A phylogenetic survey of biliary lipids in vertebrates. *J Lipid Res* **46**: 2221-2232.

31. Hofmann, A. F., L. R. Hagey, and M. D. Krasowski. 2010. Bile salts of vertebrates: structural variation and possible evolutionary significance. *J Lipid Res* **51**: 226-246.

32. Gershon, M. D. 2005. Nerves, reflexes, and the enteric nervous system: pathogenesis of the irritable bowel syndrome. *J Clin Gastroenterol* **39**: S184-193.

33. Raybould, H. E. 2007. Mechanisms of CCK signaling from gut to brain. *Current Opinions in Pharmacology* **7**: 570-574.

34. Rauch, G. J., Lyons, D.A., Middendorf, I., Friedlander, B., Arana, N., Reyes, T., Talbot, W.S. 2003. Submission and Curation of Gene Expression Data. *In*, ZFIN Direct Data Submission (http://zfin.org/).

35. Koven, W., and P. Schulte. 2012. The effect of fasting and refeeding on mRNA expression of PepT1 and gastrointestinal hormones regulating digestion and food intake in zebrafish (Danio rerio). *Fish Physiol Biochem* **38**: 1565-1575.

36. Folsch, U. R., K. Winckler, and K. G. Wormsley. 1978. Influence of repeated administration of cholecystokinin and secretin on the pancreas of the rat. *Scand J Gastroenterol* **13**: 663-671.

37. Sonobe, K., T. Sakai, M. Satoh, N. Haga, and Z. Itoh. 1995. Control of gallbladder contractions by cholecystokinin through cholecystokinin-A receptors in the vagal pathway and gallbladder in the dog. *Regul Pept* **60**: 33-46.

38. Flint, H. J., K. P. Scott, S. H. Duncan, P. Louis, and E. Forano. 2012. Microbial degradation of complex carbohydrates in the gut. *Gut Microbes* **3**: 289-306.

39. Ley, R. E., M. Hamady, C. Lozupone, P. J. Turnbaugh, R. R. Ramey, J. S. Bircher, M. L. Schlegel, T. A. Tucker, M. D. Schrenzel, R. Knight, and J. I. Gordon. 2008. Evolution of mammals and their gut microbes. *Science* **320**: 1647-1651.

40. Semova, I., J. D. Carten, J. Stombaugh, L. C. Mackey, R. Knight, S. A. Farber, and J. F. Rawls. 2012. Microbiota regulate intestinal absorption and metabolism of Fatty acids in the zebrafish. *Cell Host Microbe* **12**: 277-288.

41. Altmann, S. W., H. R. Davis, Jr., L. J. Zhu, X. Yao, L. M. Hoos, G. Tetzloff, S. P. Iyer, M. Maguire, A. Golovko, M. Zeng, L. Wang, N. Murgolo, and M. P. Graziano. 2004. Niemann-Pick C1 Like 1 protein is critical for intestinal cholesterol absorption. *Science* **303**: 1201-1204.

42. Davis, H. R., Jr., L. J. Zhu, L. M. Hoos, G. Tetzloff, M. Maguire, J. Liu, X. Yao, S. P. Iyer, M. H. Lam, E. G. Lund, P. A. Detmers, M. P. Graziano, and S. W. Altmann. 2004. Niemann-Pick C1 Like 1 (NPC1L1) is the intestinal phytosterol and cholesterol transporter and a key modulator of whole-body cholesterol homeostasis. *J Biol Chem* **279**: 33586-33592.

43. Ge, L., J. Wang, W. Qi, H. H. Miao, J. Cao, Y. X. Qu, B. L. Li, and B. L. Song. 2008. The cholesterol absorption inhibitor ezetimibe acts by blocking the sterol-induced internalization of NPC1L1. *Cell Metab* **7**: 508-519.

44. Skov, M., C. K. Tonnesen, G. H. Hansen, and E. M. Danielsen. 2011. Dietary cholesterol induces trafficking of intestinal Niemann-Pick Type C1 Like 1 from the brush border to endosomes. *Am J Physiol Gastrointest Liver Physiol* **300**: G33-40.

45. Busch-Nentwich, E., Kettleborough, R., Dooley, C. M., Scahill, C., Sealy, I., White, R., Herd, C., Mehroke, S., Wali, N., Carruthers, S., Hall, A., Collins, J., Gibbons, R., Pusztai, Z., Clark, R., and Stemple, D.L. 2013. Sanger Institute Zebrafish Mutation Project mutant data submission. *In*, ZFIN Direct Data Submission (http://zfin.org/).

46. Van Heek, M., C. F. France, D. S. Compton, R. L. McLeod, N. P. Yumibe, K. B. Alton, E. J. Sybertz, and H. R. Davis, Jr. 1997. In vivo metabolism-based discovery of a potent cholesterol absorption inhibitor, SCH58235, in the rat and rhesus monkey through the identification of the active metabolites of SCH48461. *J Pharmacol Exp Ther* **283**: 157-163.

47. Bays, H. E., D. Neff, J. E. Tomassini, and A. M. Tershakovec. 2008. Ezetimibe: cholesterol lowering and beyond. *Expert Rev Cardiovasc Ther* **6**: 447-470.

48. Clifton, J. D., E. Lucumi, M. C. Myers, A. Napper, K. Hama, S. A. Farber, A. B. Smith, 3rd, D. M. Huryn, S. L. Diamond, and M. Pack. 2010. Identification of novel inhibitors of dietary lipid absorption using zebrafish. *PLoS One* **5**: e12386.

49. Tremblay, A. J., B. Lamarche, V. Lemelin, L. Hoos, S. Benjannet, N. G. Seidah, H. R. Davis, Jr., and P. Couture. 2011. Atorvastatin increases intestinal expression of NPC1L1 in hyperlipidemic men. *J Lipid Res* **52**: 558-565.

50. Richards, M. R., J. D. Harp, D. S. Ory, and J. E. Schaffer. 2006. Fatty acid transport protein 1 and long-chain acyl coenzyme A synthetase 1 interact in adipocytes. *J Lipid Res* **47**: 665-672.

51. Melton, E. M., R. L. Cerny, C. C. DiRusso, and P. N. Black. 2013. Overexpression of human fatty acid transport protein 2/very long chain acyl-CoA synthetase 1 (FATP2/Acsvl1) reveals distinct patterns of trafficking of exogenous fatty acids. *Biochem Biophys Res Commun* **440**: 743-748.

52. Cooper, D. E., P. A. Young, E. L. Klett, and R. A. Coleman. 2015. Physiological Consequences of Compartmentalized Acyl-CoA Metabolism. *J Biol Chem* **290**: 20023-20031.

53. Lopes-Marques, M., I. Cunha, M. A. Reis-Henriques, M. M. Santos, and L. F. Castro. 2013. Diversity and history of the long-chain acyl-CoA synthetase (Acsl) gene family in vertebrates. *BMC Evol Biol* **13**: 271.

54. Thisse, B., Thisse, C. 2004. Fast Release Clones: A High Throughput Expression Analysis. *In*, ZFIN Direct Data Submission (http://zfin.org/).

55. Miyares, R. L., C. Stein, B. Renisch, J. L. Anderson, M. Hammerschmidt, and S. A. Farber. 2013. Long-chain Acyl-CoA synthetase 4A regulates Smad activity and dorsoventral patterning in the zebrafish embryo. *Dev Cell* **27**: 635-647.

56. Guitart, M., A. L. Andreu, E. Garcia-Arumi, P. Briones, E. Quintana, A. M. Gomez-Foix, and C. Garcia-Martinez. 2009. FATP1 localizes to mitochondria and enhances pyruvate dehydrogenase activity in skeletal myotubes. *Mitochondrion* **9**: 266-272.

57. Lam, S. H., C. L. Winata, Y. Tong, S. Korzh, W. S. Lim, V. Korzh, J. Spitsbergen, S. Mathavan, L. D. Miller, E. T. Liu, and Z. Gong. 2006. Transcriptome kinetics of arsenic-induced adaptive response in zebrafish liver. *Physiol Genomics* **27**: 351-361.

58. Thisse, C., and Thisse, B. 2005. High Throughput Expression Analysis of ZF-Models Consortium Clones. *In*, ZFIN Direct Data Submission (http://zfin.org/).

59. Stahl, A., D. J. Hirsch, R. E. Gimeno, S. Punreddy, P. Ge, N. Watson, S. Patel, M. Kotler, A. Raimondi, L. A. Tartaglia, and H. F. Lodish. 1999. Identification of the major intestinal fatty acid transport protein. *Mol Cell* **4**: 299-308.

60. Buttet, M., V. Traynard, T. T. Tran, P. Besnard, H. Poirier, and I. Niot. 2014. From fatty-acid sensing to chylomicron synthesis: role of intestinal lipid-binding proteins. *Biochimie* **96**: 37-47.

61. Liu, K., Y. Xu, Y. Wang, S. Wei, D. Feng, Q. Huang, S. Zhang, and Z. Liu. 2016. Developmental expression and immune role of the class B scavenger receptor cd36 in zebrafish. *Dev Comp Immunol* **60**: 91-95.

62. Otis, J. P., M. C. Shen, V. Quinlivan, J. L. Anderson, and S. A. Farber. 2017. Intestinal epithelial cell caveolin 1 regulates fatty acid and lipoprotein cholesterol plasma levels. *Dis Model Mech* **10**: 283-295.

63. Ruggles, K. V., A. Turkish, and S. L. Sturley. 2013. Making, baking, and breaking: the synthesis, storage, and hydrolysis of neutral lipids. *Annu Rev Nutr* **33**: 413-451.

64. Gluchowski, N. L., M. Becuwe, T. C. Walther, and R. V. Farese, Jr. 2017. Lipid droplets and liver disease: from basic biology to clinical implications. *Nat Rev Gastroenterol Hepatol* **14**: 343-355.

65. Zeituni, E. M., M. H. Wilson, X. Zheng, P. A. Iglesias, M. Sepanski, M. A. Siddiqi, J. L. Anderson, Y. Zheng, and S. A. Farber. 2016. Endoplasmic reticulum lipid flux influences enterocyte nuclear morphology and lipid-dependent transcriptional responses. *J Biol Chem* **291**: 23804-23816.

66. Robl, J. A., R. Sulsky, C. Q. Sun, L. M. Simpkins, T. Wang, J. K. Dickson, Jr., Y. Chen, D. R. Magnin, P. Taunk, W. A. Slusarchyk, S. A. Biller, S. J. Lan, F. Connolly, L. K. Kunselman, T. Sabrah, H. Jamil, D. Gordon, T. W. Harrity, and J. R. Wetterau. 2001. A novel series of highly potent benzimidazole-based microsomal triglyceride transfer protein inhibitors. *J Med Chem* **44**: 851-856.

67. Cuchel, M., L. T. Bloedon, P. O. Szapary, D. M. Kolansky, M. L. Wolfe, A. Sarkis, J. S. Millar, K. Ikewaki, E. S. Siegelman, R. E. Gregg, and D. J. Rader. 2007. Inhibition of

microsomal triglyceride transfer protein in familial hypercholesterolemia. *N Engl J Med* **356**: 148-156.

68. Wren, J. A., A. A. Ramudo, S. L. Campbell, V. L. King, J. S. Eagleson, J. Gossellin, and S. J. Sunderland. 2007. Efficacy and safety of dirlotapide in the management of obese dogs evaluated in two placebo-controlled, masked clinical studies in North America. *J Vet Pharmacol Ther* **30 Suppl 1**: 81-89.

69. Cartwright, I. J., and J. A. Higgins. 1999. Increased dietary triacylglycerol markedly enhances the ability of isolated rabbit enterocytes to secrete chylomicrons: an effect related to dietary fatty acid composition. *J Lipid Res* **40**: 1858-1866.

70. Quinlivan, V. H., M. H. Wilson, J. Ruzicka, and S. A. Farber. 2017. An HPLC-CAD/fluorescence lipidomics platform using fluorescent fatty acids as metabolic tracers. *J Lipid Res* **58**: 1008-1020.

71. Hui, D. Y., E. D. Labonte, and P. N. Howles. 2008. Development and physiological regulation of intestinal lipid absorption. III. Intestinal transporters and cholesterol absorption. *Am J Physiol Gastrointest Liver Physiol* **294**: G839-843.

72. Drover, V. A., D. V. Nguyen, C. C. Bastie, Y. F. Darlington, N. A. Abumrad, J. E. Pessin, E. London, D. Sahoo, and M. C. Phillips. 2008. CD36 mediates both cellular uptake of very long chain fatty acids and their intestinal absorption in mice. *J Biol Chem* **283**: 13108-13115.

73. D'Aquila, T., Y. H. Hung, A. Carreiro, and K. K. Buhman. 2016. Recent discoveries on absorption of dietary fat: Presence, synthesis, and metabolism of cytoplasmic lipid droplets within enterocytes. *Biochim Biophys Acta* **1861**: 730-747.

74. Anderson, J. L., J. D. Carten, and S. A. Farber. 2011. Zebrafish lipid metabolism: from mediating early patterning to the metabolism of dietary fat and cholesterol. *Methods Cell Biol* **101**: 111-141.

75. Asaoka, Y., S. Terai, I. Sakaida, and H. Nishina. 2013. The expanding role of fish models in understanding non-alcoholic fatty liver disease. *Dis Model Mech* **6**: 905-914.

76. Holtta-Vuori, M., V. T. Salo, L. Nyberg, C. Brackmann, A. Enejder, P. Panula, and E. Ikonen. 2010. Zebrafish: gaining popularity in lipid research. *Biochem J* **429**: 235-242.

77. Fang, L., C. Liu, and Y. I. Miller. 2014. Zebrafish models of dyslipidemia: relevance to atherosclerosis and angiogenesis. *Transl Res* **163**: 99-108.

78. Schlegel, A., and D. Y. Stainier. 2007. Lessons from "lower" organisms: what worms, flies, and zebrafish can teach us about human energy metabolism. *PLoS Genet* **3**: e199.

79. Sadler, K. C., J. F. Rawls, and S. A. Farber. 2013. Getting the inside tract: new frontiers in zebrafish digestive system biology. *Zebrafish* **10**: 129-131.

80. Esteves, A., A. Knoll-Gellida, L. Canclini, M. C. Silvarrey, M. Andre, and P. J. Babin. 2016. Fatty acid binding proteins have the potential to channel dietary fatty acids into enterocyte nuclei. *J Lipid Res* **57**: 219-232.

81. Falcinelli, S., A. Rodiles, S. Unniappan, S. Picchietti, G. Gioacchini, D. L. Merrifield, and O. Carnevali. 2016. Probiotic treatment reduces appetite and glucose level in the zebrafish model. *Sci Rep* **6**: 18061.

82. Otis, J. P., and S. A. Farber. 2013. Imaging vertebrate digestive function and lipid metabolism in vivo. *Drug Discov Today Dis Models* **10**: e11-e16.

83. Stoletov, K., L. Fang, S. H. Choi, K. Hartvigsen, L. F. Hansen, C. Hall, J. Pattison, J. Juliano, E. R. Miller, F. Almazan, P. Crosier, J. L. Witztum, R. L. Klemke, and Y. I. Miller. 2009. Vascular lipid accumulation, lipoprotein oxidation, and macrophage lipid uptake in hypercholesterolemic zebrafish. *Circ Res* **104**: 952-960.

84. Nealon, J. R., S. J. Blanksby, P. J. Donaldson, R. J. Truscott, and T. W. Mitchell. 2011. Fatty Acid uptake and incorporation into phospholipids in the rat lens. *Invest Ophthalmol Vis Sci* **52**: 804-809.

85. Hostetler, H. A., M. Balanarasimha, H. Huang, M. S. Kelzer, A. Kaliappan, A. B. Kier, and F. Schroeder. 2010. Glucose regulates fatty acid binding protein interaction with lipids and peroxisome proliferator-activated receptor alpha. *J Lipid Res* **51**: 3103-3116.

86. Huang, H., O. Starodub, A. McIntosh, B. P. Atshaves, G. Woldegiorgis, A. B. Kier, and F. Schroeder. 2004. Liver fatty acid-binding protein colocalizes with peroxisome proliferator activated receptor alpha and enhances ligand distribution to nuclei of living cells. *Biochemistry* **43**: 2484-2500.

87. Kasurinen, J. 1992. A novel fluorescent fatty acid, 5-methyl-BDY-3-dodecanoic acid, is a potential probe in lipid transport studies by incorporating selectively to lipid classes of BHK cells. *Biochem Biophys Res Commun* **187**: 1594-1601.

88. Furlong, S. T., K. S. Thibault, L. M. Morbelli, J. J. Quinn, and R. A. Rogers. 1995. Uptake and compartmentalization of fluorescent lipid analogs in larval Schistosoma mansoni. *J Lipid Res* **36**: 1-12.

89. Viktorova, E. G., L. A. Ford-Siltz, J. Nchoutmboube, and G. A. Belov. 2014. Fluorescent fatty acid analogs as a tool to study development of the picornavirus replication organelles. *J Virol Methods* **200**: 15-21.

90. Cheon, H. G., and Y. S. Cho. 2014. Protection of palmitic acid-mediated lipotoxicity by arachidonic acid via channeling of palmitic acid into triglycerides in C2C12. *J Biomed Sci* **21**: 13.

91. Wang, H., E. Wei, A. D. Quiroga, X. Sun, N. Touret, and R. Lehner. 2010. Altered lipid droplet dynamics in hepatocytes lacking triacylglycerol hydrolase expression. *Mol Biol Cell* **21**: 1991-2000.

92. Sylven, C., and B. Borgstrom. 1969. Intestinal absorption and lymphatic transport of cholesterol in the rat: influence of the fatty acid chain length of the carrier triglyceride. *J Lipid Res* **10**: 351-355.

93. Huggins, K. W., L. M. Camarota, P. N. Howles, and D. Y. Hui. 2003. Pancreatic triglyceride lipase deficiency minimally affects dietary fat absorption but dramatically decreases dietary cholesterol absorption in mice. *J Biol Chem* **278**: 42899-42905.

94. Brady, J. 1965. A simple technique for making very fine, durable dissecting needles by sharpening tungsten wire electrolytically. *Bull World Health Organ* **32**: 143-144.

95. Kates, M. 1972. Techniques of Lipidology: Isolation, Analysis, and Identification of Lipids American Elsevier Publishing Company, Inc., New York, NY.

96. Baek, J. S., L. Fang, A. C. Li, and Y. I. Miller. 2012. Ezetimibe and simvastatin reduce cholesterol levels in zebrafish larvae fed a high-cholesterol diet. *Cholesterol* **2012**: 564705.

97. Zeb, A. 2015. Chemistry and liquid chromatography methods for the analyses of primary oxidation products of triacylglycerols. *Free Radic Res* **49**: 549-564.

98. McCluer, R. H., M. D. Ullman, and F. B. Jungalwala. 1989. High-performance liquid chromatography of membrane lipids: glycosphingolipids and phospholipids. *Methods Enzymol* **172**: 538-575.

99. Samet, J. M., M. Friedman, and D. C. Henke. 1989. High-performance liquid chromatography separation of phospholipid classes and arachidonic acid on cyanopropyl columns. *Anal Biochem* **182**: 32-36.

100. Hamilton, J. G., and K. Comai. 1988. Separation of neutral lipid, free fatty acid and phospholipid classes by normal phase HPLC. *Lipids* **23**: 1150-1153.

101. Hamilton, J. G., and R. J. Karol. 1982. High performance liquid chromatography (HPLC) of arachidonic acid metabolites. *Prog Lipid Res* **21**: 155-170.

102. Khan, G. R., and F. Scheinmann. 1978. Some recent advances in physical methods for analysis and characterization of polyunsaturated fatty acids. *Prog Chem Fats Other Lipids* **15**: 343-367.

103. Ruiz-Rodriguez, A., G. Reglero, and E. Ibanez. 2010. Recent trends in the advanced analysis of bioactive fatty acids. *J Pharm Biomed Anal* **51**: 305-326.

104. Zhang, S. O., R. Trimble, F. Guo, and H. Y. Mak. 2010. Lipid droplets as ubiquitous fat storage organelles in C. elegans. *BMC Cell Biol* **11**: 96.

105. Bays, H. E., P. B. Moore, M. A. Drehobl, S. Rosenblatt, P. D. Toth, C. A. Dujovne, R. H. Knopp, L. J. Lipka, A. P. Lebeaut, B. Yang, L. E. Mellars, C. Cuffie-Jackson, E. P. Veltri, and G. Ezetimibe Study. 2001. Effectiveness and tolerability of ezetimibe in patients with primary hypercholesterolemia: pooled analysis of two phase II studies. *Clin Ther* **23**: 1209-1230.

106. Lee, S., J. M. Han, H. Kim, E. Kim, T. S. Jeong, W. S. Lee, and K. H. Cho. 2004. Synthesis of cinnamic acid derivatives and their inhibitory effects on LDL-oxidation, acyl-CoA:cholesterol acyltransferase-1 and -2 activity, and decrease of HDL-particle size. *Bioorg Med Chem Lett* **14**: 4677-4681.

107. Huang, H., O. Starodub, A. McIntosh, A. B. Kier, and F. Schroeder. 2002. Liver fatty acid-binding protein targets fatty acids to the nucleus. Real time confocal and multiphoton fluorescence imaging in living cells. *J Biol Chem* **277**: 29139-29151.

108. Atshaves, B. P., S. M. Storey, H. Huang, and F. Schroeder. 2004. Liver fatty acid binding protein expression enhances branched-chain fatty acid metabolism. *Mol Cell Biochem* **259**: 115-129.

109. Wang, J., M. A. Mitsche, D. Lutjohann, J. C. Cohen, X. S. Xie, and H. H. Hobbs. 2015. Relative roles of ABCG5/ABCG8 in liver and intestine. *J Lipid Res* **56**: 319-330.

110. Abumrad, N. A., and N. O. Davidson. 2012. Role of the gut in lipid homeostasis. *Physiol Rev* **92**: 1061-1085.

111. van Meer, G., D. R. Voelker, and G. W. Feigenson. 2008. Membrane lipids: where they are and how they behave. *Nat Rev Mol Cell Biol* **9**: 112-124.

112. Parton, R. G., and K. Simons. 2007. The multiple faces of caveolae. *Nat Rev Mol Cell Biol* **8**: 185-194.

113. Rothberg, K. G., J. E. Heuser, W. C. Donzell, Y. S. Ying, J. R. Glenney, and R. G. Anderson. 1992. Caveolin, a protein component of caveolae membrane coats. *Cell* **68**: 673-682.

114. Murata, M., J. Peranen, R. Schreiner, F. Wieland, T. V. Kurzchalia, and K. Simons. 1995. VIP21/caveolin is a cholesterol-binding protein. *Proc Natl Acad Sci U S A* **92**: 10339-10343.

115. Trigatti, B. L., R. G. Anderson, and G. E. Gerber. 1999. Identification of caveolin-1 as a fatty acid binding protein. *Biochem Biophys Res Commun* **255**: 34-39.

116. Razani, B., T. P. Combs, X. B. Wang, P. G. Frank, D. S. Park, R. G. Russell, M. Li, B. Tang, L. A. Jelicks, P. E. Scherer, and M. P. Lisanti. 2002. Caveolin-1-deficient mice are lean, resistant to diet-induced obesity, and show hypertriglyceridemia with adipocyte abnormalities. *J Biol Chem* **277**: 8635-8647.

117. Frank, P. G., S. Pavlides, M. W. Cheung, K. Daumer, and M. P. Lisanti. 2008. Role of caveolin-1 in the regulation of lipoprotein metabolism. *Am J Physiol Cell Physiol* **295**: C242-248.

118. Valasek, M. A., J. Weng, P. W. Shaul, R. G. Anderson, and J. J. Repa. 2005. Caveolin-1 is not required for murine intestinal cholesterol transport. *J Biol Chem* **280**: 28103-28109.

119. Heimerl, S., G. Liebisch, S. Le Lay, A. Bottcher, P. Wiesner, S. Lindtner, T. V. Kurzchalia, K. Simons, and G. Schmitz. 2008. Caveolin-1 deficiency alters plasma lipid and lipoprotein profiles in mice. *Biochem Biophys Res Commun* **367**: 826-833.

120. Cohen, A. W., T. P. Combs, P. E. Scherer, and M. P. Lisanti. 2003. Role of caveolin and caveolae in insulin signaling and diabetes. *Am J Physiol Endocrinol Metab* **285**: E1151-1160.

121. Frank, P. G., H. Lee, D. S. Park, N. N. Tandon, P. E. Scherer, and M. P. Lisanti. 2004. Genetic ablation of caveolin-1 confers protection against atherosclerosis. *Arterioscler Thromb Vasc Biol* **24**: 98-105.

122. Fernandez-Hernando, C., J. Yu, Y. Suarez, C. Rahner, A. Davalos, M. A. Lasuncion, and W. C. Sessa. 2009. Genetic evidence supporting a critical role of endothelial caveolin-1 during the progression of atherosclerosis. *Cell Metab* **10**: 48-54.

123. Cohen, A. W., B. Razani, W. Schubert, T. M. Williams, X. B. Wang, P. Iyengar, D. L. Brasaemle, P. E. Scherer, and M. P. Lisanti. 2004. Role of caveolin-1 in the modulation of lipolysis and lipid droplet formation. *Diabetes* **53**: 1261-1270.

124. Asterholm, I. W., D. I. Mundy, J. Weng, R. G. Anderson, and P. E. Scherer. 2012. Altered mitochondrial function and metabolic inflexibility associated with loss of caveolin-1. *Cell Metab* **15**: 171-185.

125. Parton, R. G., and M. A. del Pozo. 2013. Caveolae as plasma membrane sensors, protectors and organizers. *Nat Rev Mol Cell Biol* **14**: 98-112.

126. Field, F. J., E. Born, S. Murthy, and S. N. Mathur. 1998. Caveolin is present in intestinal cells: role in cholesterol trafficking? *J Lipid Res* **39**: 1938-1950.

127. Badizadegan, K., B. L. Dickinson, H. E. Wheeler, R. S. Blumberg, R. K. Holmes, and W. I. Lencer. 2000. Heterogeneity of detergent-insoluble membranes from human intestine containing caveolin-1 and ganglioside G(M1). *Am J Physiol Gastrointest Liver Physiol* **278**: G895-904.

128. Morroni, M., A. M. Cangiotti, and S. Cinti. 2007. Brush cells in the human duodenojejunal junction: an ultrastructural study. *J Anat* **211**: 125-131.

129. Marchiando, A. M., L. Shen, W. V. Graham, C. R. Weber, B. T. Schwarz, J. R. Austin, 2nd, D. R. Raleigh, Y. Guan, A. J. Watson, M. H. Montrose, and J. R. Turner. 2010. Caveolin-1-dependent occludin endocytosis is required for TNF-induced tight junction regulation in vivo. *J Cell Biol* **189**: 111-126.

130. McConnell, R. E., A. E. Benesh, S. Mao, D. L. Tabb, and M. J. Tyska. 2011. Proteomic analysis of the enterocyte brush border. *Am J Physiol Gastrointest Liver Physiol* **300**: G914-926.

131. Siddiqi, S., A. Sheth, F. Patel, M. Barnes, and C. M. Mansbach, 2nd. 2013. Intestinal caveolin-1 is important for dietary fatty acid absorption. *Biochim Biophys Acta* **1831**: 1311-1321.

132. Nabeyama, A., and C. P. Leblond. 1974. "Caveolated cells" characterized by deep surface invaginations and abundant filaments in mouse gastro-intestinal epithelia. *Am J Anat* **140**: 147-165.

133. Nusrat, A., C. A. Parkos, P. Verkade, C. S. Foley, T. W. Liang, W. Innis-Whitehouse, K. K. Eastburn, and J. L. Madara. 2000. Tight junctions are membrane microdomains. *J Cell Sci* **113 (Pt 10)**: 1771-1781.

134. Carten, J. D., and S. A. Farber. 2009. A new model system swims into focus: using the zebrafish to visualize intestinal metabolism in vivo. *Clin Lipidol* **4**: 501.

135. Nixon, S. J., A. Carter, J. Wegner, C. Ferguson, M. Floetenmeyer, J. Riches, B. Key, M. Westerfield, and R. G. Parton. 2007. Caveolin-1 is required for lateral line neuromast and notochord development. *J Cell Sci* **120**: 2151-2161.

136. Fang, P. K., K. R. Solomon, L. Zhuang, M. Qi, M. McKee, M. R. Freeman, and P. C. Yelick. 2006. Caveolin-1alpha and -1beta perform nonredundant roles in early vertebrate development. *Am J Pathol* **169**: 2209-2222.

137. Gabor, K. A., D. Kim, C. H. Kim, and S. T. Hess. 2015. Nanoscale imaging of caveolin-1 membrane domains in vivo. *PLoS One* **10**: e0117225.

138. Singh, R. D., Y. Liu, C. L. Wheatley, E. L. Holicky, A. Makino, D. L. Marks, T. Kobayashi, G. Subramaniam, R. Bittman, and R. E. Pagano. 2006. Caveolar endocytosis and microdomain association of a glycosphingolipid analog is dependent on its sphingosine stereochemistry. *J Biol Chem* **281**: 30660-30668.

139. Schubert, W., P. G. Frank, B. Razani, D. S. Park, C. W. Chow, and M. P. Lisanti. 2001. Caveolae-deficient endothelial cells show defects in the uptake and transport of albumin in vivo. *J Biol Chem* **276**: 48619-48622.

140. Chanthick, C., R. Kanlaya, R. Kiatbumrung, S. N. Pattanakitsakul, and V. Thongboonkerd. 2016. Caveolae-mediated albumin transcytosis is enhanced in dengue-infected human endothelial cells: A model of vascular leakage in dengue hemorrhagic fever. *Sci Rep* **6**: 31855.

141. Ghitescu, L., and M. Bendayan. 1992. Transendothelial transport of serum albumin: a quantitative immunocytochemical study. *J Cell Biol* **117**: 745-755.

142. Ghitescu, L., A. Fixman, M. Simionescu, and N. Simionescu. 1986. Specific binding sites for albumin restricted to plasmalemmal vesicles of continuous capillary endothelium: receptor-mediated transcytosis. *J Cell Biol* **102**: 1304-1311.

143. Dobrinskikh, E., K. Okamura, J. B. Kopp, R. B. Doctor, and J. Blaine. 2014. Human podocytes perform polarized, caveolae-dependent albumin endocytosis. *Am J Physiol Renal Physiol* **306**: F941-951.

144. Singh, R. D., V. Puri, J. T. Valiyaveettil, D. L. Marks, R. Bittman, and R. E. Pagano. 2003. Selective caveolin-1-dependent endocytosis of glycosphingolipids. *Mol Biol Cell* **14**: 3254-3265.

145. Cao, J., A. Navis, B. D. Cox, A. L. Dickson, M. Gemberling, R. Karra, M. Bagnat, and K. D. Poss. 2016. Single epicardial cell transcriptome sequencing identifies Caveolin 1 as an essential factor in zebrafish heart regeneration. *Development* **143**: 232-243.

146. Cao, G., G. Yang, T. L. Timme, T. Saika, L. D. Truong, T. Satoh, A. Goltsov, S. H. Park, T. Men, N. Kusaka, W. Tian, C. Ren, H. Wang, D. Kadmon, W. W. Cai, A. C. Chinault, T. B. Boone, A. Bradley, and T. C. Thompson. 2003. Disruption of the caveolin-1 gene impairs renal calcium reabsorption and leads to hypercalciuria and urolithiasis. *Am J Pathol* **162**: 1241-1248.

147. Madison, B. B., L. Dunbar, X. T. Qiao, K. Braunstein, E. Braunstein, and D. L. Gumucio. 2002. Cis elements of the villin gene control expression in restricted domains of the vertical (crypt) and horizontal (duodenum, cecum) axes of the intestine. *J Biol Chem* **277**: 33275-33283.

148. Drab, M., P. Verkade, M. Elger, M. Kasper, M. Lohn, B. Lauterbach, J. Menne, C. Lindschau, F. Mende, F. C. Luft, A. Schedl, H. Haller, and T. V. Kurzchalia. 2001. Loss of caveolae, vascular dysfunction, and pulmonary defects in caveolin-1 gene-disrupted mice. *Science* **293**: 2449-2452.

149. Razani, B., J. A. Engelman, X. B. Wang, W. Schubert, X. L. Zhang, C. B. Marks, F. Macaluso, R. G. Russell, M. Li, R. G. Pestell, D. Di Vizio, H. Hou, Jr., B. Kneitz, G. Lagaud, G.

J. Christ, W. Edelmann, and M. P. Lisanti. 2001. Caveolin-1 null mice are viable but show evidence of hyperproliferative and vascular abnormalities. *J Biol Chem* **276**: 38121-38138.

150. Vogel, U., K. Sandvig, and B. van Deurs. 1998. Expression of caveolin-1 and polarized formation of invaginated caveolae in Caco-2 and MDCK II cells. *J Cell Sci* **111 (Pt 6)**: 825-832.

151. Hansen, G. H., L. L. Niels-Christiansen, L. Immerdal, and E. M. Danielsen. 2003. Scavenger receptor class B type I (SR-BI) in pig enterocytes: trafficking from the brush border to lipid droplets during fat absorption. *Gut* **52**: 1424-1431.

152. Parker, S., D. S. Walker, S. Ly, and H. A. Baylis. 2009. Caveolin-2 is required for apical lipid trafficking and suppresses basolateral recycling defects in the intestine of Caenorhabditis elegans. *Mol Biol Cell* **20**: 1763-1771.

153. Hansen, G. H., L. Immerdal, E. Thorsen, L. L. Niels-Christiansen, B. T. Nystrom, E. J. Demant, and E. M. Danielsen. 2001. Lipid rafts exist as stable cholesterol-independent microdomains in the brush border membrane of enterocytes. *J Biol Chem* **276**: 32338-32344.

154. Danielsen, E. M., and G. H. Hansen. 2006. Lipid raft organization and function in brush borders of epithelial cells. *Mol Membr Biol* **23**: 71-79.

155. Singh, R. D., E. L. Holicky, Z. J. Cheng, S. Y. Kim, C. L. Wheatley, D. L. Marks, R. Bittman, and R. E. Pagano. 2007. Inhibition of caveolar uptake, SV40 infection, and beta1-integrin signaling by a nonnatural glycosphingolipid stereoisomer. *J Cell Biol* **176**: 895-901.

156. Luangrath, V., M. R. Brodeur, D. Rhainds, and L. Brissette. 2008. Mouse CD36 has opposite effects on LDL and oxidized LDL metabolism in vivo. *Arterioscler Thromb Vasc Biol* **28**: 1290-1295.

157. Nassir, F., B. Wilson, X. Han, R. W. Gross, and N. A. Abumrad. 2007. CD36 is important for fatty acid and cholesterol uptake by the proximal but not distal intestine. *J Biol Chem* **282**: 19493-19501.

158. Pepino, M. Y., O. Kuda, D. Samovski, and N. A. Abumrad. 2014. Structure-function of CD36 and importance of fatty acid signal transduction in fat metabolism. *Annu Rev Nutr* **34**: 281-303.

159. Febbraio, M., N. A. Abumrad, D. P. Hajjar, K. Sharma, W. Cheng, S. F. Pearce, and R. L. Silverstein. 1999. A null mutation in murine CD36 reveals an important role in fatty acid and lipoprotein metabolism. *J Biol Chem* **274**: 19055-19062.

160. Poirier, H., P. Degrace, I. Niot, A. Bernard, and P. Besnard. 1996. Localization and regulation of the putative membrane fatty-acid transporter (FAT) in the small intestine. Comparison with fatty acid-binding proteins (FABP). *Eur J Biochem* **238**: 368-373.

161. Ring, A., S. Le Lay, J. Pohl, P. Verkade, and W. Stremmel. 2006. Caveolin-1 is required for fatty acid translocase (FAT/CD36) localization and function at the plasma membrane of mouse embryonic fibroblasts. *Biochim Biophys Acta* **1761**: 416-423.

162. Yedgar, S., T. E. Carew, R. C. Pittman, W. F. Beltz, and D. Steinberg. 1983. Tissue sites of catabolism of albumin in rabbits. *Am J Physiol* **244**: E101-107.

163. Veilleux, A., E. Grenier, P. Marceau, A. C. Carpentier, D. Richard, and E. Levy. 2014. Intestinal lipid handling: evidence and implication of insulin signaling abnormalities in human obese subjects. *Arterioscler Thromb Vasc Biol* **34**: 644-653.

164. Gustavsson, J., S. Parpal, M. Karlsson, C. Ramsing, H. Thorn, M. Borg, M. Lindroth, K. H. Peterson, K. E. Magnusson, and P. Stralfors. 1999. Localization of the insulin receptor in caveolae of adipocyte plasma membrane. *FASEB J* **13**: 1961-1971.

165. Gafencu, A., M. Stanescu, A. M. Toderici, C. Heltianu, and M. Simionescu. 1998. Protein and fatty acid composition of caveolae from apical plasmalemma of aortic endothelial cells. *Cell Tissue Res* **293**: 101-110.

166. Cao, H., K. Gerhold, J. R. Mayers, M. M. Wiest, S. M. Watkins, and G. S. Hotamisligil. 2008. Identification of a lipokine, a lipid hormone linking adipose tissue to systemic metabolism. *Cell* **134**: 933-944.

167. Djousse, L., N. L. Weir, N. Q. Hanson, M. Y. Tsai, and J. M. Gaziano. 2012. Plasma phospholipid concentration of cis-palmitoleic acid and risk of heart failure. *Circ Heart Fail* **5**: 703-709.

168. Puri, P., M. M. Wiest, O. Cheung, F. Mirshahi, C. Sargeant, H. K. Min, M. J. Contos, R. K. Sterling, M. Fuchs, H. Zhou, S. M. Watkins, and A. J. Sanyal. 2009. The plasma lipidomic signature of nonalcoholic steatohepatitis. *Hepatology* **50**: 1827-1838.

169. Cai, Q., L. Guo, H. Gao, and X. A. Li. 2013. Caveolar fatty acids and acylation of caveolin-1. *PLoS One* **8**: e60884.

170. Dietzen, D. J., W. R. Hastings, and D. M. Lublin. 1995. Caveolin is palmitoylated on multiple cysteine residues. Palmitoylation is not necessary for localization of caveolin to caveolae. *J Biol Chem* **270**: 6838-6842.

171. Yang, X., E. E. Schadt, S. Wang, H. Wang, A. P. Arnold, L. Ingram-Drake, T. A. Drake, and A. J. Lusis. 2006. Tissue-specific expression and regulation of sexually dimorphic genes in mice. *Genome Res* **16**: 995-1004.

172. Cooper, A. D., R. Nutik, and J. Chen. 1987. Characterization of the estrogen-induced lipoprotein receptor of rat liver. *J Lipid Res* **28**: 59-68.

173. Schlegel, A., C. Wang, B. S. Katzenellenbogen, R. G. Pestell, and M. P. Lisanti. 1999. Caveolin-1 potentiates estrogen receptor alpha (ERalpha) signaling. caveolin-1 drives ligand-independent nuclear translocation and activation of ERalpha. *J Biol Chem* **274**: 33551-33556.

174. Lorbek, G., M. Perse, S. Horvat, I. Bjorkhem, and D. Rozman. 2013. Sex differences in the hepatic cholesterol sensing mechanisms in mice. *Molecules* **18**: 11067-11085.

175. Link, J. C., X. Chen, C. Prien, M. S. Borja, B. Hammerson, M. N. Oda, A. P. Arnold, and K. Reue. 2015. Increased high-density lipoprotein cholesterol levels in mice with XX versus XY sex chromosomes. *Arterioscler Thromb Vasc Biol* **35**: 1778-1786.

176. Yoon, M., S. Jeong, C. J. Nicol, H. Lee, M. Han, J. J. Kim, Y. J. Seo, C. Ryu, and G. T. Oh. 2002. Fenofibrate regulates obesity and lipid metabolism with sexual dimorphism. *Exp Mol Med* **34**: 481-488.

177. Baigent, C., A. Keech, P. M. Kearney, L. Blackwell, G. Buck, C. Pollicino, A. Kirby, T. Sourjina, R. Peto, R. Collins, R. Simes, and C. Cholesterol Treatment Trialists. 2005. Efficacy and safety of cholesterol-lowering treatment: prospective meta-analysis of data from 90,056 participants in 14 randomised trials of statins. *Lancet* **366**: 1267-1278.

178. Kwan, K. M., E. Fujimoto, C. Grabher, B. D. Mangum, M. E. Hardy, D. S. Campbell, J. M. Parant, H. J. Yost, J. P. Kanki, and C. B. Chien. 2007. The Tol2kit: a multisite gateway-based construction kit for Tol2 transposon transgenesis constructs. *Dev Dyn* **236**: 3088-3099.

179. Bourseau-Guilmain, E., J. A. Menard, E. Lindqvist, V. Indira Chandran, H. C. Christianson, M. Cerezo Magana, J. Lidfeldt, G. Marko-Varga, C. Welinder, and M. Belting. 2016. Hypoxia regulates global membrane protein endocytosis through caveolin-1 in cancer cells. *Nat Commun* **7**: 11371.

180. Truett, G. E., P. Heeger, R. L. Mynatt, A. A. Truett, J. A. Walker, and M. L. Warman. 2000. Preparation of PCR-quality mouse genomic DNA with hot sodium hydroxide and tris (HotSHOT). *Biotechniques* **29**: 52, 54.

181. Otis, J. P., D. Sahoo, V. A. Drover, C. L. Yen, and H. V. Carey. 2011. Cholesterol and lipoprotein dynamics in a hibernating mammal. *PLoS One* **6**: e29111.

182. Heron, M. 2012. Deaths: Leading Causes for 2008. *National Vital Statistics Reports* **60**.

183. Cederbaum, A., C. Lieber, D. Beattie, and E. Rubin. 1975. Effect of chronic ethanol ingestion on fatty acid oxidation by hepatic mitochondria. *Journal of biological chemistry*: 5122-5129.

184. Wheeler, M. D. 2003. Endotoxin and Kupffer cell activation in alcoholic liver disease. *Alcohol Res Health* **27**: 300-306.

185. Rubin, E., and C. Lieber. 1968. Alcohol-Induced Hepatic Injury in Nonalcoholic Volunteers. *New England Journal of Medecine*: 869-876.

186. Passeri, M. J., A. Cinaroglu, C. Gao, and K. C. Sadler. 2009. Hepatic steatosis in response to acute alcohol exposure in zebrafish requires sterol regulatory element binding protein activation. *Hepatology* **49**: 443-452.

187. Yin, C., K. J. Evason, J. J. Maher, and D. Y. Stainier. 2012. The basic helix-loop-helix transcription factor, heart and neural crest derivatives expressed transcript 2, marks hepatic stellate cells in zebrafish: analysis of stellate cell entry into the developing liver. *Hepatology* **56**: 1958-1970.

188. Lin, J. N., L. L. Chang, C. H. Lai, K. J. Lin, M. F. Lin, C. H. Yang, H. H. Lin, and Y. H. Chen. 2015. Development of an Animal Model for Alcoholic Liver Disease in Zebrafish. *Zebrafish* **12**: 271-280.

189. You, M., M. Fischer, M. A. Deeg, and D. W. Crabb. 2002. Ethanol induces fatty acid synthesis pathways by activation of sterol regulatory element-binding protein (SREBP). *J Biol Chem* **277**: 29342-29347.

190. Howarth, D. L., C. Yin, K. Yeh, and K. C. Sadler. 2013. Defining hepatic dysfunction parameters in two models of fatty liver disease in zebrafish larvae. *Zebrafish* **10**: DO1: 10.1089/zeb.2012.0821.

191. Howarth, D. L., A. M. Vacaru, O. Tsedensodnom, E. Mormone, N. Nieto, L. M. Costantini, E. L. Snapp, and K. C. Sadler. 2012. Alcohol disrupts endoplasmic reticulum function and protein secretion in hepatocytes. *Alcoholism, clinical and experimental research* **36**: 14-23.

192. Tsedensodnom, O., A. M. Vacaru, D. L. Howarth, C. Yin, and K. C. Sadler. 2013. Ethanol metabolism and oxidative stress are required for unfolded protein response activation and steatosis in zebrafish with alcoholic liver disease. *Dis Model Mech* **6**: 1213-1226.

193. Howarth, D. L., M. Passeri, and K. C. Sadler. 2011. Drinks like a fish: using zebrafish to understand alcoholic liver disease. *Alcohol Clin Exp Res* **35**: 826-829.

194. Salazar, G., and M. Antunano. 2005. Medical Facts for Pilots: Publication AM-400-94/2. *In*. A. E. D. FAA Civil Aerospace Medical Institute, editor, Oklahoma City.

195. Lickwar, C. R., J. G. Camp, M. Weiser, J. L. Cocchiaro, D. M. Kingsley, T. S. Furey, S. Z. Sheikh, and J. F. Rawls. 2017. Genomic dissection of conserved transcriptional regulation in intestinal epithelial cells. *PLoS Biol* **15**: e2002054.

196. Unger, R. H. 1995. Lipotoxicity in the pathogenesis of obesity-dependent NIDDM. Genetic and clinical implications. *Diabetes* **44**: 863-870.

197. Listenberger, L. L., D. S. Ory, and J. E. Schaffer. 2001. Palmitate-induced apoptosis can occur through a ceramide-independent pathway. *The Journal of biological chemistry* **276**: 14890-14895.

198. D'Alessandro, M. E., A. Chicco, and Y. B. Lombardo. 2008. Dietary fish oil reverses lipotoxicity, altered glucose metabolism, and nPKCepsilon translocation in the heart of dyslipemic insulin-resistant rats. *Metabolism: clinical and experimental* **57**: 911-919.

199. Stanley, W. C., and F. A. Recchia. 2010. Lipotoxicity and the development of heart failure: moving from mouse to man. *Cell metabolism* **12**: 555-556.

200. Schaffer, J. E. 2003. Lipotoxicity: when tissues overeat. *Current opinion in lipidology* **14**: 281-287.

201. Song, B.-J., K.-H. Moon, N. U. Olsson, and J. Norman Salem. 2008. Prevention of alcoholic fatty liver and mitochondrial dysfunction in the rat by long-chain polyunsaturated fatty acids. *Journal of Hepatology* **49**: 262-273.

202. Nanji, A., C. Mendenhall, and S. French. 1989. Beef fat prevents alcoholic liver disease in the rat. *Alcohol Clin Exp Res* **13**: 15-19.

203. Kim, K., N. Jung, K. Lee, J. Choi, S. Kim, J. Jun, E. Kim, and D. Kim. 2013. Dietary omega-3 polyunsaturated fatty acids attenuate hepatic ischemia/reperfusion injury in rats by modulating toll-like receptor recruitment into lipid rafts. *Clinical Nutrition* **32**: 855-862.

204. Widmer, R. J., A. J. Flammer, L. O. Lerman, and A. Lerman. 2015. The Mediterranean diet, its components, and cardiovascular disease. *Am J Med* **128**: 229-238.

Biography

Vanessa H. Quinlivan was born in 1984 and grew up in Latrobe, PA. She attended the Massachusetts Institute of Technology in Cambridge, MA as an undergraduate, where she majored in Biology. As an undergraduate researcher, she participated in the Mars Gravity Biosatellite Program. She also worked in the Department of Environmental Engineering, where she studied interactions between oceanic cyanobacteria and bacteriophages (with Sallie Chisholm), resulting in a publication in the journal *Environmental Microbiology* entitled "Portal protein diversity and phage ecology."

In 2006, Vanessa began working as a laboratory manager and instructor for the Science department of Tidewater Community College in Chesapeake, VA. In 2008, she worked as a technician for the Biology department at the College of William & Mary in Williamsburg, VA.

In 2011, Vanessa completed a M.S. in Biology at the College of William & Mary, having researched gene regulation of environmental responses in *Helicobacter pylori* with Mark Forsyth. She was also a teaching assistant for several courses including the HHMI Phage Lab. An article resulting from this work, "Repetitive sequence variations in the promoter region of the adhesion encoding gene *sabA* of *Helicobacter pylori* affect transcription," is published in the Journal of Bacteriology.

Vanessa began the Ph.D. program in Cellular, Molecular, and Developmental Biology and Biophysics at the Johns Hopkins University in Baltimore, MD in 2011. She worked as a teaching assistant for laboratory courses in Cell Biology and Biochemistry. Vanessa completed three laboratory rotations in which she studied protein-protein interactions important for cell division in yeast (with Andy Hoyt), DNA repair mechanisms in radiation-resistant archaea (with Jocelyne DiRuggiero), and membrane protein folding in *E. coli* (with Karen Fleming), before joining Steven Farber's laboratory in 2012.